ESPOO 2008 VTT PUBLICATIONS 701

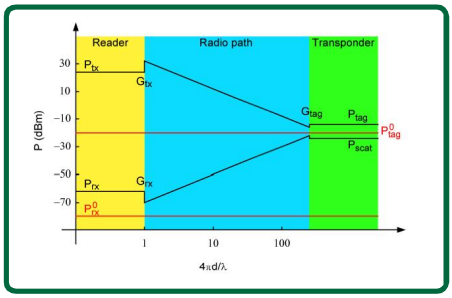

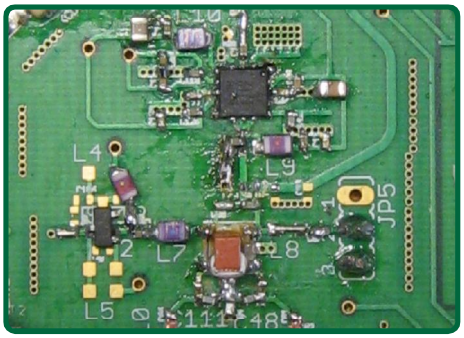

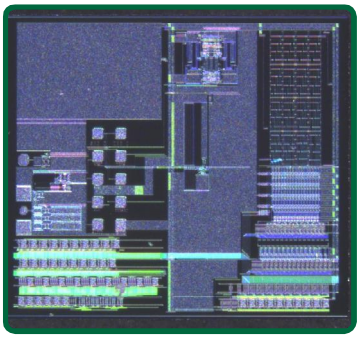

Pekka Pursula

Analysis and Design of UHF and Millimetre Wave Radio Frequency Identification

VTT PUBLICATIONS 701

Analysis and Design of UHF and Millimetre Wave Radio Frequency Identification

Pekka Pursula

Dissertation for the degree of Doctor of Science in Technology to be presented with due permission of the Faculty of Information and Natural Sciences, for public examination and debate in Auditorium AS1, Helsinki University of Technology (Espoo, Finland) on the 30th of January, 2009, at 12 noon.

ISBN 978-951-38-7133-8 (soft back ed.)
ISSN 1235-0621 (soft back ed.)

ISBN 978-951-38-7134-5 (URL: http://www.vtt.fi/publications/index.jsp)
ISSN 1455-0849 (URL: http://www.vtt.fi/publications/index.jsp)

JULKAISIJA – UTGIVARE – PUBLISHER

VTT, Vuorimiehentie 3, PL 1000, 02044 VTT
puh. vaihde 020 722 111, faksi 020 722 4374

VTT, Bergsmansvägen 3, PB 1000, 02044 VTT
tel. växel 020 722 111, fax 020 722 4374

VTT Technical Research Centre of Finland, Vuorimiehentie 3, P.O. Box 1000, FI-02044 VTT, Finland
phone internat. +358 20 722 111, fax +358 20 722 4374

VTT, Tietotie 3, PL 1000, 02044 VTT
puh. vaihde 020 722 111, faksi 020 722 7012

VTT, Datavägen 3, PB 1000, 02044 VTT
tel. växel 020 722 111, fax 020 722 7012

VTT Technical Research Centre of Finland, Tietotie 3, P.O. Box 1000, FI-02044 VTT, Finland
phone internat. +358 20 722 111, fax +358 20 722 7012

Cover: A platform-tolerant UHF RFID transponder antenna (above left); A power budget diagram of an UHF RFID System (above right); The adaptive RF front end of an EPC Gen2 UHF RFID reader (below left, courtesy of Perlos Corporation); And a UHF RFID transponder IC with a sensor interface (below right).

Edita Prima Oy, Helsinki 2008

Pursula, Pekka. Analysis and Design of UHF and Millimetre Wave Radio Frequency Identification [UHF- ja millimetriaaltoalueen radiotunnistusjärjestelmien tutkimus ja suunnittelu]. Espoo 2008. VTT Publications 701. 82 p. + appendices 51 p.

Keywords Radio frequency identification, RFID, ultra high frequency, UHF, millimetre waves, millimetre wave identification, MMID, antenna, scattering, backscattering modulation, scattering measurement, reader device, adaptive rf front end.

Abstract

Radio frequency identification (RFID) is an asymmetric radio protocol, where uplink communication (from transponder to reader) is implemented with backscattering modulation. The idea was first demonstrated in the 1940's. One of the first consumer applications of RFID was access control, and key cards based on an inductive near field coupling are widely used even today. The introduction of Schottky diodes to CMOS processes enabled passive RFID, i.e. transponders without a battery, at ultra high frequencies (UHF) with reasonable cost and read range in the end of 1990's. This has opened up new applications and inspired new research on RFID.

This thesis studies the radio frequency (RF) components and general RF phenomena in RFID at UHF and millimetre waves. The theoretical analysis of the radio path reveals that the read range of a passive UHF system is ideally limited by the downlink, i.e. the power transfer from reader to the transponder. However, the architecture of the reader RF front end is critical, because the transmitted signal may couple a significant amount of noise to the receiver, overpowering the faint reflection from the transponder. In the thesis, two adaptive RF front ends are introduced to eliminate the noise coupling from the transmitter.

One of the most critical problems with UHF RFID has been the detuning of transponder antennas on different mounting platforms. The detuning may significantly diminish the read range of the transponder, especially on metal surfaces. In this thesis, two backscattering-based measurement techniques for the transponder antennas are presented. The detuning effect has been studied using these measurement techniques, and a platform tolerant-antenna is introduced.

RFID at millimetre waves enables miniaturisation of the reader antenna, and widening the data bandwidth over short distances. This could be used to access wirelessly mass memories with wide data bandwidth. A semi-passive or active transponder could communicate, e.g., with automotive radars. The millimetre wave identification (MMID) has been theoretically studied and experimentally verified at 60 GHz.

Pursula, Pekka. Analysis and Design of UHF and Millimetre Wave Radio Frequency Identification [UHF- ja millimetriaaltoalueen radiotunnistusjärjestelmien tutkimus ja suunnittelu]. Espoo 2008. VTT Publications 701. 82 s. + liitteet 51 s.

Avainsanat Radio frequency identification, RFID, ultra high frequency, UHF, millimetre waves, millimetre wave identification, MMID, antenna, scattering, backscattering modulation, scattering measurement, reader device, adaptive rf front end.

Tiivistelmä

Radiotunnistus (RFID) on lyhyen kantaman radioprotokolla, jossa yksinkertaisen tunnisteen muisti voidaan lukea langattomasti lukijalaitteen avulla. Tiedonsiirto tunnisteesta lukijalaitteeseen perustuu tunnisteen takaisinsironnan moduloimiseen. Tekniikka on osoitettu kokeellisesti toimivaksi jo 1940-luvulla. Radiotunnistuksen ensimmäisiä kuluttajasovelluksia on induktiivisiin kulkukortteihin ja lukulaitteisiin perustuva kulunvalvonta, jota käytetään tänäkin päivänä yleisesti. Passiivisten, eli paristottomien, tunnisteiden valmistaminen UHF-taajuusalueelle halpeni merkittävästi 1990-luvulla, kun Schottky-diodi integroitiin onnistuneesti CMOS-prosessiin.

Tässä väitöskirjassa on tutkittu radiotunnistusjärjestelmien radiotaajuisia komponentteja ja ilmiöitä UHF- ja millimetriaaltoalueella. Teoreettisen analyysin perusteella tehonsyöttö lukijalta tunnisteelle rajoittaa passiivisen UHF RFID -järjestelmän toimintaetäisyyden noin kymmeneen metriin. Lukijan vastaanottama signaali on tällä etäisyydellä heikko lähettimen kohinaan verrattuna. Tässä väitöskirjassa on esitetty kaksi mukautuvaa radioetuastetta lähettimen kohinan eristämiseksi vastaanottimesta.

Tunnisteantennin sivuunvirittyminen on yleinen ongelma radiotunnistuksessa. Antennin kiinnitysalustan johtavuus tai dielektrisyys muuttaa antennin resonanssitaajuutta, mikä voi estää tunnisteen havaitsemisen. Väitöskirjassa on kehitetty kaksi takaisinsirontaan perustuvaa antennimittausmenetelmää ilmiön tutkimiseksi. Lisäksi työssä esitellään antennirakenne, joka voidaan kiinnittää useille erityyppisille pinnoille antennin toiminnallisuuden heikentymättä.

Millimetriaaltoalueella radiotunnistuksessa voidaan käyttää erittäin laajaa tiedonsiirtokaistaa lyhyillä etäisyyksillä langattoman massamuistin nopeaan lukemiseen. Toisaalta pitkän kantaman sovelluksessa esimerkiksi autotutkia voitaisiin käyttää lukijalaitteina. Väitöskirjassa on tutkittu millimetriaaltojen käyttöä radiotunnistuksessa teoreettisesti sekä osoitettu tekniikan toimivuus kokeellisesti 60 GHz:n taajuudella.

Preface

The work leading to this thesis has been carried out at the Centre of Sensors and Wireless Devices at VTT Technical Research Centre of Finland, Espoo, Finland, during 2003 – 2008. The thesis has been supported by The Finnish Foundation for Technology Promotion (TES), The Foundation of The Finnish Society of Electronics Engineers (EIS), and The Espoo Culture Foundation. The financial support is gratefully acknowledged.

I was introduced to RFID by my instructor, Dr. Timo Varpula. I thank Timo for the opportunity to work on the subject and for all the advice during the years. The work has been supervised by two professors, Kimmo Saarinen and Matti Kaivola. I wish to thank them both for their support. Professor Heikki Seppä deserves special thanks for the long discussions on RFID, universe and everything. Many problems in the prototypes were solved during these sessions with mind-blowing speed. I also thank the reviewers of the dissertation, Dr. Catherine Dehollain from EPFL of Switzerland and professor Lauri Sydänheimo from Tampere University of Technology for their time and effort on the quality of the thesis. I'm also keen to thank professor Pavel Nikitin from University of Washington, USA, for promising to act as the opponent in the defense.

I'm indebted to all the co-authors and colleagues. Especially Dr. Mervi Hirvonen, Dr. Tauno Vähä-Heikkilä, Dr. Nadine Pesonen and M.Sc. Kaarle Jaakkola, among others, have counseled me whenever needed. The advice of Dr. Kaj Nummila and all the other senior research staff has been invaluable. I want to thank all of my friends, especially those around the Round Table, whether at TKK or Gallows.

Sincere thanks for my parents Toini and Matti who have tiredlessly supported and encouraged me all my life. I wouldn't be here without You. I also want to thank my brother Antti for being there for me.

I thank Aino and and Ilmari for making daddy to think something else than his research, and reminding him of the joy of discovery. Finally, I thank my wife, Eeva, for everything: Like a night in the forest, like a walk in the rain...

Pekka Pursula, Espoo, December 2nd 2008.

List of Publications

Backscattering Communication and Applications

I P. Pursula, J. Marjonen, H. Ronkainen, and K. Jaakkola, "Wirelessly Powered Sensor Transponder for UHF RFID", *Transducers & Eurosensors'07 Conference*, Lyon, France, June 10 – 14, 2007, pp. 73 – 76.

II P. Pursula, T. Vähä-Heikkilä, A. Müller, D. Neculoiu, G. Konstantinidis, A. Oja, and J. Tuovinen, "Millimeter-Wave Identification – A New Short-Range Radio System for Low-Power High Data-Rate Applications", *IEEE Transactions on Microwave Theory and Techniques*, Vol. 56, Issue 10, pp. 2221 – 2228, October 2008.

Transponder Antenna Design and Measurement

III M. Hirvonen, P. Pursula, K. Jaakkola, and K. Laukkanen, "Planar Inverted-F Antenna for Radio Frequency Identification", *IEE Electronics Letters*, Vol. 40, Issue 14 , pp. 848 – 849, July 2004.

IV P. Pursula, M. Hirvonen, K. Jaakkola, and T. Varpula, "Antenna Effective Aperture Measurement with Backscattering Modulation", *IEEE Transactions on Antennas and Propagation*, Vol. 55, No. 10, pp. 2836 – 2843, October 2007.

V P. Pursula, D. Sandström, and K. Jaakkola, "Backscattering-Based Measurement of Reactive Antenna Input Impedance", *IEEE Transactions on Antennas and Propagation*, Vol. 56, No. 2, pp. 469 – 474, February 2008.

Adaptive RF Front End for Reader Device

VI P. Pursula, M. Kiviranta, and H. Seppä, "UHF RFID Reader with Reflected Power Canceller", accepted in *IEEE Microwave and Wireless Component Letters*, to be published in January 2009.

VII P. Pursula and H. Seppä, "Hybrid Transformer-Based Adaptive RF Front End for UHF RFID Mobile Phone Readers", *IEEE International Conference on RFID*, Las Vegas, USA, April 16 – 17, 2008, pp. 150 – 155.

Author's Contribution

I The author is the responsible author of the paper. The author designed the air interface and the protocol of the system. He contributed to the RF front end design and is responsible for the RF -related measurements. The author wrote the paper except for Sections 1 and 3.2. He presented the paper as an oral contribution in the conference.

II The author is the responsible author of the paper. The author derived the equations of operation and gathered the other results and the review of components in Sections II and III. He participated in the measurements and analysed the measurement results. He wrote the paper except for Section IV.

III This is a collaborative paper. The author is responsible for the antenna measurements and the analysis of the measurement results together with M. Hirvonen. The author wrote the paragraph on the measurement method.

IV The author is the responsible author of the paper. The author derived the theory and analysed the measurement results and uncertainty. He is responsible for the wireless measurements together with M. Hirvonen. The author wrote the paper.

V The paper is based on an original idea by the author. He is responsible for the theoretical analysis, measurements and the analysis of the measurement results together with D. Sandström. The author wrote Sections I, V and VI.

VI The author is the responsible author of the paper. The author designed and developed the UHF reader prototype, and he was responsible for the measurements. The theoretical analysis is a collaborative work by all the authors. The author wrote Sections I, III and parts of IV.

VII The author is the responsible author of the paper. The author is responsible for all simulations, measurements and the analysis of the measurement results. The theoretical analysis is a collaborative work by all the authors. The author wrote Sections I, III, IV, V and parts of VI. He presented the paper as an oral contribution in the conference.

The papers are referred to throughout the thesis by their Roman numerals [I] – [VII].

Contents

Abstract . . . 3
Tiivistelmä . . . 4
Preface . . . 5
List of Publications . . . 6
Author's Contribution . . . 7
Contents . . . 8

1 Introduction **9**
1.1 History . . . 13
1.2 Regulations and Standards . . . 15

2 Communication by Backscattering Modulation **17**
2.1 Effective Aperture and Radar Cross Section . . . 18
2.2 Effect of Modulation . . . 20
2.3 Power Transfer and Received Power . . . 23
2.4 Transponder Sensitivity . . . 24
2.5 Reader Sensitivity . . . 27
2.6 Read Range of UHF RFID . . . 27
2.7 Millimetre Wave Identification . . . 30
2.8 Limitations of the Free-Space Model . . . 31
2.9 Summary . . . 34

3 Transponder Antennas **35**
3.1 Backscattering from Antennas . . . 35
3.2 Measurement of Transponder Antennas . . . 36
3.3 Power Transfer . . . 38
3.4 Input Impedance . . . 41
3.5 Transponder Antenna Requirements . . . 44
3.6 Platform Tolerance . . . 45
3.7 Overview of Platform-Tolerant Antennas . . . 46
3.8 Summary . . . 48

4 RFID Reader **49**
4.1 Isolator Review . . . 50
4.2 Dynamic Range . . . 53
4.3 Reader with Common Isolation Techniques . . . 55
4.4 Adaptive RF Front End . . . 59
4.5 Impedance Bridge as an Adaptive RF Front End . . . 63
4.6 Summary . . . 66

5 Conclusion **68**

References . . . 70
Errata . . . 81
Publications . . . 83

1 Introduction

Radio Frequency Identification (RFID) has gained lot of interest and publicity in the recent years. In particular in industries, where logistics are central to the business, RFID-based processes have been tested, piloted and implemented with enthusiasm verging on hype [1]. Radio frequency identification has promised to deliver unprecedented visibility of goods within the logistics chain, because the long read range enables automatic identification, which replaces manual work.

In addition to logistics, the applications of radio frequency identification seem almost endless [2]. Access control is the most typical application, since many companies use RFID-based key cards in their offices. Car immobilisers are based on RFID [3]. The technique is used for collecting road tolls [4], as well as for timing in mass sports events [5]. Cattle, pets, and a few people carry transponders for identification [6]. Systems that enable localisation of transponders have been used e.g. in hospitals for patient and personnel safety as well as for the control of the medical equipment inventory [7]. Recently, short range readers under the near-field communication (NFC) standard have been integrated to mobile phones [8]. At the same time, sensors are being implemented within RFID systems, which opens ever-more applications.

Sensor networks have been envisioned to be the next mega trend after the Internet. A major drawback, however, exists. The sensor nodes need power for operation, and batteries tend to run empty, even though the life time of a battery in a sensor node has been extended to ten years. Passive RFID provides an efficient solution to the problem: Powering the sensor node remotely from the reader eliminates the battery.

But what actually is the technology behind RFID? The system consists of a reader device and a number of transponders. The transponders are attached to the objects to be identified. They include a memory, where an identification code and possible additional information on the object are stored. The reader can access the memory of a nearby transponder, and read the information stored in the memory.

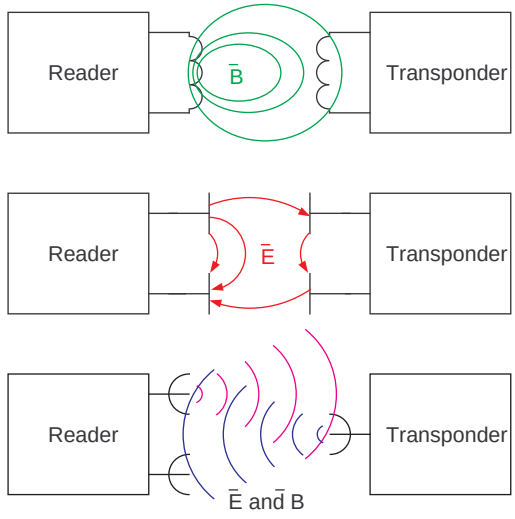

Figure 1.1. Physical coupling between reader and transponder: Inductive coupling uses the magnetic field $\bar{B}$ of a coil (top). Capacitive coupling utilises the electric field $\bar{E}$ of a capacitor (centre). Electromagnetic coupling is based on wave propagation of both $\bar{E}$ and $\bar{B}$ (bottom).

A variety of RFID systems exist. The systems differ in terms of range, size, cost and underlying technology and can be classified based on different characteristics, such as *coupling, operation frequency, transponder powering* and *implementation*.

The physical coupling between the reader and the transponder can be based on magnetic field (inductive coupling), electric field (capacitive coupling) or radiation field (electromagnetic coupling). These coupling methods are illustrated in Fig. 1.1. The inductive and capacitive couplings utilise the near-fields of a coupling element, i.e. a coil and a capacitor, respectively. The nature of the near-fields limits the read range approximately to the size of the coupling element. The electromagnetic coupling is based on electromagnetic waves, which are generated by an antenna, and which propagate far from the antenna.

The operation frequency of near-field systems varies from low to high frequencies, i.e, from 100 kHz to 13.56 MHz. The 13.56 MHz band is globally reserved for inductive RFID. Electromagnetically coupled systems operate at higher frequencies, usually from 400 MHz to 5 GHz, even though research takes place also in the millimetre waves, up to 60 and 77 GHz. Most of the electromagnetically coupled systems operate at ultra high frequencies (UHF), i.e. around 900 MHz.

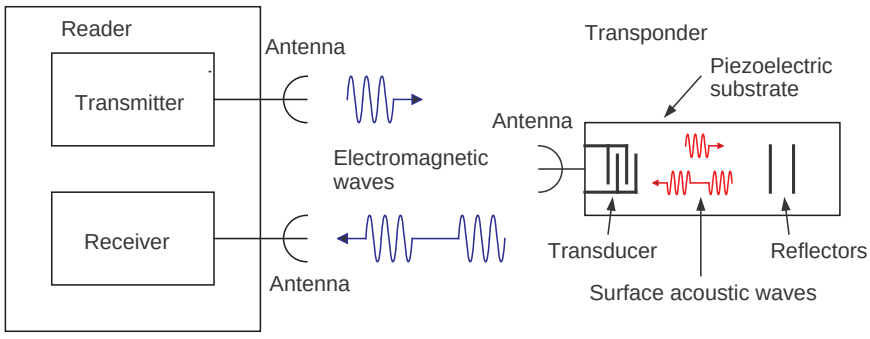

Figure 1.2. The operation principle of SAW RFID. The reader sends a short pulse of electromagnetic (EM) waves, which are transformed to surface acoustic waves (SAW) in the transponder. The waves are reflected with different time delays and transformed back to EM waves for transmission to the reader.

A passive transponder is powered up by the reader transmission. A semi-passive transponder has a battery, but relies on backscattering modulation for uplink (transponder to reader) communication. This enables a longer range than with a passive transponder, while providing a long battery lifetime. Active transponders generate also the carrier for uplink communications from the power of the battery.

The transponder memory can be implemented with microelectronics on silicon or with printing technology on an organic or an inorganic substrate. Also surface acoustic wave (SAW) propagation on a piezoelectric material can be used. The integrated circuits (IC) on silicon include a state machine that runs a program much like a microprocessor. The transponders based on printed organic or inorganic transistors have the same operational principle. In SAW RFID, the slow propagation of surface acoustic waves is utilised to create reflections of the reader transmission with different time delays (Fig. 1.2).

Most of the recent interest in RFID has been concentrated on silicon-based passive electromagnetically coupled systems at UHF. These systems deliver more than 5 metres of reliable read range with transponders that cost less than 10 Euro cents. The other systems can be superior in other aspects. For example, inductive systems can deliver much better security and encryption features [2], and SAW-based systems deliver a longer range [9].

Printed electronics might provide another low-cost implementation of the transponders in the future. The transponder antenna for HF and UHF RFID can be printed with ink that includes metallic nanoparticles (see

e.g. [10]). The transistors for the transponder electronics can be printed with inorganic or organic semiconductor ink. A mobility of 0.1 cm^2/Vs is achieved in organic transistors [11]. Inorganic semiconductors have been used in printed electronics to fabricate higher quality transistors with mobilities of 80 cm^2/Vs [12], but they are still slower and lossier than the transistors on silicon, where the bulk electron mobility is 1500 cm^2/Vs. Functional systems have been implemented for frequencies up to 13.56 MHz, both organic [13] and inorganic [12], but often the protocols of the systems are simplified (see e.g. [14]), and they do not comply with the standards.

This Thesis studies passive electromagnetically coupled RFID systems at UHF and millimetre waves. The study concentrates on silicon-based systems, even though some of the analysis is independent of the transponder implementation. This choice reflects the author's opinion of the most feasible RFID system configuration. The ultra high frequency provides a good compromise between size and read range, and the maturity of the silicon technology makes it the best choice both technically and economically, at least for many years to come.

The author has been involved in proposing RFID at millimetre waves, a technique called Millimetre Wave Identification (MMID). Millimetre waves span up in frequency from 30 GHz, where the wavelength of the radiation is below 1 cm. The advantages of millimetre waves include high data rates, small directional antennas, and the possibility to use automotive radars as reader devices. MMID is technically feasible today, even though the components are expensive. But the technology is becoming economically more attractive with CMOS-processes scaling up to 60 GHz and beyond.

The operational principle of passive UHF RFID is summarised in Fig. 1.3. The reader transmits a modulated carrier signal. The transponder rectifies the carrier to power itself up. Downlink communication, i.e. from reader to transponder, includes amplitude modulated commands. The uplink communication (from transponder to reader) is realised with backscattering modulation. The reader sends a carrier signal when the transponder responds. The transponder IC modulates its input impedance, which leads to a modulation of the signal scattered by the transponder. Both amplitude and phase modulation can be utilised. The signal transfer from the transponder to the reader is based on reflection, like in the optical bar code systems. But in RFID, at radio frequencies, a coherent detection of the reflection can be used, which makes the detection more sensitive. This is emphasised in Fig. 1.3 by drawing the common local oscillator for the transmitter and the receiver.

The understanding of antenna scattering and its detection is crucial to

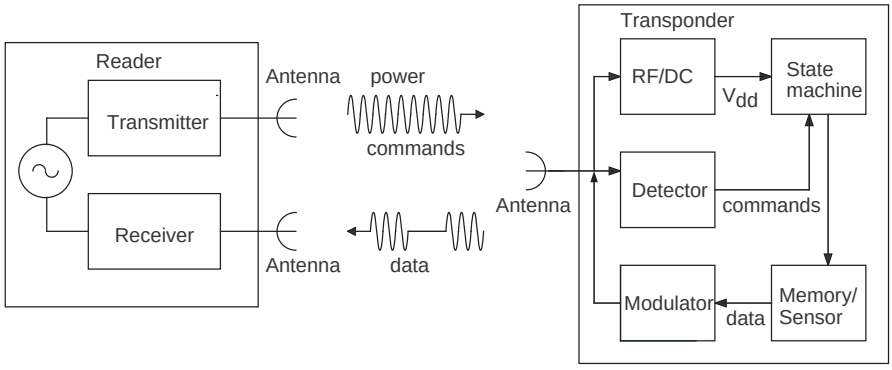

Figure 1.3. Components of a passive UHF RFID system. A reader with coherent detection (left) and a transponder with an antenna connected to a silicon-based integrated circuit (right).

the reliability of an RFID system. This Thesis studies the radio frequency (RF) components, i.e. the transponder antenna and reader front end, and the antenna scattering. In the next chapter, the fundamental theory for transponder powering and communication by backscattering modulation is derived. The analysis is applied to UHF, where an RFID chip for sensor applications is also presented [I]. The RFID concept is extended to millimetre waves theoretically and experimentally [II].

In Chapter 3, the transponder antenna and its scattering are further discussed. A platform-tolerant transponder antenna structure is presented [III]. The scattering of transponders is measured, and two scattering-based measurement techniques for transponder antenna characterisation are introduced [IV, V]. Last, but not least, the RFID reader device is studied in Chapter 4. The development of two RFID readers with adaptive RF front ends is presented [VI, VII].

1.1 History

Electromagnetic coupling is based on electromagnetic wave propagation, which was first predicted by Maxwell, when he derived the electromagnetic wave equations in 1864 [15]. Hertz was the first to experimentally generate and detect electromagnetic waves beginning in 1888. The development of the radio technology culminated in Marconi making his famous transmission of data over the Atlantic Ocean in 1901. Tesla was experimenting

with the wireless radio at the same time, but is known better for his experiments on wireless power transfer. He had several patents relating to power transfer. Even though Tesla imagined using wireless power transfer over considerable distances, the power transfer systems described by him are basically near-field systems, consisting of two coupled resonant circuits [16]. For global wireless power transfer he suggested using the earth as a resonator [17]. In 1900, in one of his patents [16], Tesla rejects the use of electromagnetic waves for power transfer:

"It is to be noted that the phenomenon here involved in the transmission of electrical energy is one of true conduction and is not to be confounded with the phenomena of electrical radiation which have heretofore been observed and which from the very nature and mode of propagation would render practically impossible the transmission of any appreciable amount of energy to such distances as are of practical importance."

It took half a century before radio wave power transmission was developed further. Friis derived the transmission equation in 1946 [18]. High microwave power transfer has been developed since the 1950s, and a power of 30 kW was transferred over a distance of 1 mile in 1975 [19]. Nowadays, radio waves are used in the passive electromagnetically coupled RFID systems for wireless power transfer of micro- and milliwatts over distances of up to 10 m.

In 1948, Stockman proposed using modulated backscattering for communication [20]. He used corner reflectors and modulated the backscattering by moving one of the metal plates of the reflector. For example, by modulating the reflector plate by voice he succeeded in transferring the signal over a hundred yards.

King was one of the first to measure and interpret antenna scattering as a function of antenna load [21] in 1949. The theory was developed further by Harrington, who derived the scattering equation for loaded scatterers using a linear three-port network in 1964 [22]. Since then the research field has diversified and load modulation has been used for example in electric field measurements [23], as well as the measurement of antenna gain [24], antenna input impedance [25], and antenna scattering matrix [26]. The author has studied backscattering-based measurement techniques in the case of RFID in [IV, V]. Today's RFID technology relies on backscattering modulation for uplink communication.

The history of RFID cannot be written without mentioning the passive microphone developed by Theremin. The microphone was placed within the Great Seal of Unites States and presented to the US Ambassador in Berlin by the Russians in 1946. The microphone was used for spying for

six years, before it was found by the Americans in 1952. The device was completely passive, including only an antenna and a cavity resonator with a moving diaphragm [27].

During World War II, the Royal Air Force used an RFID based system to identify friendly aeroplanes. The Interrogate-Friend-or-Foe (IFF) system was similar to the transponders that commercial aeroplanes carry nowadays. The transponders are active, and usually use UHF frequencies at around 1 GHz [28].

The inductive RFID systems have been widely adopted for access control since the 1990s. In the beginning of the 2000s, they were standardised under the Near-Field Communication (NFC) Forum, which has lead to readers embedded in mobile phones (see e.g. [8]).

A passive UHF RFID system was first demonstrated in 1975 by Koelle, Depp and Freyman [29]. Commercial systems began to emerge in the 1980s, but the development of Schottky diodes on a CMOS circuit in the 1990s can be considered a breakthrough [30]. This advance allowed long-range and low-cost transponders, see e.g. [31, 32]. At this time, also standardisation under the International Organization for Standardization (ISO) and the Auto-ID Center (now EPCglobal) began.

1.2 Regulations and Standards

To ensure the successful coexistence of the myriads of radio devices of our daily lives, the electromagnetic spectrum is divided into separate bands for different radio applications. Unfortunately, a global band for the UHF RFID does not exist, but the allocated bands vary from region to region. The frequency bands and allowed transmission (TX) power for a number of regions are summarised in Table 1.1. The transmission power is expressed as equivalent isotropic radiated power (eirp), i.e., $P_{eirp} = G_{tx}P_{tx}$, where G_{tx} is the transmitter antenna gain and P_{tx} the power fed to the antenna. The equivalent radiated power (erp) is similarly defined, but uses antenna gain over dipole (dBd). The two are related as $P_{eirp} = 1.64P_{erp}$.

In addition to the radio regulations, the physical layer of RFID systems, including modulation, encoding etc., is standardised by the International Standardisation Organisation and EPCglobal. These have issued the UHF RFID air interface standards ISO 18000-6 [33] and EPC Gen2 [34], respectively. The standards are identical, except for a few application identifier bits in the transponder memory mapping. These standards have become

Table 1.1. Radio regulations on UHF RFID in different regions.

Region	Frequency (MHz)	TX Power (maximum)	Regulation	Ref
Europe	869.4 – 869.65	0.5 W_{erp}	EN 300 220	[35]
Europe	865 – 868	2.0 W_{erp}	EN 302 208	[35]
USA	902 – 928	4.0 W_{eirp}	FCC Part 15	[36]
Korea	908.5 – 914	4.0 W_{eirp}		
Japan	952 – 954	4.0 W_{eirp}		
China	840.25 – 844.75	2.0 W_{erp}		[37]
China	920.25 – 924.75	2.0 W_{erp}		[37]

the most utilised in the field in recent years.

The physical layers of some air-interface standards and protocols are presented in Table 1.2. The study presented in this thesis can be utilised for any modulation and coding scheme, and the air interface standards are not discussed further. The allocated frequency and the allowed power define the fundamental limits of the RFID system read range, as will be seen in the next chapter.

Table 1.2. Physical layers of some air-interface standards and protocols for UHF RFID.

Standard/ Protocol	Downlink		Uplink		Ref
	Modulation	Encoding	Modulation	Encoding	
ISO 18000-6A	ASK	PIE	ASK	FM0	[33]
ISO 18000-6B	ASK	Man-chester	ASK	FM0	[33]
ISO 18000-6C	(PR-) ASK	PIE	ASK PSK	FM0 MMS	[33]
EPC Gen2	(PR-) ASK	PIE	ASK PSK	FM0 MMS	[34]
Tagidu	PR-ASK	PIE	PSK	FM0 NRZ 3Phase1	[32]

PIE = pulse interval encoding
(PR-)ASK = (phase reversal) amplitude shift keying
PSK = phase shift keying
MMS = Miller-modulated subcarrier
NRZ = non-return to zero

2 Communication by Backscattering Modulation

A passive RFID system has two principal constraints limiting its operation: the power transfer to the transponder and the power received by the reader. The electromagnetic wave propagation phenomena are crucial to the success of RFID, and have been widely studied. One of the first analyses of the RFID read zone was presented by Rao et al. [38]. The power transfer to a transponder was analysed as a function of antenna load by Karthaus and Fischer [39]. Nikitin and Rao [40, 41] included a number of unidealities in the discussion, e.g. multipath propagation and polarisation. Recently, Fuschini et al. [42] have analysed the transponder antenna scattering further. The author has studied the phenomena in [II, IV].

The two-way power budget of an RFID system is presented in Fig. 2.1. The figure describes a passive UHF RFID with a transponder near its maximum operational range. The system has two critical power levels,

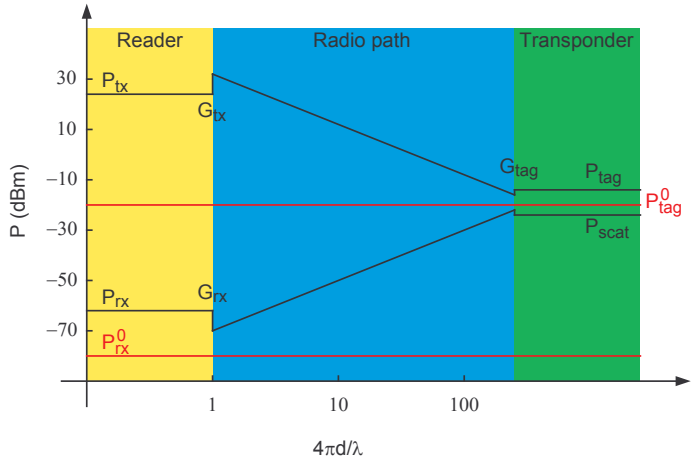

Figure 2.1. Power budget diagram of an RFID system.

the transponder sensitivity P^0_{tag} and the reader sensitivity P^0_{rx}, i.e. the minimum power levels required by the transponder and the reader.

Figure 2.1 shows the symmetry of the up- and downlinks in an RFID system. The radio path is equal in both directions. The effect of the antenna gain is shown as steps in the power level. The transponder uses some of the incident power for powering up the integrated circuit (IC) and some for backscattering modulation. The modulation loss determines the difference of the power P_{tag} transferred to the IC and the scattered power P_{scat}. The power budget of an RFID system is comprehensively discussed in the next sections.

2.1 Effective Aperture and Radar Cross Section

The power transfer to the transponder and the power scattered by the transponder are described in terms of the effective aperture A_e and the radar cross section σ of the transponder antenna, respectively. To derive equations for the effective aperture and the radar cross section, the transponder is modelled as a series circuit shown in Fig. 2.2. The circuit consists of series resistances and reactances of an antenna (subscript A) and a load (subscript L), and a voltage source with amplitude V describing the incident radiation field.

The effective aperture A_e and the radar cross section σ can be expressed in terms of the power dissipated in the load and antenna resistances, respectively [43]

$$\begin{aligned} A_e &= \frac{\frac{1}{2}R_L|I|^2}{S}, \\ \sigma &= \frac{\frac{1}{2}G_A R_A|I|^2}{S}. \end{aligned} \tag{2.1}$$

Here I is the complex amplitude of the current in the circuit. The antenna gain G_A in the radar cross section equation takes into account the antenna losses and directivity when the scattered power is re-radiated. The power is normalised to the incident field power intensity S, which is related to the voltage V. In a conjugate match, the power dissipated in the load and antenna resistances are equal, and they can be identified with the available power in the Friis equation [18]

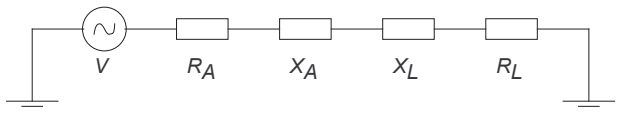

Figure 2.2. The series model of a loaded antenna.

$$\frac{V^2}{8R_A} = \frac{G_A\lambda^2}{4\pi}S. \tag{2.2}$$

Combining Eqs. (2.1) and (2.2), the effective aperture and the radar cross section can be written as [IV]

$$\begin{aligned} A_e &= \frac{G_A\lambda^2}{4\pi}\frac{4R_AR_L}{(R_A+R_L)^2+(X_A+X_L)^2}, \\ \sigma &= \frac{G_A^2\lambda^2}{4\pi}\frac{4R_A^2}{(R_A+R_L)^2+(X_A+X_L)^2}. \end{aligned} \tag{2.3}$$

The equations consist of a maximum aperture term multiplied by a mismatch term. The mismatch term can be expressed with the aid of a reflection coefficient, known as the Kurokawa power reflection coefficient [44, 45]

$$\Gamma = \frac{Z_L - Z_A^*}{Z_L + Z_A}. \tag{2.4}$$

The current in the circuit can now be written as

$$I = \frac{V}{Z_A + Z_L} = \frac{V}{2R_A}\left(1-\Gamma\right). \tag{2.5}$$

The power dissipated in the load has two expressions in terms of the reflection coefficient,

$$\begin{aligned} P_L &= \frac{1}{2}R_L|I|^2 \\ &= \frac{V^2R_L}{8R_A^2}\left|1-\Gamma\right|^2 \\ &= \frac{V^2}{8R_A}\frac{4R_LR_A}{|Z_L+Z_A|^2} \\ &= \frac{V^2}{8R_A}\left(1-|\Gamma|^2\right). \end{aligned} \tag{2.6}$$

The expression on line 2 of Eq. (2.6) follows directly from Eq. (2.1). The expression on line 4 can be considered as the product of the incident power and the power transmission coefficient. Now the equations for the effective aperture and radar cross section can then be written as [II]

$$\begin{aligned} A_e &= \frac{G_A \lambda^2}{4\pi} \left(1 - |\Gamma|^2\right), \\ \sigma &= \frac{G_A^2 \lambda^2}{4\pi} |1 - \Gamma|^2 . \end{aligned} \tag{2.7}$$

The mismatch terms now look more familiar.

In a conjugate match, i.e. for $\Gamma = 0$, the expressions in Eq. (2.7) reduce to the well-known aperture equations presented already by Friis [18] and Harrington [22]

$$\begin{aligned} A_e &= \frac{G_A \lambda^2}{4\pi} \\ \sigma &= \frac{G_A^2 \lambda^2}{4\pi} = G_A A_e. \end{aligned} \tag{2.8}$$

2.2 Effect of Modulation

To achieve actual data transfer in the uplink, a modulation between two load impedance states Z_1 and Z_2, or reflection coefficients Γ_1 and Γ_2, is required. Assuming an FM0 coding scheme, which is used in the EPC Gen2 RFID standard [34], a square wave can be taken as the modulation waveform. Explicitly, the modulation has the form

$$\Gamma(t) = \begin{cases} \Gamma_1 & , \quad \frac{2\pi}{\omega_m}\left(k - \frac{1}{2}\right) < t < \frac{2\pi k}{\omega_m} \\ \Gamma_2 & , \quad \frac{2\pi k}{\omega_m} < t < \frac{2\pi}{\omega_m}\left(k + \frac{1}{2}\right) \end{cases}, \tag{2.9}$$

where ω_m is the modulation frequency, and k is an integer. The effect of the duty cycle of the modulation waveform is further explored in [46].

The power available to the transponder is the average of the powers in each individual load state. Thus the effective aperture becomes [II]

$$A_e^m = \frac{G_A \lambda^2}{4\pi} \left(1 - \frac{1}{2}\left[|\Gamma_1|^2 + |\Gamma_2|^2\right]\right), \tag{2.10}$$

where the superscript m is added to denote the modulated case.

The current I in the circuit includes contributions at all the harmonics of the modulation frequency. Hence also the radar cross section has components on all the frequencies. The zeroth harmonic, i.e. the DC component, describes the scattering at the carrier frequency, and the other harmonic contributions of the modulation frequency form a comb of sidebands around the carrier.

In [IV], the radar cross section component σ_1 at the fundamental modulation frequency is calculated using Fourier expansion of the modulated current. In [II], the radar cross section σ_0 at the carrier frequency and the radar cross section σ_m, which describes the scattered power at all the harmonics of the modulation frequency, are presented. The Fourier expansion is now elaborated here to link these radar cross section terms together.

The Fourier series of the current is calculated in [IV], but not expressed with the reflection coefficient. However, the Fourier series of a square wave is well known, and can be expressed in terms of the reflection coefficient

$$\begin{aligned} I &= \frac{1}{2}I_0 + \sum_{k=1,3,5,\ldots} I_k \sin(k\omega_m t) \ \text{, where} \\ I_0 &= \frac{V}{2R_A}[2 - (\Gamma_1 + \Gamma_2)], \\ I_k &= \frac{V}{2R_A}\frac{2}{k\pi}(\Gamma_1 - \Gamma_2). \end{aligned} \tag{2.11}$$

The scattered power of each of the frequency components can be calculated by squaring the corresponding Fourier component of the frequency. The radar cross section components become

$$\begin{aligned} \sigma_0 &= \frac{G_A^2\lambda^2}{4\pi}\left|1 - \frac{1}{2}(\Gamma_1 + \Gamma_2)\right|^2, \\ \sigma_k &= \frac{G_A^2\lambda^2}{4\pi}\frac{2}{k^2\pi^2}|\Gamma_1 - \Gamma_2|^2. \end{aligned} \tag{2.12}$$

In [IV], a square modulation of the load reactance was studied. The load impedances $Z_1 = Z_A^* + j\Delta X$ and $Z_2 = Z_A^* - j\Delta X$ are used. Equations (11) and (14) in [IV] give the effective aperture A_e^m and the radar cross section σ_1. The effective aperture is an average of the apertures of the individual impedance states, as suggested by Eq. (2.10). Using Eq. (2.12) for the case of the reactive modulation, the radar cross section σ_1 becomes

$$\sigma_1 = \frac{\lambda^2 G_A^2}{4\pi} \frac{16}{\pi^2} \frac{R_A^2 \Delta X^2}{(R^2 - X^2 + \Delta X^2)^2 + 4R^2 X^2}, \tag{2.13}$$

which is the equation given by the analysis in [IV] (see also Errata).

The radar cross section σ_m associated with the overall scattered power can be calculated from the sum of the terms σ_k, i.e. $\sigma_m = \Sigma_k \sigma_k$. Using the definition of the Riemann Zeta Function $\zeta(x)$ [47],

$$\zeta(2) = \sum_{k=1,2,3,\ldots} \frac{1}{k^2} = \frac{\pi^2}{6}, \tag{2.14}$$

the sum included in the radar cross section can be calculated as

$$\sum_{k=1,3,5,\ldots} \frac{1}{k^2} = \sum_{k=1,2,3,\ldots} \frac{1}{k^2} - \frac{1}{4} \sum_{k=1,2,3,\ldots} \frac{1}{k^2} = \frac{\pi^2}{8}.$$

Hence, the modulated radar cross section becomes [II]

$$\sigma_m = \frac{G_A^2 \lambda^2}{16\pi} |\Gamma_1 - \Gamma_2|^2 = \frac{G_A^2 \lambda^2}{4\pi} m. \tag{2.15}$$

This is the radar cross section that describes the information carrying scattering. Here, $m = \frac{1}{4} |\Gamma_1 - \Gamma_2|^2$ is the modulation index or modulation loss. It can have values $0 \leq m \leq 1$.

The result for σ_0 in Eq. (2.12) and σ_m in Eq. (2.15) can also be derived by arranging the modulated current to even and odd terms

$$I = \frac{V}{2R_A} \left[1 - \frac{1}{2} (\Gamma_1 + \Gamma_2) + \frac{1}{2} (\Gamma_1 - \Gamma_2) \Theta(t) \right], \tag{2.16}$$

where $\Theta(t)$ is a square wave with unity amplitude

$$\Theta(t) = \begin{cases} -1 & , \quad \frac{2\pi}{\omega_m} \left(k - \frac{1}{2}\right) < t < \frac{2\pi k}{\omega_m} \\ 1 & , \quad \frac{2\pi k}{\omega_m} < t < \frac{2\pi}{\omega_m} \left(k + \frac{1}{2}\right) \end{cases}. \tag{2.17}$$

The radar cross section terms σ_0 and σ_m follow directly, if the odd and even currents are inserted to Eq. (2.1). However, this analysis does not provide an expression for the terms σ_k for $k = 1, 2, 3, ...$ associated with the harmonics of the modulation frequency. The Fourier analysis provided also the term σ_1, and enabled comparing the expressions and analyses in [II] and [IV].

The analysis presented above did not make any assumptions concerning the type of the load modulation. The reflection coefficient suffices to describe the modulation in terms of the transferred and scattered power. In general, the transponder modulates both the amplitude and the phase of the scattered signal. The analysis gives the scattered power, independent of the type of modulation.

Usually, mainly either load resistance or reactance is modulated. Amplitude and phase modulation can arise from both types of load modulation. For example, modulation of the load resistance with states $Z_1 = 0 - jX_A$ and $Z_2 = R_A/2 - jX_A$ gives the reflection coefficients $\Gamma_1 = 1$ and $\Gamma_2 = 1/3$. Because the reflection coefficients have the same phase, but unequal magnitude, amplitude modulation arises. On the other hand, states $Z_1 = 0 - jX_A$ and $Z_2 = \infty - jX_A$ lead to reflection coefficients $\Gamma_1 = 1$ and $\Gamma_2 = -1$. They are equal in magnitude but opposite in phase. Hence phase modulation arises. In a similar manner, reactive load modulation can give rise to both amplitude and phase modulation.

Because of its simplicity, a switched capacitor or a switched resistor modulator is often used. Hence the scattered signal will include both phase and amplitude modulation. The reader needs quadrature downmixers to detect both amplitude and phase modulation and advanced algorithms are required for optimal detection.

2.3 Power Transfer and Received Power

Using the effective aperture from Eq. (2.10), the power P_{tag} transferred to the transponder can be calculated from the Friis equation

$$P_{tag} = A_e^m \frac{G_{tx} P_{tx}}{4\pi d^2}, \tag{2.18}$$

where the subscript tx stands for the reader transmitter and d is the distance between the transponder and the reader. The transferred power must be higher than the transponder sensitivity P_{tag}^0, which depends greatly on the properties of the transponder. The sensitivity P_{tag}^0 describes the minimum RF power that must be transferred to the integrated circuit (IC) of the transponder.

Often the unmodulated aperture A_e in Eq. (2.7) is used in the Friis equation instead of the average aperture A_e^m of Eq. (2.10). There are many reasons for this. First, the impedances of both of the IC modulation states are not always known. Usually only one impedance state is given in publi-

cations. Further, the modulation index is often quite low, less than -6 dB. Hence the error due to the simpler expression is small. The IC properties are further discussed in Section 2.4.

The power P_{rx} received by the reader is given by the radar equation using the modulated radar cross section from Eq. (2.15)

$$P_{rx} = \sigma_m \frac{\lambda^2 G_{tx} P_{tx} G_{rx}}{(4\pi)^3 d^4}, \tag{2.19}$$

where the subscript rx stands for the reader receiver (see Errata). The received power must be greater than the reader sensitivity P^0_{rx}, which is limited by the noise seen by the receiver. This will be further discussed in Section 2.5 and Chapter 4.

Which one of Eqs. (2.18) and (2.19) imposes the more stringent limit for the range of the RFID system? It depends on many parameters of the system: the antenna gains, distance, and especially on the transponder and reader sensitivities. An overview of state-of-the-art transponder ICs and readers needs to be presented to determine proper values of the sensitivities P^0_{tag} and P^0_{rx}.

2.4 Transponder Sensitivity

The sensitivity of a passive transponder IC depends mainly on the transponder DC power consumption and rectifier efficiency η. The efficiency is usually only 10 – 40 %, because of RF power leaks to substrate through paracitic elements and because the incident voltages are low compared with the threshold voltage and thermal noise of the rectifying element. The parasitic leakage can be diminished by using a narrow-line-width process and a high-resistivity substrate. The DC power consumption depends on the circuit functionality. Memory access consumes less power than sensor interfacing, for example.

In [I], a sensor RFID IC is presented. The block diagram and chip photograph of the sensor chip are presented in Fig. 2.3. The IC has a 10 bit analog-to-digital converter (ADC) for an external sensor. The IC includes all RF and baseband analog and digital electronics that are needed for the wireless readout of the external sensor.

Table 2.1 presents an overview of the passive UHF RFID ICs published in the literature. The sensitivity is often expressed in terms of a DC current consumption from a certain voltage. Whenever possible, the sensitivity has been transformed to the RF power incident to the IC, which is referred

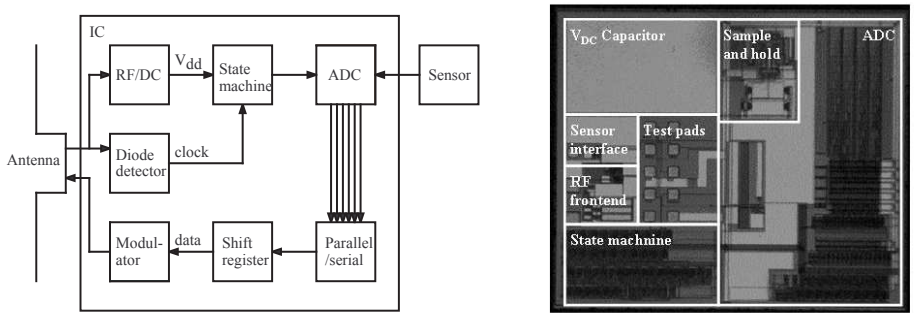

Figure 2.3. The block diagram (left) and photograph (right) of the wireless sensor IC [I].

to as P^0_{tag}. The modulation index m, which is needed to calculate the radar cross section σ_m, depends on the modulator design. Common designs include a capacitance diode, a switched capacitor and a switched resistor. Unfortunately the modulation index m and the rectifier efficiency η are presented in only a few publications.

In addition to the passive UHF chips, Table 2.1 includes a SAW-based sensor chip [48], one inductive sensor system on package [49], and one semi-passive memory IC [50]. The transponder sensitivity varies at least by a factor of 1000, depending on the chip functionality. Roughly, the chips can be divided into two classes: memory ICs and sensor ICs.

The memory ICs have a sensitivity of the order of 1 – 10 μW_{RF}. The ICs with the sensors or sensor interfaces require more power, from 100 μW_{RF} to 10 mW_{RF}. This is not surprising, as high precision and power consumption are contradictory optimisation parameters in ADCs, which can be understood to be a consequence of the thermal noise in resistors: the greater the resistor, the less power is dissipated, but the higher is the noise generated. Unfortunately the RF sensitivity of the sensor IC in [51] is not provided, but assuming a typical rectifier efficiency of $\eta = 20$ %, the sensitivity would be about 25 μW_{RF}.

The 10 bit ADC sensor readout presented in [I] stands up well in the comparison. The power consumption of the IC is only 30 μW_{DC}. All the other sensor ICs in Table 2.1 have much higher power consumption, except for [51]. To date, the chip presented in [I] seems to be the only published UHF RFID IC with an ADC for external sensors. However, sensor ICs for RFID are commercially interesting, and a lot of unpublished development is probably carried out by the industry.

Table 2.1. Review of RFID Integrated circuits.

f_0 (MHz)	Z_L (Ω)	m (dB)	Sensitivity (μW_{RF})	Sensitivity (μW_{DC})	η (%)	Process	Features	Ref	Year
915	—	—	—	—	—	SAW	analog uplink, temp sensor	[48]	1987
865	6-j210	-6	16.7	3.0	18	0.5 μm CMOS +Schottky		[39]	2003
860 – 960	—	—	—	5.1	—	0.25 μm CMOS	10 bit? ADC, internal temp and photo sensor	[51]	2005
3	—	—	—	341	—	3 μm BiCMOS	inductive, analog uplink, external sensors for temp, pressure, RH%	[49]	2005
2 450	5-j130	<-6	2.7	1.0	37	0.5 μm Si on Sapphire		[52]	2005
450 & 900	12-j10	—	—	4 000	—	0.25 μm CMOS	5 bit ADC, uplink 7 Mbit/s up-/downlink 900/450 MHz	[53]	2006
915	—	—	400 – 1 000	—	—	not integrated	10 bit ADC, EPC Gen1	[54]	2007
869	22-j145	-12	4 300 (250)	30 (30)	0.7 (12)	1.5 μm BiCMOS (+Schottky)	10 bit ADC	[I]	2007
953	—	—	80	29	36	0.35 μm CMOS		[55]	2007
2 450	92-j867	—	12.5	—	—	1 μm CMOS +Schottky	ISO-18000-4B, semi-passive	[50]	2007
860 – 960	27-j200	—	15.8	—	—	CMOS	EPC Gen2	[56]	2008

2.5 Reader Sensitivity

Table 2.2 presents a review of the receiver parameters of published and commercialised RFID readers. The most important parameters are the reader sensitivity and the input compression point P_{1dB}. The sensitivity describes the lowest received signal power that can be differentiated from noise. The input compression describes the highest incident power that the receiver tolerates. In general, the higher the input compression point, the worse the sensitivity. The sensitivity and input compression will be discussed further in Chapter 4.

The sensitivity is limited by the noise in the receiver. This includes the thermal noise of the receiver itself, but also the transmitter noise has an impact: Because the receiver and the transmitter are operating simultaneously at the same frequency, the transmitter signal easily couples to the receiver. Hence, the sensitivity is a function of the incident carrier power, or the TX–RX coupling. The reader ICs [57, 58] have two operating modes: The best sensitivity is achieved with the lowest P_{1dB} and vice versa.

The ICs and commercialised readers have a sensitivity of -96 – -70 dBm at a reliable communication level defined by a reasonably low bit error rate (BER) or packet error rate (PER) and a different incident carrier power. In [VI] a sensitivity of even -100 dB is achieved with unity signal-to-noise ratio (SNR). In practice, at least an SNR = 10 dB is required for reliable communication (approximately BER $< 10^{-3}$ [46, 58]). The bandwidths of the readers are similar, even though they are presented differently. Hence, the reader presented in [VI] has a similar sensitivity to the commercial readers, but a higher compression point. However, the sensitivity in [VI] is still 20 dB over the thermal noise limit. The reader dynamic range will be further discussed in Chapter 4.

2.6 Read Range of UHF RFID

After reviewing the transponders and the readers, it is now possible to choose some typical values for transponder and reader sensitivity to analyse the system. For a graphical analysis of the read range, typical UHF RFID system parameters are chosen. The transponder sensitivity $P^0_{tag} = 10\mu$W is 2 dB better than the EPC Gen2 chip in [56]. The reader sensitivity $P^0_{rx} = -100$ dBm is the best value in the reader review presented in Table 2.2.

Table 2.2. Review of Readers.

Sensitivity (dBm/Hz)	Sensitivity (dBm)	Δf	P_{1dB} (dBm)	Process	Features	Ref	Year
—	—	—	—	—	ISO 18000-6C	[59]	2007
—	-96 – -80 (BER 0.1 %)	40 kbit/s	—	not integrated	ISO 18000-6C	[60]	2007
—	-96 – -83 (PER 1 %)	40 kbit/s	4 – 11	0.18 μm SiGe BiCMOS	ISO 18000-6C	[57]	2007
—	-80 – -70 (BER 0.001 %)	40 kbit/s	-10 – 8	0.18 μm CMOS	ISO 18000-6	[58]	2008
-155 – 140	-100 – -85 (SNR 1)	200 kHz	15	not integrated		[VI]	2008

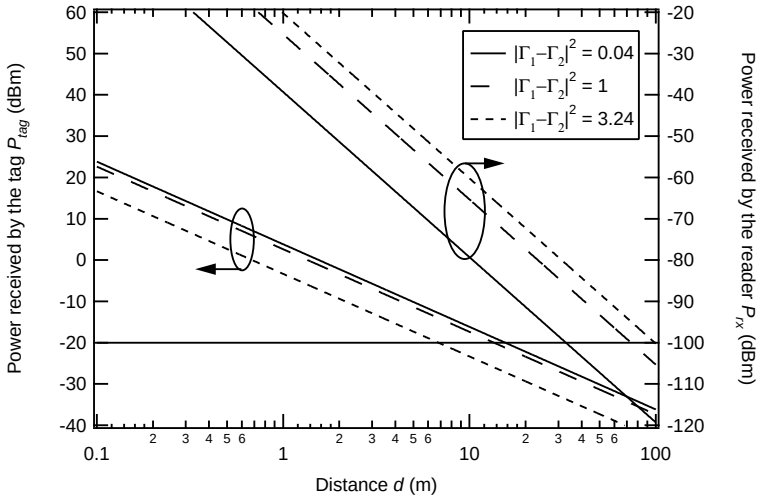

Figure 2.4. The limiting factors on the UHF RFID range at 867 MHz with $G_{tx}P_{tx}$ = 2 W_{erp}, G_{rx} = 8 dBi, G_A = 0 dBi [II].

The link budget of the RFID system is summarised in Fig. 2.4 (see Errata). Both the transferred and received powers are presented as a function of the operational distance at 867 MHz with several modulation index values. Ideal modulation is assumed, i.e. $\Gamma_1 = -\Gamma_2$. The power scales have been set in such a way that the horizontal line represents both P^0_{tag} and P^0_{rx}.

Naturally, the more power is scattered, the less power is transferred to the transponder. The choice of the modulation index depends greatly on the system variables. If the range is limited by the power transfer, the modulation should be as shallow as possible ($m \approx 0$), and vice versa: If the scattered power is the limiting factor, the modulation should be as deep as possible ($m \approx 1$).

According to Fig. 2.4, the read range of a typical passive RFID system at UHF is power transfer limited to a range of 10 m. However at $d = 10$ m, the power received by the reader is only 20 dB higher than the sensitivity of the reader. This margin can be easily lost, if the transmitter noise couples to the receiver. Hence reader architecture is also important, especially because the transponders are becoming ever more sensitive with the introduction of semi-passive transponders.

The chips usually use a low modulation factor, such as the measured value m = -16 – -6 dB [41]. It can also be seen that modulation indexes smaller than $m = -6$ dB do not significantly affect the range. Because small modulation indexes are typically used in UHF RFID, the unmodulated

effective aperture can be used in Eq. (2.18), which gives the form

$$r_{max} = \frac{\lambda}{4\pi}\sqrt{\frac{G_{tag}G_{tx}P_{tx}}{P^0_{tag}}\tau}, \tag{2.20}$$

where τ is the mismatch term

$$\tau = \frac{4R_AR_L}{(R_A+R_L)^2+(X_A+X_L)^2}. \tag{2.21}$$

The mismatch term can have values $0 \leq \tau \leq 1$. Equation (2.20) is often referred to as the read range equation for UHF RFID.

2.7 Millimetre Wave Identification

What if the carrier frequency RFID was at the millimetre waves? The idea of RFID at millimetre waves was first proposed in [61] and analysed in more detail in [II]. Before that, the highest frequency used for RFID was 24 GHz by Biebl [62].

The main differences between the RFID and MMID systems is the wavelength, which scales the effective aperture and the radar cross section. MMID also enables communication at higher data rate, because a wide bandwidth is available e.g. at 60 GHz.

At millimetre waves small antennas can give very high gain. However, this cannot be used to increase the gain of the transponder, as this makes the transponder only accessible from the main beam direction — a direction that is not known in many applications. Thus the transponders use a low-gain antenna.

The read range of MMID at 60 GHz is graphically analysed in Fig. 2.5 (see Errata), which suggests that passive operation is limited to the centimetre range by power transfer to the transponder. On the other hand, the signal-to-noise ratio at the receiver is very high at the low distances, allowing the widening of the data (and noise) bandwidth. Even gigabit data transfer would be possible to a distance of a few cm, which could be used in wireless passive mass memories. Of course, low directivity antenna is required also for the reader to satisfy the far-field criterion for the Friis equation.

In [II] also semi-passive MMID is discussed. Its range is limited by the reader sensitivity, which would allow a range of a few meters, as seen from

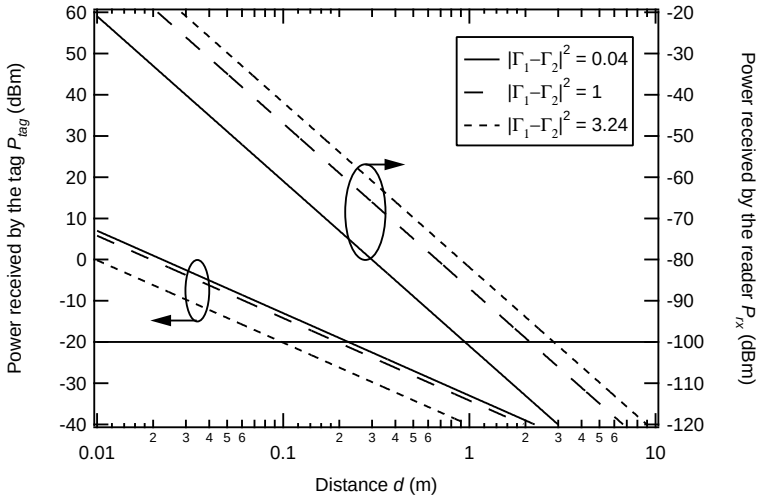

Figure 2.5. The limiting factors on the MMID range at 60 GHz with $G_{tx}P_{tx}$ = 2 W_{erp}, G_{rx} = 20 dBi, G_A = 0 dBi [II].

Fig. 2.5. This enables an application similar to today's RFID, where an ID code is transferred over a few meters. The narrow-beamed antenna of the MMID reader could deliver pinpoint accuracy in the localisation of the transponders, which is not possible with UHF RFID.

An active MMID could deliver a range of a hundred metres. This could be used in road environment, where automotive radars could be used as readers [II]. The radars already have all hardware required.

Figure 2.5 presents only one possible configuration for the MMID system. The range can be extended by more sensitive transponders, higher gain antennas, etc. The backscattering modulation is verified in [II] at 60 GHz and in [63] at 77 GHz. The spectrum of a modulated backscattered signal is shown in Fig. 2.6. Even though the bandwidth of the measurement is small, the measurement proves that MMID can be implemented with a better transponder modulator and a more sensitive reader device.

2.8 Limitations of the Free-Space Model

The range equation (Eq. (2.20)) was derived for ideal free-space conditions. A multitude of unidealities effect the performance of the RFID system in real-life situations, which will now be shortly commented.

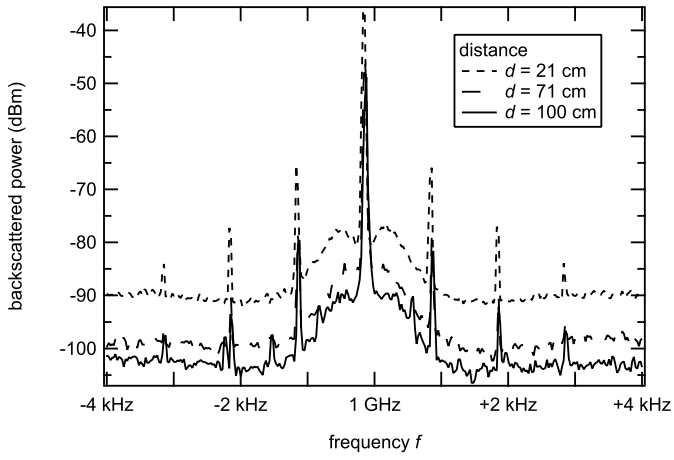

Figure 2.6. Measured backscattered spectra. Resolution bandwidth is 100 Hz and the data has been averaged over 100 samples [II].

First of all, Eqs. (2.18) and (2.19) are valid in the far field, usually defined by the criterion $d > 2D^2/\lambda$, where D is the greatest dimension of the antennas [43]. At UHF the reader antenna is usually a $\lambda/2$ -patch. Hence the far field criterion can be written as $d > \lambda/2 \approx 18$ cm.

Transmitter Noise

The transmitted signal couples to the receiver through the near-field of the reader antenna and through environmental reflections. The attenuation in the coupling can be as low as -20 dB – -30 dB. The transmitted signal carries amplitude and phase noise originating in the oscillator and the power amplifier, which can then dominate over the noise generated at the receiver. The high sensitivity of the reader, which was used in the range analysis, requires high isolation between the transmitter and the receiver. This will be further discussed in Chapter 4.

Mismatch

The read range analysis assumed ideal backscattering modulation, where $\Gamma_1 = -\Gamma_2$. This implies best possible power matching between the antenna and the load. Good matching is even more important than usual: Increasing the mismatch deteriorates the backscattering modulation faster than it diminishes the power transfer. Measurements of the effect are presented in Fig. 2.7.

A typical source of mismatch is a change in the environment within the near-field of the transponder antenna. In general, a change in the

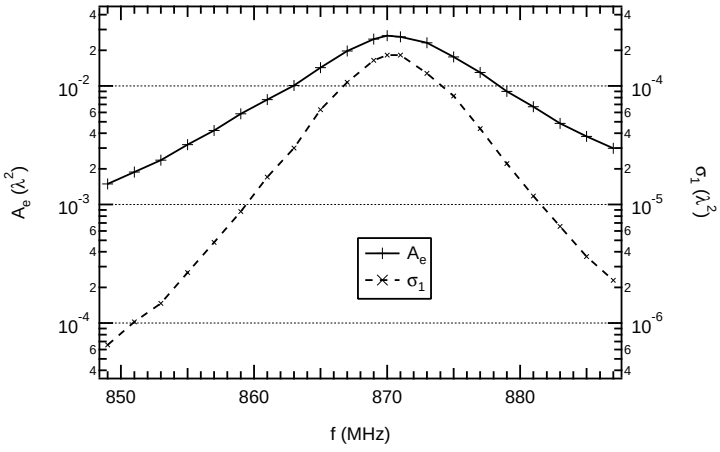

Figure 2.7. The measured aperture A_e and radar cross section σ_1 of a transponder in free space [IV].

antenna surroundings effects the antenna input port impedance. The effect is discussed in Chapter 3.

Fading

When the environment is full of reflectors and scatterers, signals arrive at the same point via different paths. This multipath propagation leads to interference. The destructive interference creates areas of diminished RF field. In simple geometries, the areas of diminished field can be calculated, but in practice this is impossible. Hence measurements and statistical fading analysis must be used. The fading effect is considered in more detail in [41] and measurements on fading in backscattering communication at 2.45 GHz can be found in [64].

Polarisation

The power transfer and the received scattered power are affected by the transponder and reader antenna polarisations. At UHF, usually linearly polarised transponder antennas and circularly polarised reader antennas are used. This ensures operation regardless of polarisation, but introduces a polarisation loss of $p = -3$ dB. The polarisation loss is a function of the polarisations and inclinations of the reader and transponder antenna [41].

The polarisation loss can be taken into account in the range analysis by replacing the transponder antenna gain G_A by the term pG_A. Hence the loss will affect power transfer in the first and the radar cross section in the second order. In the range equation the polarisation mismatch term is found under the square root.

2.9 Summary

In this chapter, the fundamental equations for the powering of the transponder and the communication by backscattering modulation have been discussed. The equations have been applied to passive UHF RFID, whose range was shown to be limited by the power transfer, if the reader sensitivity is not deteriorated by the transmitter noise. The analysis was also applied to millimetre wave RFID, or MMID. Experimental verification of the theory at 60 GHz was also presented.

A review of the integrated circuits of the UHF transponders, as well as reader circuits was presented. As far as the author is aware of, the sensor IC presented in the Thesis is the only published IC with an ADC for external sensors. The chip provides a 10 bit ADC with a power consumption of 30 μW_{DC}, which is in the same order of magnitude than other sensor ICs with a 10 bit ADC.

3 Transponder Antennas

This chapter takes a closer look at the transponder antennas. First the antenna scattering is further discussed. The more thorough treatment of the antenna scattering reveals possibilities for characterising the transponder antennas by their scattering. Two measurement techniques are presented. Finally, transponder antenna requirements are discussed, and a transponder antenna design is introduced and compared with other published transponder antennas.

3.1 Backscattering from Antennas

King [21] and Harrington [22] developed a general antenna scattering theory from a general linear three-port model. The three ports describe the input ports of a transmitting (subscript tx), receiving (subscript rx) and scattering (subscript a) antennas. By writing a three-port impedance matrix for the system and assuming that the scattering antenna port's current and voltage satisfy Ohm's law with the load impedance Z_L, an equation for the received signal can be written as

$$V_{rx} = \left(Z_{rx-tx} - \frac{Z_{tx-a} Z_{rx-a}}{Z_D + Z_L} \right) I_{tx}, \tag{3.1}$$

where Z_D is the input impedance of the scattering antenna. According to the Eq. (3.1), the scattering can be considered to consist of two parts: the structural mode scattering (the first term), and the antenna mode , or re-radiated, scattering (latter term). The structural mode scattering does not depend on the antenna load, and the antenna mode scattering is load-dependent.

The definitions of the structural and antenna mode scattering are ambiguous. In practice they cannot be distinguished from each other by measurements. Equation (3.1) would suggest that the structural mode scatter-

ing can be measured by attaching an open load to the scattering antenna port. However, several other definitions are used in the literature. Sometimes the structural mode scattering refers to short-circuit scattering, at other times to scattering with a matched load [65]. In this thesis, the structural scattering refers to the scattering with an open load, as suggested by Eq. (3.1). This definition is also used in [V].

Equation (3.1) is derived for a general antenna, only assuming a linear three-port model with a linear load, and it holds for all kinds of antennas. In the previous chapter, the equivalent model of Fig. 2.2 leads to a similar equation for the current in the circuit, namely the Eq. (2.5).

However, compared to Eq. (3.1), Eq. (2.5) describes a special case, where the structural scattering term $Z_{rx-tx} = 0$. The equivalent model in Fig. 2.2 describes a minimum scattering antenna, which is defined as an antenna that scatters as much power as is transferred to the load, when connected to a matched load [65]. From this definition it follows, that with an open load, the antenna does not scatter any power. Yet the definition requires that the antenna scatters with the same pattern as it radiates.

The definition of a minimum scattering antenna seems very restricting, but it turns out to be very useful. For example, electric dipoles are minimum scattering antennas. Other common RFID transponder antennas, such as the patch and planar inverted-F antenna (PIFA), are not minimum scattering antennas, especially as they may scatter in different modal distributions, i.e. with different pattern than they radiate [65, 66]. However, the analysis presented in the previous chapter can be used to describe the modulated backscattering from all types of antennas. In [67], the antenna mode scattering, which is affected by the load, is derived independently of the model of Fig. 2.2. The result is similar to Eq. (2.5). Further the modulated radar cross section σ_m in Eq. (2.15) does not contain the structural mode scattering term, but is only a function of the difference of the antenna mode scattering with different loads [68]. Hence, σ_m of Eq. (2.15) is valid for all antennas, but σ_0 of Eq. (2.12) holds only for minimum scattering antennas.

3.2 Measurement of Transponder Antennas

A design goal of a transponder antenna is the maximisation of the mismatch term τ in the read range equation (2.20). In principle, the mismatch can be measured by connecting a feed line to the antenna feed port and

measuring the reflection with a network analyser. However, the transponder antennas are very small, and the feed line cannot be efficiently isolated from the antenna radiation and near fields. Hence, the feed line inevitably affects the antenna radiation pattern, and input impedance. The coupling effects are complicated, and the antenna impedance cannot be simply deembedded from the measured results. Some antenna structures, such as a dipole antenna, allow a symmetric feed line to be attached perpendicular to the electric fields, which the antenna generates. In these cases, accurate measurements can be carried out, but with a more complex antenna structure this is not possible.

The integrated circuits (ICs) of the transponders have a capacitive input impedance (see Table 2.1). The matching elements required for direct matching to the capacitive IC are incorporated into the antenna, making the input impedance of the antenna highly inductive, which leads to a high reflection from a 50-ohm feed line. In addition to this, it is not always clear, whether the antenna should be fed with a single-ended (referred to ground) or a symmetric signal, as in the case of the PIFA presented in [III]. These unique properties of the transponder antennas tend to increase the feed line radiation, and hence diminish the accuracy of feed line measurements.

In [IV] the antenna radiation pattern is measured with the backscattering and feed line methods, and the result is compared with simulations. It is clearly seen, that the radiation pattern of a small antenna is badly distorted in the feed line measurement — even though a matching circuit and an optical feed are used.

The backscattering from transponder antennas is discussed and measured in [69], but the scattering has not been used to characterise the antenna power transfer or input impedance. The feed line problem has been solved in [70] by contactless near-field measurement of the radiation pattern. Also commercial devices for wireless measurements of RFID transponders are available. The devices can measure both the power transfer and the received backscattered power, see e.g. [71].

In this Thesis two scattering-based techniques for measuring the mismatch term are presented. In [IV] and [72] a method for measuring the effective aperture expressed in Eq. (2.7), effectively measuring the power transferred to the load of the antenna. The technique presented in [V] relies on Eq. (3.1) to measure the input impedance of the transponder antenna, from which the mismatch term τ can be calculated.

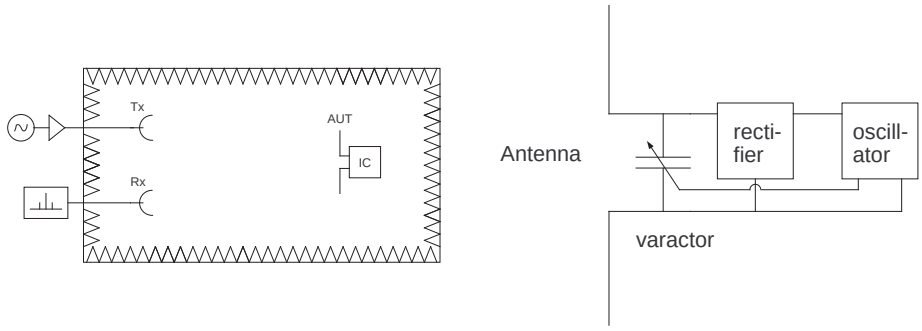

Figure 3.1. Aperture measurement. The measurement setup (left) and the block diagram of the antenna – chip system (right) [IV].

3.3 Power Transfer

In [IV], the antenna under test (AUT) is connected to an IC chip that has a low-frequency oscillator inside it, as shown in Fig. 3.1. The power for the operation of the oscillator is generated from the incident RF power. The oscillator drives a modulator at the input of the chip, causing backscattering modulation, which is seen as sidebands in the scattered signal.

The chip is designed so that the RF power $P_{rf,0}$ necessary for its operation is known. The Friis equation can now be written in the form [IV]

$$A_e = \frac{P_{rf,0}}{S_{ref}} \frac{P_{tx,ref}}{P_{tx,0}}. \tag{3.2}$$

First, the reference power intensity $S_{ref} = S(P_{tx,ref})$ is measured with a transmission power of $P_{tx,ref}$ by placing a reference antenna at the location of the AUT. Then the reference antenna is replaced by the AUT, and transmission power is slowly ramped up at the transmitter. When the power transferred to the IC reaches $P_{rf,0}$, the load modulation begins, and sidebands appear at the receiver. The lowest transmit power that wakes the sidebands is the critical transmit power $P_{tx,0}$.

Equation (3.2) provides a procedure to measure the antenna aperture, and hence the mismatch term τ. The measurement is simple and robust, because the scattered power levels are not needed to calculate the result. Equation (3.2) can be used to measure antenna radiation patterns and bandwidth.

In [IV], the measurements of a PIFA-type antenna [III] are carried out in

free space and on two different sizes of metal platforms to study the effect of the mounting platform. The radiation patterns are presented in Fig. 3.2 and compared with simulations (Fig. 3.3) and feed line measurements (Fig. 3.4). The feed line is connected to the PIFA through the metal platform, so that the platform shields the antenna from feed line coupling. The results of the aperture measurement (Fig. 3.2) comply with the simulations (Fig. 3.3) with all the sizes of the metal platform, but the smaller the platform, the worse the results of the feed line measurement (Fig. 3.4).

The bandwidth measurement gives direct information on the mismatch term τ. The measured effective aperture of the PIFA is presented in Fig. 3.5 as a function of frequency. The reactive part of both the IC and the antenna change fast as a function of the frequency, whereas the real parts are almost constant. Hence, the measurement result shown in Fig. 3.5 can be considered to present the reactive mismatch in the term τ. The measurement helps to identify the frequency, at which the reactive mismatch is at its minimum, but cannot be used to measure the resistive mismatch, as the measured effective aperture consists of the product of the antenna gain and the mismatch term. Hence, the absolute value of the aperture at its maximum is also the product of these two terms, and the magnitudes of those cannot be extracted from this measurement only.

Figure 3.5 shows the measured aperture at three different mounting platforms. As an example, the aperture is 3 dB greater on a big metal plate than in free space. It would be tempting to state that this is due to the change from an omnidirectional (free space) to a hemispherical (metal) radiation pattern, but the effect could also be due to a change in antenna input impedance. Without further measurements, the effects cannot be distinguished.

Despite its limitations, the aperture measurement gives direct information on the antenna behaviour with the correct loading, and in an actual application environment. The method is robust, and the measurements can be carried out in a normal laboratory environment, or in an RFID application environment. The measurement method has been found useful, not only by the author, but also by other RFID antenna developers, who have used the method developing several antenna structures, e.g. [73, 74, 75].

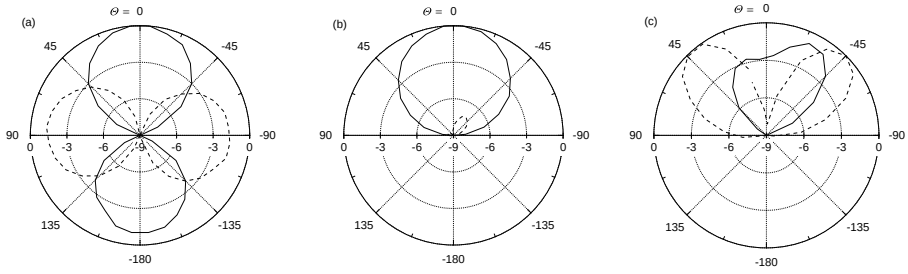

Figure 3.2. The radiation patterns of the PIFA measured with the aperture method: (a) in free space, (b) on (150 mm)^2 metal and (c) on (600 mm)^2 metal. The solid line (—) denotes the co-polarisation and the dashed line (- -) the cross-polarisation [IV].

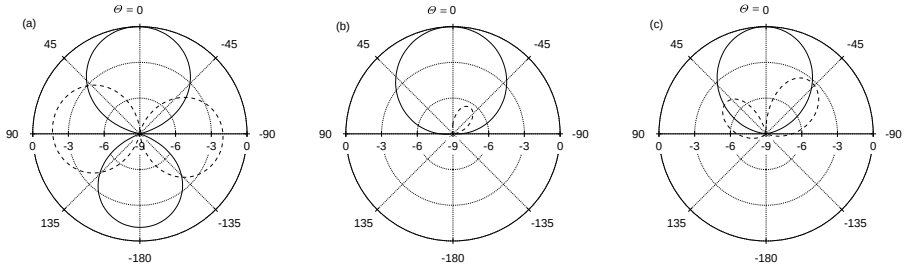

Figure 3.3. The radiation patterns of the PIFA simulated with HFSS: (a) in free space, (b) on (150 mm)^2 metal and (c) on infinite metal. The solid line (—) denotes the co-polarisation and the dashed line (- -) the cross-polarisation [IV].

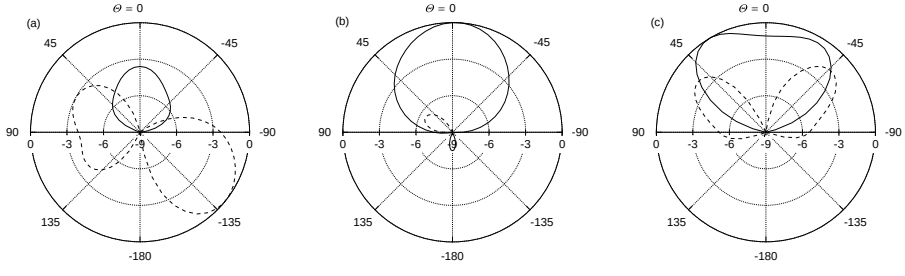

Figure 3.4. The radiation patterns of the PIFA measured with the feed line method: (a) in free space, (b) on (150 mm)^2 metal and (c) on (600 mm)^2 metal. The solid line (—) denotes the co-polarisation and dashed line (- -) the cross-polarisation [IV].

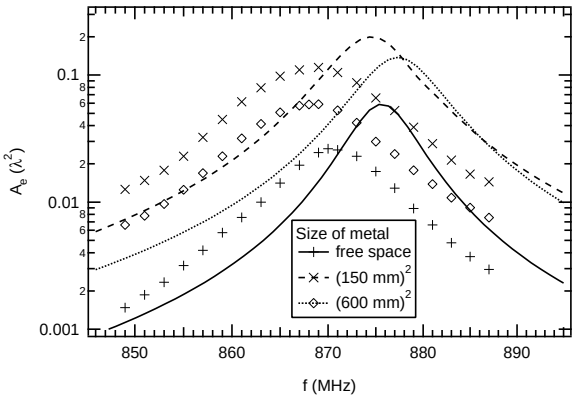

Figure 3.5. The measured (markers) and calculated (lines) apertures of the PIFA on different platforms as a function of frequency [IV].

3.4 Input Impedance

To obtain information on both the resistive and reactive mismatch, Eq. (3.1) can be used to measure the input impedance Z_D of the antenna. This approach is a more conventional one. While the author has not seen the aperture of the antenna measured earlier as presented in [IV], a multitude of other antenna measurement methods based on the backscattered field have been reported.

Already in 1963, Harrington proposed the use of active loads to measure field strengths by backscattering [23]. In 1979, Appel-Hansen [24] presented a method for antenna gain measurement. He used short-circuited transmission lines of different lengths as the load of the AUT. Mayhan et al. [25] presented a method for measuring the antenna input impedance in 1994. Wiesbeck and Heidrich [26] went a step further in 1998 by measuring the whole scattering matrix of an antenna with two radiation (both polarisations) and several load ports.

The technique presented in [V] is an extension of the method developed by Mayhan et al. in [25], who considered only real antenna load impedances. But because the transponder antenna input impedance is highly inductive, it is necessary to use capacitive loads. In [V], the theory is expanded for reactive loads, and measurements of two transponder antennas are presented.

Equation (3.1) has four unknown parameters, but it describes bistatic scattering, i.e. separate transmission and receiving antennas are used. In monostatic case, the terms Z_{tx-a} and Z_{rx-a} are equal. Hence, measurement

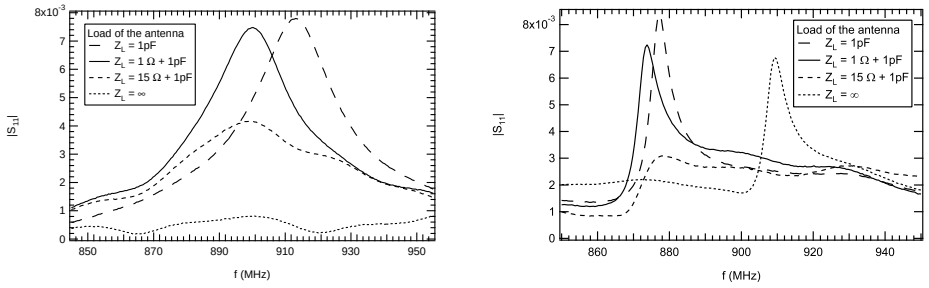

Figure 3.6. The measured scattering parameters S_{11} with different loads of the Palomar antenna (left) and the PIFA (right) [V].

of the scattering with three known loads gives a group of three equations with three unknowns. The solution for the input impedance is [V]

$$Z_D = \frac{Z_m - AZ_c}{A - 1}, \tag{3.3}$$

where A contains the measured scattered fields

$$A = \frac{S_c - S_o}{S_m - S_o}. \tag{3.4}$$

The used loads Z (and the respective measured scattered fields S) are: open load $Z_o = \infty$ (S_o), capacitive match $Z_c \approx -jX_A$ (S_c) and conjugate match $Z_m \approx R_A - jX_A$. The result reduces to the one given in [25], if capacitive match is taken to be a short circuit ($Z_c = 0$) and Z_m is purely resistive.

Equation (3.3) has three noteworthy aspects. First, the equation does not include any coupling constants from the measurement apparatus to the antenna, and only linear coupling is assumed. Therefore the measurements can be carried out in free space as in [25], or in a gigahertz transverse electromagnetic mode (GTEM) cell [76], [V]. Further, the scattered fields only appear as a ratio of two differences in the equation. Hence, a simple background reduction from every scattered field does not affect the results, if the background remains constant over the measurement. Finally, the equation does not take into account polarisation coupling in the AUT. Most antennas have two orthogonal radiation ports, i.e. two polarisations are radiated. Accurate results are only to be expected in the case of antennas, where one of the polarisations is highly dominant, such as electric dipole.

The two antennas measured in [V] are the Palomar antenna [32], an electrical dipole in a spiral, and a PIFA similar to the one described in [III]. The scattered fields of the antennas with several loads are presented in Fig. 3.6.

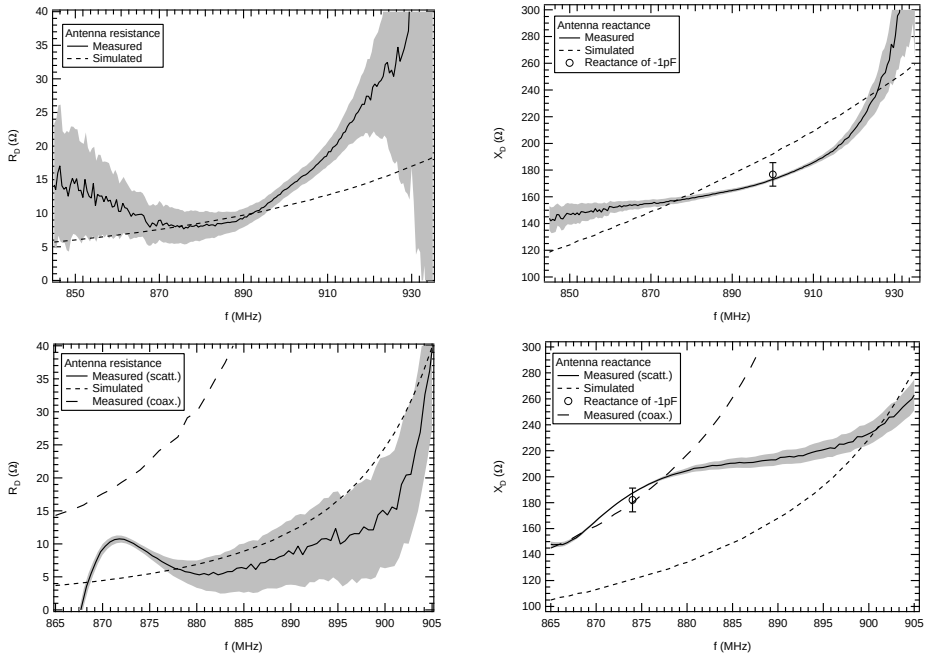

Figure 3.7. The measured and simulated input impedances $Z_D = R_D + jX_D$ of the Palomar antenna (above) and the PIFA (below). The grey area represents the uncertainty in the measured value [V].

The model in Fig. 2.2 suggests that a short-circuited antenna would scatter a fourfold power compared with the matched antenna. Fig. 3.6 shows that an approximately twofold scattered field is detected from the short-circuited antenna compared with the matched case. This, again, justifies the model used in Chapter 2.

Figure 3.7 presents the input impedance results for the two antennas. The grey area in the figure represents the random uncertainty derived in [V]. The error arises from residual background scattering and displacement error, and is a strong function of the reference loads. The optimal choice of the reference loads is considered in the error analysis in [V]. The error is found to be the smallest when reactive matching is the best, which is also seen in Fig. 3.7. Hence, all the loads have capacitive matching. The resistive loads are to be chosen far apart, i.e. an open, a matched and a shorted load.

The results are in a good agreement with the simulations and the feed line measurements in the case of the dipole. The results of the PIFA are reasonable in the immediate neighbourhood of the resonance peak, but clearly unphysical farther away from the peak. The PIFA radiates a significant

amount of power to the other polarisation, which is not measured, and not considered in the simple model, which the analysis is based on. Hence, a systematic error is to be expected.

The measurement technique is reliable when measuring electrical dipoles and other antennas that have a single dominant polarisation. The electrical dipoles present a major proportion of the RFID transponder antennas. However, when the antennas radiate a significant amount of power to both polarisations, the results are only indicative. In such a cases, both polarisations should be measured and the analysis developed further.

3.5 Transponder Antenna Requirements

All transponder antennas in RFID applications need to satisfy three main requirements: 1) The antenna must have a simple structure that is mass-producible with low cost; 2) the tag must be small in size; and 3) it must (in its own part) provide long read range. The design process and considerations for transponder antennas are well summarised in [77].

In general, there are two types of antennas are on the market. First, labels that usually employ an electric dipole. The dipole is easy to manufacture with a roll-to-roll process using only one metallisation layer on a thin plastic foil. The antenna and matching elements are patterned to the same metallisation layer for direct match to the capacitive RFID IC. This makes it possible to manufacture very low cost transponders, even less than 10 Euro cents. Second, there are antennas that have at least two metal layers. Typical designs are a patch, a planar inverted-F antenna (PIFA), and an electric dipole on a metal plane. The antennas can be attached to metal and other surfaces, and they often have a robust casing. Both the more complex antenna structure and the sturdier casing make the antennas more expensive, typically a few Euros. These antennas are often called platform tolerant, universal, or metal-mount transponders.

Independent of the antenna structure, the low form factor required implies low directivity of the transponder antenna. This seems to lower the read range according to Eq. (2.20), but actually helps to increase the read reliability in many applications. Usually the transponder location and orientation cannot be accurately known. Hence a high-gain, narrow-beam transponder would be hard to access, because the main beam direction is not known. Hence, low-gain transponders are suggested also for MMID applications [II].

The third requirement basically implies low loss and good matching to the IC. The second and third requirements are closely related, because the antenna size limits the gain and the bandwidth of the antenna: The smaller the antenna, the narrower the band and lower the gain [78, 79].

3.6 Platform Tolerance

One-layer electric dipoles are very sensitive to their immediate surroundings, i.e. the dielectrics and conductors in their near field. The dielectrics and metals detune the antenna. When the resonance shifts from the desired frequency, the input impedance of the antenna changes. The detuning affects both real and imaginary parts of the input impedance. Hence, the mismatch term τ in the range equation (Eq. (2.20)) decreases, diminishing the read range. The effect can be very strong, making it practically impossible to read the transponder at all. The detuning has been studied and measured e.g. in [80, 81].

The antennas with two metal layers are less sensitive to the electric properties of the materials near the antenna, especially to the material of the mounting platform. The antennas are not detuned, and their input impedance is not influenced by the mounting platform. This is called platform tolerance.

The effect of the mounting platform on the transponder antenna has been found to be crucial to the success of UHF RFID since at least 1999, when Foster [82] concluded that narrow-beamed antennas are preferable in order to achieve better isolation from the mounting platform. However, also the near field of the antenna couples to the mounting platform. The whole current distribution of the antenna must be taken into account when studying the effect of the mounting platform [83, 84].

The mounting platform of the antenna also affects the radiation pattern, especially on metal platforms. However, the detuning usually has the stronger effect on the read range. The change in the radiation pattern has been measured in [85] for electrical dipoles and in [IV] for a platform tolerant PIFA.

The PIFA presented in [III] is one of the first published platform-tolerant antennas. Due to the interest on the research field, it has also been very widely referenced to. Later structures that offer better platform tolerance are published, but the read range achieved from the metal surface was unprecedented in 2004. The structure of the PIFA is presented in Fig. 3.8. It contains only two metal layers and two contacts between them.

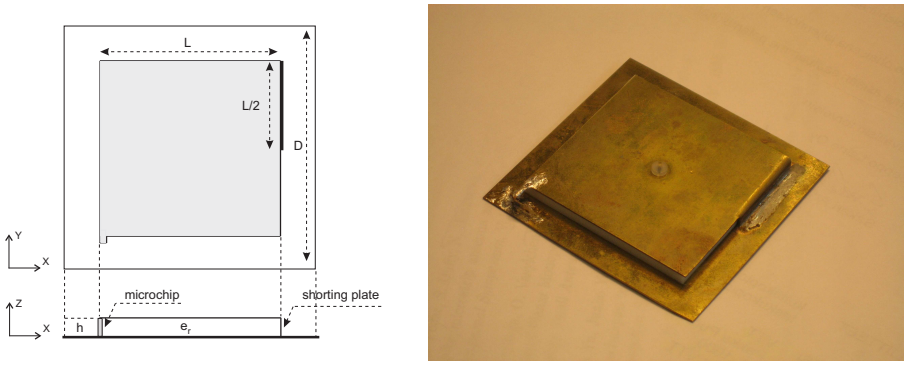

Figure 3.8. The structure (left) and photograph (right) of the PIFA: D = 59 mm, L = 45 mm, h = 3 mm, and ε_r = 2.1 (Teflon) [III].

3.7 Overview of Platform-Tolerant Antennas

Numerous transponder antenna structures have been published. In this section, a review of published platform-tolerant transponder antennas is presented. The review includes antennas published in peer-reviewed journals, some of which are commercialised. A transponder that is commercialised, but not published, is included in order to give an example of a dipole-on-metal transponder [86]. The overview is summarised in Table 3.1.

Platform-tolerant antennas have three basic structures: a dipole on a ground plane, a patch, and a PIFA. The comparison of the antennas is complicated, because different transponder ICs and radio regulations are used in the publications. Comparing only antenna gains is not relevant either, because impedance matching is the key issue. The difference of the read ranges on different platforms describes the platform tolerance, and wider band (Δf) antennas lend themselves better to mass production. The absolute read ranges in particular cannot be directly compared between the transponders, because the transmission power and other components of the system, e.g. the reader and the transponder sensitivity, strongly affect the result.

Low-profile antennas tend to be narrow-banded. The bandwidth can be increased using a dual resonance [87, 88]. The same technique has been used in [89] to achieve a dual-band operation. The commercialised transponders [86, 88] have a higher bandwidth than the other transponders.

The use of metamaterials, like electronic band gap structures (EBGs) and artificial magnetic conductors (AMCs) have been widely studied [90,

Table 3.1. Review of metal-mount transponders.

Read Range (m) metal	free space	TX Power	Δf (MHz)	f_0 (MHz)	Z_L (Ω)	IC	Structure	Size (mm^3)	Ref	Year
4 – 5	2	0.5 W_{erp}	15	869	7-j170	Tagidu	PIFA	59 × 59 × 3	[III]	2004
1.0	0.5	—	—	915	1200	—	IFA	200 × 160 × 10	[93]	2004
1.9	1.5	—	—	915	1200	—	Patch, EBG	100 × 100 × 6.4	[90]	2004
—	—	—	57	915	6-j125	—	Patch	74 × 24 × 3	[87]	2006
10	7	2 W_{erp}	13	867, 915	10-j160	Tagidu	PIFA	62 × 51 × 3	[89]	2006
4.8 – 5.2	6	—	27	915	15-j140	Alien AL-9238	Patch	86 × 50 × 5	[73]	2006
4.5 – 4.9	5	—	26	915	6.2-j127	Alien ALN-9338-R	shorted Patch	50 × 47 × 3	[74]	2007
—	—	—	10	900	12-j300	Philips	dipole, AMC	100 × 100 × 5	[91]	2007
3.5 – 4.2	2.7	—	26	915	14.3-j62	TI	Patch	80 × 40 × 1.6	[75]	2008
4	2.5	4 W_{eirp}	100	915	40-j120	Impinj EPC Gen2	Patch	79 × 31 × 10	[88]	2008
8.5	7	4 W_{eirp}	100	915	40-j120	Impinj EPC Gen2	Patch	155 × 32 × 10	[88]	2008
6.0	4.2	2 W_{eirp}	12	910	6-j125	Alien EPC Gen2	dipole, AMC	121 × 34 × 3.5	[92]	2008
5 – 7		—	100	910	—	Impinj/NXP EPC Gen2	dipole on metal	224 × 24 × 8	[86]	—

91, 92]. The structures include at least three metal layers. Table 3.1 does not indicate any significant performance improvement due to the use of metamaterials. The reason is that the transponders must be small, but the EBG and AMC ground planes require a size of several wavelengths to work properly [91].

3.8 Summary

In this chapter, the development and measurement of transponder antennas was discussed. Two backscattering-based measurement techniques were presented, and the antenna scattering studied with the techniques. The backscattering-based measurements give better results than feed line measurements, because near-field of the small antenna couples to the feed line.

A platform-tolerant PIFA antenna for the transponder was presented, and compared with other antennas found in the literature. The PIFA was one of the first published platform-tolerant antennas. When published, it provided an unprecedented read range on metal.

4 RFID Reader

Most radio devices used daily in modern society are transceivers, i.e. they include both a transmitter and a receiver, but usually the receiver and transmitter signals are isolated by multiplexing. Possible physical multiplexing schemes are frequency (FDM) or time division multiplexing (TDM), and several digital multiplexing schemes also exist, like the code division multiplexing (CDM). For example in GSM, both FDM and TDM are used. The transmitter and receiver have separate frequency ranges with about a hundred channels (FDM), and each frequency channel is divided into random time slots to allow multiple user within a single channel (TDM). The physical multiplexing schemes efficiently isolate the transmitter and receiver signals, allowing the receiver and transmitter modules to be independently designed and implemented.

Physical multiplexing cannot be used to isolate the receiver and transmitter signals in passive RFID. Even though the data transfer in RFID is time-division multiplexed, i.e. the reader and the transponder do not send data at the same time, the reader has to be sending a continuous wave (CW) signal, when the transponder is sending, since the transponder uses the CW signal from the reader to power itself, and as a carrier for the backscattering modulation.

The fact that the receiver is used simultaneously at the same frequency as the transmitter has its drawbacks, but also benefits [VI, VII]. The obvious drawback is the requirement for high dynamic range in the receiver [46]. The received signal is as low as -70 dBm, but the transmitter signal up to +36 dBm_{eirp} can have as high a coupling as -20 dB to the receiver. The high power of the incident carrier can saturate the receiver. The incident carrier also carries the transmitter noise into the receiver. To minimise these effects, high isolation between the transmitter and the receiver is required.

Most RFID receivers have a direct conversion detector. Because the transmitter and the receiver are co-located, the transmitted (tx) signal is generated from the same local oscillator (lo) that is used for downmixing

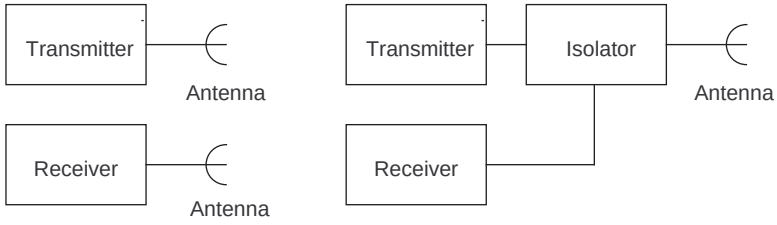

Figure 4.1. Principal architectures of a bistatic (left) and a monostatic (right) reader.

the received (rx) signal. Because the radio path is short compared to the modulation wavelength, $\lambda_m = 2\pi c/\omega_m$, the noises of the rx and lo signals are at least partially correlated, which may actually help to increase the dynamic range. The phenomenon is called range correlation [94].

The RFID reader can be realised mono- or bistatic (Fig. 4.1), i.e. having a single or separate antennas for transmitting and receiving. If monostatic architecture is used, the RF front end needs an isolator between the transmitter and the receiver. Common isolation techniques include a circulator and a directional coupler, or else an adaptive front end can be used. The adaptive RF front end adds an additional compensation signal to the input of the receiver. The feedback from the receiver keeps the amplitude of the compensation signal is equal and the phase opposite to the incident carrier. These isolation techniques are presented in Fig. 4.2 for a monostatic reader.

4.1 Isolator Review

The common isolation techniques in case of the RFID reader have been described in [41, 95]. The circulator can provide up to -30 dB isolation, but the antenna reflection loss is rarely below -20 dB, which limits the isolation to -20 dB, too. A weakly coupled directional coupler can deliver up to -40 dB isolation with ca. -10 dB reception loss [96]. Separate antennas for transmission and reception can give -30 dB isolation, but is inconvenient in practice.

Because these common isolation techniques do not provide a sufficient solution in an RFID reader, the issue has been widely studied in the recent years. The research falls in two categories. On the other hand, the isolation of a directional coupler has been increased [96, 97, 98, 99], and on the other hand adaptive RF front ends have been designed [100], [VI, VII].

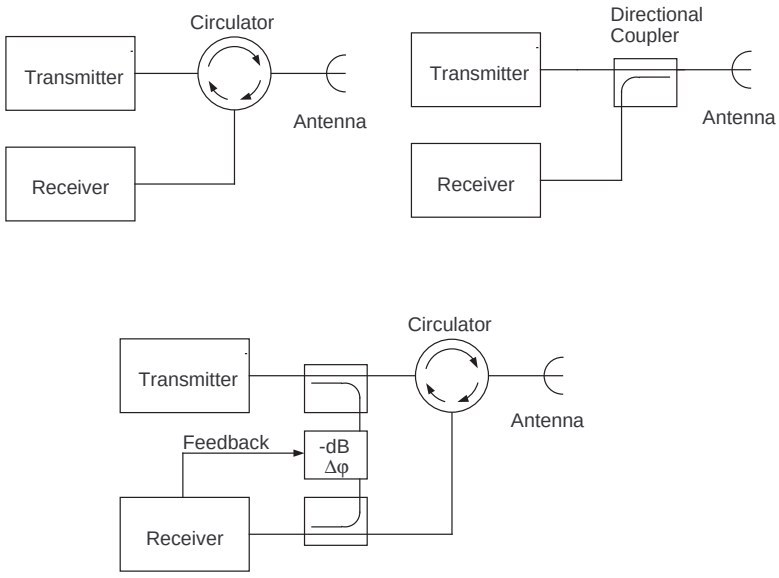

Figure 4.2. Common isolation techniques for the RFID reader front end: a circulator (above left), a directional coupler (above right), and an adaptive front end (below).

Additionally, an antenna including a hybrid to provide the isolation has been suggested in [101]. The review of the published isolator elements is summarised in Table 4.1.

The directional couplers provide -45 – -60 dB isolation with -11 – -15 dB coupling. The high isolation is achieved by choosing the load in the matched port of the coupler according to the antenna impedance [97, 98, 99], but it is not reported, how the impedance is realised or varied. If the matched port impedance is not adaptive, the isolation will diminish, if the antenna impedance is changing. Especially in hand-held devices, the antenna impedance will vary due to the user hand moving in the antenna near-field.

This Thesis introduces two truly adaptive RF front ends. In [VII], an adaptive RF front end for mobile devices is presented. The front end is considered to be a impedance measurement bridge, which is very similar to the idea of using a directional coupler and a tunable load. The coupler achieves a -50 to -60 dB isolation with a -7 dB coupling.

The adaptive RF front end presented in [VI] is similar to the circuit in [100]. The papers were published independently of each other at the same time. The design used in [VI] is based on a patent filed in 2005 [102].

Table 4.1. Review of Isolators.

f_0 (MHz)	L_{tx-rx} (dB)	L_{tx-ant} (dB)	L_{ant-rx} (dB)	F (dB)	P_{1dB} (dBm)	Size (mm)	Adaptive	Ref	Year
860 – 960	-64	—	-15	—	—	58 × 34	No	[97]	2006
860 – 960	-36	8	8	—	—	450 × 200 × 30	No, incl. antenna	[101]	2006
912	-45	—	-11	—	—	1.5 × 1.5	No	[96]	2007
865 – 869	-50	-3	- 7	12	—	40 × 40	Yes	[VII]	2008
920	-65	—	-10.5	—	—	46 × 34	No	[98]	2008
908 – 914	-60	—	-3	—	—	—	Yes	[100]	2008
908 – 914	-60	—	-15	—	—	50 × 12	No	[99]	2008
865 – 869	—	—	—	20	15	100 × 100	Yes	[VI]	2005/2008

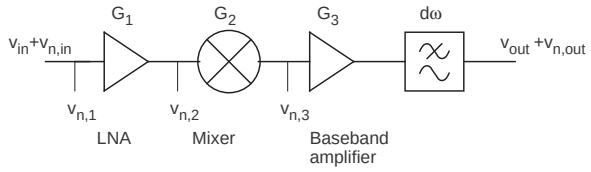

Figure 4.3. Block diagram of a cascade receiver.

Similar structures have later been patented also by others [103]. Both [VI] and [VII] analyse noise due to the tunable impedance and the tuner in greater detail than any of the other publications discussed here.

In this chapter, the dynamic range of an RFID reader is analysed. Three isolation techniques are considered: a circulator, a directional coupler, and an adaptive front end as described in [VI]. The adaptive impedance bridge described in [VII] will then be discussed in the context of a mobile reader, where additional design limitations in power consumption and size exist.

4.2 Dynamic Range

The dynamic range of a receiver describes the highest and the lowest signal that can be inserted into the receiver, so that the data can still be successfully detected. At low-power, the limiting factor is the noise of the receiver. This is described by the receiver sensitivity S. At high-power, the receiver saturation deteriorates the receiver functionality. Saturation is described by input compression point P_{1dB}. The dynamic range is the ratio of the input compression point and the input sensitivity.

Receiver Sensitivity

To compare the receiver noise with the incoming signal, the concept of input-referred noise is used. It is illustrated in Fig. 4.3. The receiver consists of a low-noise amplifier (LNA), a mixer, and a baseband amplifier, which all add their noise to the signal. The noise is white and is modelled as as input referred noise source with spectral density v_n. Every stage also has its gain G (or loss in case of diode ring mixers). The signal at the output is $v_{out} = G_1G_2G_3v_{in}$ and the noise spectral density is $v_{n,out} = G_3(v_{n,3} + G_2[v_{n,2} + G_1\{v_{n,1} + v_{n,in}\}])$. The noise is referred to the input by dividing with the cascade gain, i.e. $v_{n,ref} = v_{n,out}/(G_1G_2G_3)$. The input-

referred noise $v_{n,ref}$ takes into account the noises of the latter stages, and it can be compared directly to the incident signal.

If one calculates the signal-to-noise ratios (SNR) at input and baseband output, one gets

$$\begin{aligned} \frac{SNR_{in}}{SNR_{out}} &= 1 + v_{n,1}/v_{n,in} + \frac{v_{n,2}/v_{n,in}}{G_1} + \frac{v_{n,3}/v_{n,in}}{G_1 G_2} \\ &= F_1 + \frac{F_2 - 1}{G_1} + \frac{F_3 - 1}{G_1 G_2}, \end{aligned} \tag{4.1}$$

which is the well-known equation for the noise figure F of a cascade system [104].

To determine the receiver sensitivity, i.e. the weakest signal to be detected, we have to limit the noise bandwidth df of the receiver. The overall input-referred noise power S is an integral of the noise voltage spectral density divided by the impedance level R of the receiver.

$$S = \frac{1}{R} \int_0^\infty |v_{n,ref}(f)|^2 df. \tag{4.2}$$

This is also called the sensitivity of the receiver. Here the sensitivity is defined for the signal-to-noise ratio being SNR = 1. The sensitivity can also be defined by referring to some value of the bit error ratio (BER), as seen in the reader review in Table 2.2. Usually an SNR>10 dB is required for a reasonably low bit error ratio (BER) [46, 58].

Input Compression

The receiver has a gain that is usually measured with a small incoming signal. However, if the signal power is increased, at some power level, the receiver will saturate, i.e. the gain begins to diminish. The output power of RF devices is limited. When the limit is reached, the device cannot drive more power to the load impedance. The saturation causes not only diminishing gain, but also distortion.

Saturation can be described by several parameters, such as the third-order intercept point $IP3$, which is based on the amount of harmonics generated, or the 1 dB compression point P_{1dB}, which is based on the gain compression. In this context we use the 1 dB input compression point, which is defined as the input power P_{in} that causes the receiver gain to diminish by 1 dB. The definition is clarified by Fig. 4.4. The input compression point is a convenient measure for the saturation, because it is easy

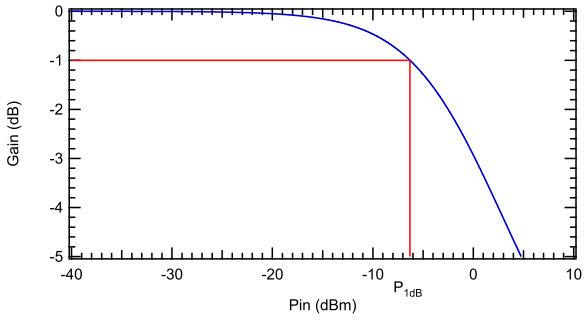

Figure 4.4. Definition of the input compression point P_{1dB}. The gain of the receiver drops by 1 dB at the input power P_{1dB}.

to measure. In the context of RFID, the input compression is caused by the carrier signal at f_0, not the information carrying sidebands, which carry very low power. Thus we have $P_{in} \approx P_{in}(f = f_0)$.

The generation of harmonics also introduces third order mixing products that can diminish the signal significantly. In [46], it is shown that at certain phase and amplitude values of the incoming carrier signal, the third order mixing products can cancel the signal altogether. This would be seen in Fig. 4.4 as a deep notch at the gain slope.

4.3 Reader with Common Isolation Techniques

In [VI] an RFID reader with an adaptive RF front end is presented. The reader design enables comparing a bistatic common reader with a one having an adaptive RF front end, because the adaptive front end can be shut down. This is called the *open loop* case in [VI], because the feedback loop is opened. The *closed loop* case describes the adaptive RF front end. The photograph of the circuitry is presented in Fig. 4.5.

Sensitivity

A block diagram of a bistatic RFID reader is presented in Fig. 4.6. The dynamic range analysis presented here is valid for a circulator and a directional coupler, too. In phasor notation, the local oscillator voltage signal is of the form $V_{LO} = (A + \delta A)\exp(j\omega_0 t + j\delta\varphi)$, where the amplitude and phase noises are denoted by δA and $\delta\varphi$, respectively. The power amplifier has complex gain G_{TX}. In practice the power amplifier adds white noise

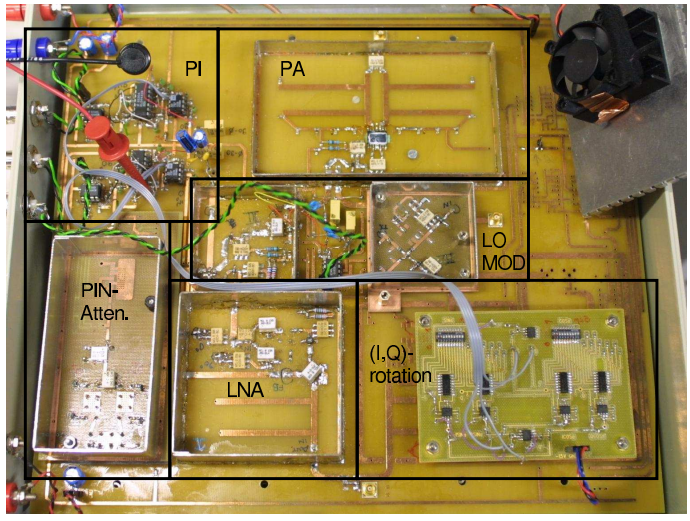

Figure 4.5. Photograph of the RFID reader circuitry presented in [VI].

to the signal, but this can be neglected, because phase noise dominates it by tens of decibels. Now the transmitted signal can be written as

$$V_{TX} = G_{TX}(A + \delta A)\exp(j\omega_0 t + j\delta\varphi). \tag{4.3}$$

The transmitted signal couples to the receiver with a complex coupling $L_{TX/RX}$. The coupling arises from reader architecture and environment. The magnitude of the coupling has been estimated for various architectures in [41]. In bistatic systems coupling of -30 dB is typical, and for monostatic systems a coupling of -20 dB is to be expected. The coupling is actually limited by the antenna return loss.

The transponder modulates the transmitted CW signal with data that we assume to be sinusoidal at frequency ω_{mod} and noiseless, for simplicity. Hence, the signal incident on the receiver is

$$\begin{aligned} V_{RX} &= L_{TX/RX}G_{TX}(A + \delta A)\exp(j\omega_0 t + j\delta\varphi) \\ &+ L_{path}(A + \delta A)\exp(j[\omega_0 + \omega_{mod}]t + j\delta\varphi), \end{aligned} \tag{4.4}$$

where L_{path} is the complex attenuation of the radio path (reader-tag-reader).

The receiver gain is G_{RX} and the noise of the whole cascade receiver is described by its input-referred noise voltage $v_{n,ref}$. The signal is then

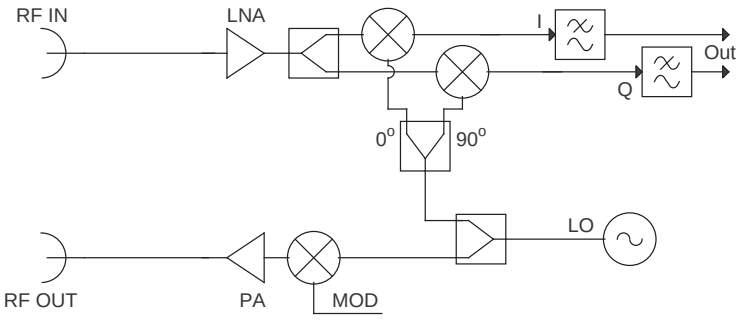

Figure 4.6. Block diagram of a bistatic common reader configuration.

detected by a mixer (conversion loss included in the receiver gain) using the same local oscillator that was used for tx. Because the radio path is short compared with the modulation wavelength, the phase and amplitude noises correlate, eliminating the phase noise [94]. The amplitude noise is amplified by the correlation, but the use of a balanced mixer suppresses it by tens of decibels (term L_A). Hence the baseband signal is of the form

$$\begin{aligned} V_{BB} &= G_{RX} L_{TX/RX} G_{TX} (A^2 + 2 L_A A \delta A) \\ &+ G_{RX} n_{ref} + G_{RX} L_{path} G_{TX} A^2 \exp(j\omega_{mod} t), \end{aligned} \tag{4.5}$$

where the amplitude noise term at the modulation frequency is omitted, because we have $L_A L_{path} \ll 1$.

The first term in Eq. (4.5) describes a DC voltage that is proportional to the incident carrier power. As the coupling coefficient $L_{TX/RX}$ also has a definite phase, mixing the signal down in two orthogonal phases, as shown in Fig. 4.6, gives a complete description of the incident carrier amplitude and phase. The second term is an amplitude noise term that is proportional to the incident carrier power. The third term describes the white noise, i.e. the noise figure of the receiver. The fourth term is the signal from the transponder.

The noise can be referred to the input to give an expression for the sensitivity [VI]

$$S = S_{RX} + \alpha_O P_{in}. \tag{4.6}$$

Here, the term S_{RX} describes the white noise of the receiver. The latter term is due to the transmitter noise and is proportional to the incident carrier power.

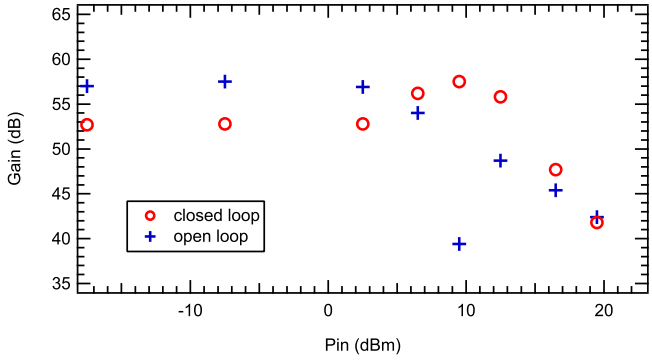

Figure 4.7. Measured gain from RF input single sideband to baseband output at 20 kHz offset from the carrier as a function of the incident carrier power. Signal power is kept constant throughout the measurement and only the carrier power is altered [VI].

Input Compression

In the reader shown in Fig. 4.6, the input compression is limited by the low-noise amplifier (LNA) or the mixer. The compression points of the devices depend greatly on the technology they are fabricated with.

The prototype described in [VI] has a diode ring mixer (Mini-Circuits JMS-2LH) with $P_{1dB} \approx 5$ dBm , and LNA (Mini-Circuits MAV-11SM) with $P_{1dB} \approx 7$ dBm. The input compression is determined by the mixer, and it should be ca. -5 dBm.

The measurement of the open loop case shown in Figs. 4.7 and 4.8 describes the common reader. The input compression point and the reader sensitivity are $P_{1dB} \approx +4$ dBm and $s \approx -160$ dBm/Hz, respectively. There is additional attenuation due to the filters and the coupler circuits before the LNA. Figure 4.8 also clearly shows the effect of the carrier-induced amplitude noise term, which raises the sensitivity above P_{in} = -5 dBm.

In the worst case, the incident carrier power can be up to +10 dBm. Hence, the compression point has to be raised. The simplest way to do this would be to add attenuation before the LNA, or replace the circulator with a directional coupler in the case of a monostatic reader. This deteriorates the sensitivity. The noise of the latter stages has a higher impact, and the sensitivity will rise more than just by the amount of the added attenuation. The compression point, on the other hand, rises only by the amount of the attenuation.

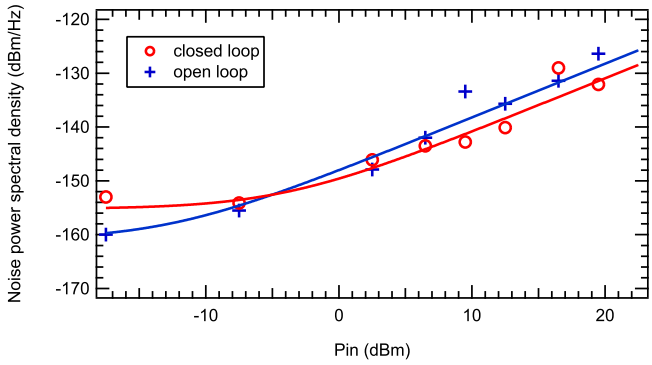

Figure 4.8. Measured input-referred noise at 50 kHz offset from the carrier as a function of the incident carrier power [VI].

The attenuator significantly decreases the signal-to-noise ratio at low incident carrier power, when the receiver white noise is the dominant noise mechanism. However, because the attenuator affects equally to the signal and carrier induced noises, the signal-to-noise ratio is not affected at high incident carrier power, when the carrier-induced noise is dominant. However, the higher white noise is the dominant noise mechanism at higher incident power levels.

4.4 Adaptive RF Front End

Feedback Principle

Another approach to dynamic range improvement is the use of feedback. The DC component of the mixer output signal describes the incident carrier amplitude and phase, and this signal can be used as an input for an adaptive RF isolator circuit. The feedback is described in [VII], and the block diagram of the front end with feedback is presented in Fig. 4.9.

The basic idea of the circuit is to add a compensation signal of equal magnitude and opposite phase to the incident signal. The feedback signal c_F can be calculated by equating it with the open loop feedback signal c_{FO}. The signal incident on the LNA becomes

$$c_F + c_R = c_R \frac{1}{1 - c_D^* c_D G\left(\omega_R - \omega_0\right)}, \tag{4.7}$$

where c_D describes the phase shift in the loop. To eliminate the coupling from the receiver, but to let the signal from the transponder pass

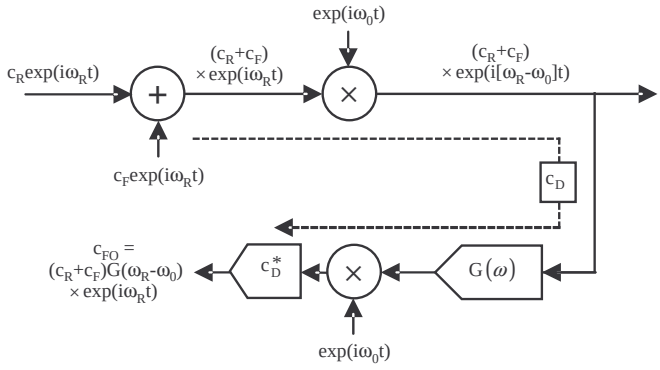

Figure 4.9. Signal flow of the quadrature feedback in the case of complex-valued signals [VI].

unhindered, the loop gain is selected to be of low-pass type with a cut-off frequency well below the data band, i.e. $G(\omega) = -G_0/(1 + i\omega/\omega_C)$. Additionally, a perfect phase compensation is assumed. Now the signal incident on the LNA is

$$c_R + c_F = c_R \left(1 + G_0 \frac{\omega_C}{\omega_C + i\,(\omega_R - \omega_0)}\right)^{-1}. \tag{4.8}$$

Below the cut-off frequency, the feedback suppresses all signals by $(1+G_0)$, and above the cut-off the signals are not affected.

Sensitivity

In Fig. 4.10, a bistatic reader with an adaptive RF front end is shown. The circuit is described in [VI]. The reader utilises quadrature feedback for carrier suppression. The idea has earlier been exploited in frequency modulated continuous wave (FMCW) radars, where the receiver exhibits similar carrier coupling from the reader [105, 106].

The sensitivity analysis begins with the incident signal, which is identical to the traditional reader (see Eq. (4.4)). A compensation signal of the form

$$V_{FB} = (C + \delta C)(A + \delta A)\exp(j\omega_0 t + j\delta\varphi) + n_{FB} \tag{4.9}$$

is added to the incident signal. The compensation signal carries the same noise as the incident signal, but also new noise terms from the baseband loop amplifiers, i.e. white noise n_{FB} and non-white amplitude noise δC,

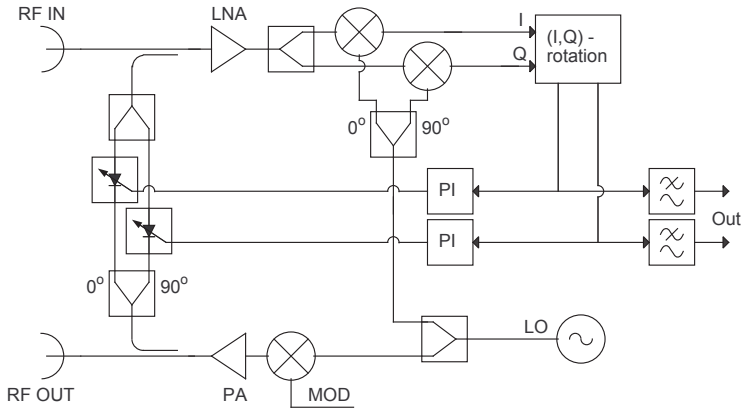

Figure 4.10. Block diagram of a bistatic reader with an adaptive RF front end [VI].

which can arise, e.g. from leakage of the carrier-induced amplitude noise through the loop.

When the feedback is closed, according to Eq. (4.7), the signal incident on the LNA is suppressed at the feedback band by $(1+G_0)$. With high gain, i.e. $G_0 \gg 1$, the compensation signal is equal in magnitude and opposite in phase compared with the incident carrier signal, giving

$$C = -L_{TX/RX} G_{TX} A. \tag{4.10}$$

The incoming carrier and the compensation signal carry correlated amplitude noise δA with them. The noise is correlated within the feedback and data bands due to range correlation [94]. Hence, when suppressing the carrier at the feedback band, the amplitude noise is suppressed also at the data band by the factor $(1 + G_0)$.

The feedback will introduce its own noise sources to the system. The feedback signal will emit at least white noise n_{FB} due to thermal sources. Also, the amplitude term cannot be assumed to be completely filtered by the loop gain. The noncorrelated amplitude noise term δC may arise for example from amplitude-noise leakage from the downmixer, or from PIN-diode shot noise. These noise components do not affect the feedback, and can be directly added to the signal.

The signal incident to the LNA can now be written as

$$\begin{aligned} V_{RX} + V_{FB} &= \frac{1}{1+G_0} L_{TX/RX} G_{TX} (A + \delta A) \exp(j\omega_0 t + j\delta\varphi) \\ &+ A(C\frac{\delta C}{C} + n_{FB}) \\ &+ L_{path}(A + \delta A) \exp(j[\omega_0 + \omega_{mod}]t + j\delta\varphi). \end{aligned} \tag{4.11}$$

Here the first and second terms describe the incident carrier and its amplitude noise, respectively. These are suppressed by the loop feedback band gain also at the data band due to signal correlation. The third term is the amplitude noise introduced by the feedback loop. It has been emphasised that the amplitude noise term δC is dependent on the compensation signal voltage C, i.e. on the incident carrier power. The fourth term is the white noise of the baseband amplifiers and the last term is the signal from the transponder.

Again, the phase noise is correlated and suppressed in the downmixer. Hence, in the case of high loop gain ($G_0 \gg 1$), the baseband signal becomes

$$\begin{aligned} V_{BB} &= \frac{1}{G_0} L_{TX/RX} G_{TX} (A^2 + 2AL_A \delta A) \\ &+ L_{TX/RX} G_{TX} A^2 \frac{\delta C}{C} + A^2 n_{FB} \\ &+ L_{path} A^2 \exp(j\omega_{mod} t), \end{aligned} \tag{4.12}$$

where we have used the feedback criterion $C = -L_{TX/RX} G_{TX} A$. In terms of power, the receiver sensitivity is [VI]

$$S = S_{RX} + S_F + \frac{\alpha_O P_{in}}{G_0} + \alpha_F P_{in}. \tag{4.13}$$

The carrier amplitude noise is suppressed by the loop gain, but additional white and amplitude-dependent terms arise. In practice this means, that sensitivity at low incident power is somewhat higher because of the feedback white noise S_F, but at higher incident power, the sensitivity can be better than without the feedback, if $\alpha_F < \alpha_O$.

Input Compression

The linearity is limited by the feedback loop. The criteria in Eq. (4.7) and the subsequent reasoning hold as long as the feedback loop can drive sufficient power to the input of the LNA. Hence, the compression is defined

by the active component in the feedback loop. A PIN diode attenuator similar to that in [107] is an optimum choice here, because it can handle high power up to 20 dBm, and still have basically thermally limited noise characteristics. Use of a diode ring mixer easily limits the output power to about 0 dBm, which falls short by 10 dB. Adding an amplifier after the mixer in the feedback loop increases S_F by the gain of the amplifier, making it an infeasible solution. Both the sensitivity and the linearity, i.e. the dynamic range of the receiver, are determined by the upmixer component in the feedback loop [VI].

The sensitivity and compression point of a realised adaptive front end in [VI] can be seen in Figs. 4.7 and 4.8. The front end is measured with the feedback loop both closed and open, giving a comparison between a traditional reader with LNA and an adaptive front end. It is seen that the feedback increases the white noise level by almost 10 dB, but noise suppression leads to a smaller noise term due to the incident carrier. At the same time, the input compression point of the receiver is increased by more than 10 dB.

4.5 Impedance Bridge as an Adaptive RF Front End

In hand-held devices, there are three main design objectives. The devices must be small in size and power consumption, and it has to be mass producible with low cost. Hence physically small antennas have to be used in hand-held devices. The small antennas tend to be narrow-banded in nature and sensitive to near-field effects, e.g. dielectric loading by the user hand. The mobile RFID reader has generated several small antenna designs [108, 109, 110]. The mobile phone manufacturers have been developing RFID readers. In [58], an integrated UHF RFID reader IC described by Samsung, and a prototype of a mobile phone with an embedded RFID reader is presented in [111] by Nokia.

In addition to delivering isolation and high dynamic range, the adaptive RF front end can be used to tune the reader antenna to the operating frequency, despite the user hand. This optimises the impedance matching between the power amplifier (PA) and the antenna, enabling a high read range with low power consumption.

In [VII] an adaptive front end with a four-port isolator is described. The block diagram and the circuit model of the reader RF front end are

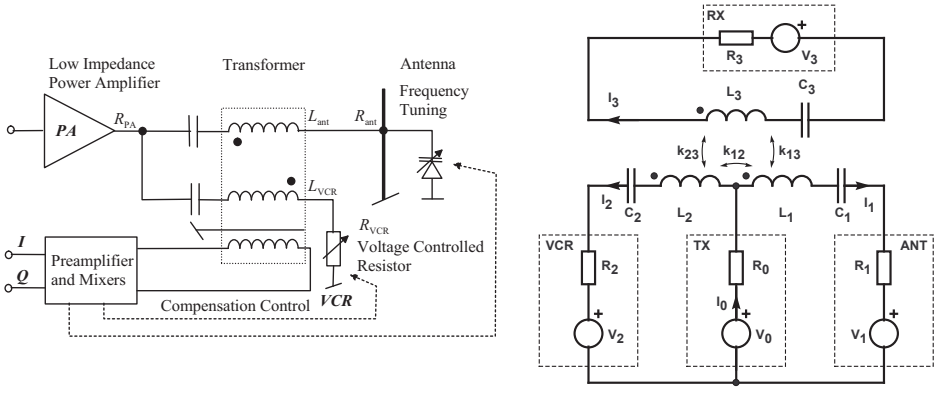

Figure 4.11. Block diagram (left) and circuit model (right) of an impedance bridge as an adaptive front end [VII].

presented in Fig. 4.11 and a photograph of the prototype in Fig. 4.12. The isolator is realised as a hybrid transformer with unequal coupling between the antenna and voltage controlled resistor (VCR) ports. Hence, the device could be described as a directional coupler. The directional coupler adds attenuation to the rx path, compromising the sensitivity of the receiver. However, in situations, where the backscattered signal is relatively high, i.e. the operating range is short, the solution is feasible. This is the case with a hand-held reader, which usually transmits a lower power (100 – 500 mW) to save battery.

The bridge enables increasing the compression point in the same manner than with the adaptive front end described in [VI], but with less components. Only a transformer, a PIN diode and a varactor, instead of two directional couplers, two PIN diode attenuators and two power dividers are needed. Hence, the transformer-based solution is better for size-critical applications, e.g. hand-held devices.

The bridge can be thoroughly analysed by writing the network equations of the circuit model presented in Fig. 4.11. The operation principle is simple. The antenna is tuned to resonance by the varactor. The branches of the bridge are also in resonance, i.e. L_1 resonates with C_1, as well as L_2 with C_2. Isolation is achieved by tuning the VCR resistance to

$$\frac{R_1}{R_2} = \frac{M_{13}}{M_{23}} = \frac{k_{13}}{k_{23}}\sqrt{\frac{L_1}{L_2}}. \tag{4.14}$$

A measurement of the prototype described in [VII] is shown in Fig. 4.13, with the isolation and rx and tx gains given as a function of frequency.

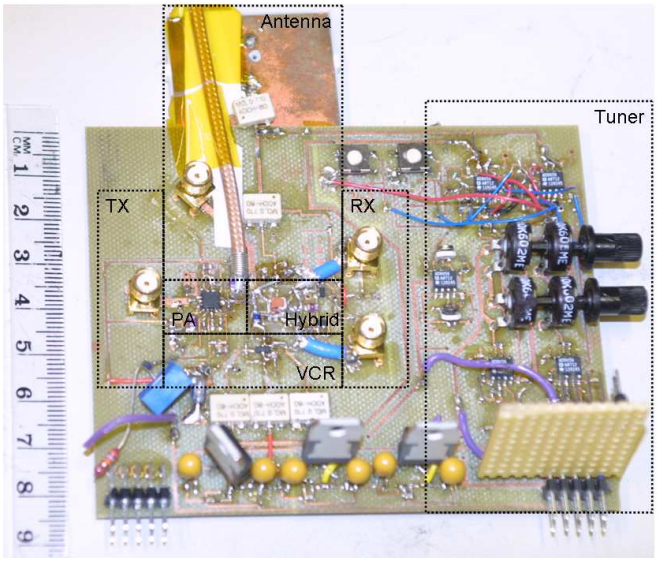

Figure 4.12. Photograph of the impedance bridge prototype [VII].

The power dissipated in the loads R_1 and R_2 depends only on the resistances according to

$$\frac{P_1}{P_2} = \frac{R_2}{R_1} = n, \tag{4.15}$$

which defines the power ratio n. Because inductance of a wire wound coil is proportional to the square of the turns of wire in the coil, the power ratio n describes also the ratio of turns in coils L_1 and L_2 (see Eq. 4.14). Hence the hybrid transformer can be designed for any power ratio between the loads. The power ratio n also affects the gain in tx and rx paths, G_{TX} and G_{RX} respectively, and hence the noise figure F of the bridge as a receiver. Theoretical results can be summarised as [VII]

$$\begin{aligned} G_{TX} &= \left(1 + \frac{1}{n}\right)^{-1}, \\ G_{RX} &\propto \frac{1}{n^2}, \\ F &\propto n^3. \end{aligned} \tag{4.16}$$

For power saving, i.e. for achieving low transmission loss, a high value of n would be preferable, but the noise figure increases fast with increasing n.

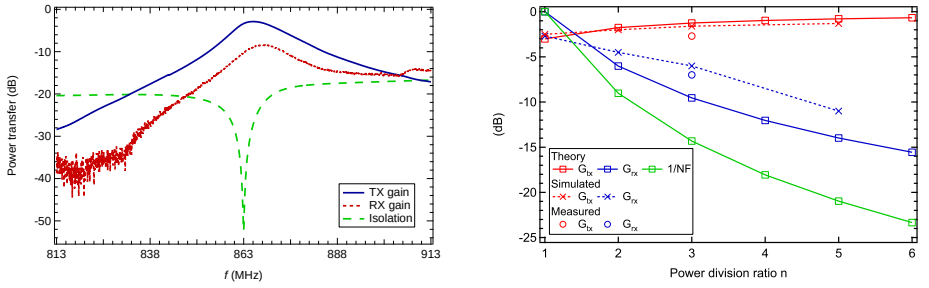

Figure 4.13. Measured results of isolation and tx and rx gains of the bridge as a function of frequency (left), and transmission and reception gains (G_{TX} and G_{RX}), and the noise figure F of the bridge at isolation frequency as a function of the power ratio n (right) [VII].

Thus a compromise has to be found. The compromise taken in [VII] is n≈3. The analytical results of Eq. (4.16), simulations of the bridge and measurement results are summarised in Fig. 4.13. The figure shows that the measurements are in good agreement with the theory and simulations.

4.6 Summary

In this chapter, RFID readers with three different isolation techniques have been discussed, i.e. the common reader with a bistatic configuration (or a circulator), a common reader with a directional coupler, and a reader with an adaptive RF front end. The design and development of two adaptive RF front ends was presented: a full power (0.5 W_{erp}) reader in [VI] and a lower power reader for mobile applications in [VII]. The sensitivity and compression point of the readers was analysed and measured, and they were compared to other published isolation techniques and readers.

The dynamic range of the different reader architectures is summarised here. Typical values of sensitivity and input compression point of the readers are schematically presented in Fig. 4.14. The values are based on the measurements in [VI], except for the geometry with directional coupler, which has been calculated based on the measurement results of the bistatic reader and the measurement results of the attenuation of the impedance bridge in [VII]. Using a directional coupler is equal to adding attenuation in front of the receiver of the bistatic reader.

The attenuation at the receiver can be used to rise the input compression

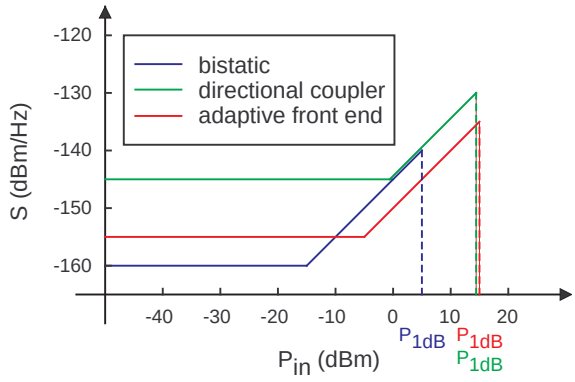

Figure 4.14. Typical sensitivity S and input compression point P_{1dB} of different reader architectures as a function of the incident carrier power P_{in}.

point, but it also diminishes the dynamic range: Sensitivity is increased more than the compression point due to the noise contribution of latter stages. The impedance bridge used in [VII] is similar to the directional coupler, but the adaptivity enables small size and low power consumption, which are essential in mobile devices.

At best, the dynamic range of the published readers is comparable to that of a the bistatic reader (see Table 2.2). Hence, the adaptive front end presented in [VI] has supreme dynamic range.

5 Conclusion

In this Thesis, RF components and phenomena in passive UHF RFID systems were studied. The basic equations for transponder powering and backscattering communication were derived. The analysis was applied to RFID at UHF and millimetre waves. The read range of passive UHF RFID is limited by the power transfer to the transponder, provided that the sensitivity of the reader is not compromised by the coupling from the transmitter. To ensure this, high isolation between the transmitter and the receiver of the reader is required. The sensitivity of the transponders is improving with the introduction of semipassive transponders. The more sensitive the transponders become, the more important the reader sensitivity will be.

In the Thesis, the dynamic range of the RFID reader was analysed in detail, and the development of two RFID readers with adaptive RF front ends was presented. The sensitivity and compression point of the readers was analysed and measured and compared to other readers published in literature. The reader with adaptive front end presented in [VI] has the highest dynamic range among them all. It combines low noise characteristics and high input compression, enabling longer range RFID systems.

The UHF RFID is applied in logistics and in retail industry for tracking ever smaller pallets and boxes, and recently even item level tagging has been introduced. Hence, even consumers could begin to use handheld readers to access further information on the merchandise. Mobile phone manufacturers have already shown interest for integrating an UHF RFID reader into mobile phones [111], even though the devices are not yet rolled out to the general public. A reader in a small mobile phone is very prone to disturbances caused by the user hand and other objects in the imminent near environment of the reader antenna. An adaptive RF front end, such as the one presented in [VII], is needed for efficient and reliable operation.

The adoption of RFID in new applications and environments demands also suitable transponder antennas. Tagging of an item cannot be economically feasible, if placing the transponder on an item requires an RF

specialist, or if a transponder antenna has to be specially developed for every different item. Even though an ultimate universal transponder, fitting every application, is a day-dream, research on platform-tolerant antennas has already lead to several designs, such as the one introduced in [III]. The development has been rapid in the recent years. First universal transponders emerged less than five years ago, and nowadays there are at least a dozen companies selling their designs. However, most of the universal transponders are expensive, costing tens of times as much as the 10 cent labels. Hence, the design of a specialised low cost antenna is still feasible for tagging mass products.

In the future, passive sensor nodes, like the one introduced in [I], could be utilised to measure room temperature, moisture, pressure in tires, etc. And the consumer could access the node with the reader in his/her cell phone. Another future development in the field of RFID will propably be the adoption of higher carrier frequencies in the microwave and millimetre wave ranges. The higher carrier frequency does not affect the operating principles of RFID, but it will modify the compromise between power transfer and backscattering modulation. The millimetre RFID, or millimetre wave identification (MMID), was analysed in [II]. Power transfer at millimetre waves is not feasible, but semipassive systems could provide features impossible to implement with UHF. At millimetre waves, data bandwidth of hundreds of megabits could be implemented. A reader antenna with narrow beam could be used to select a single transponder in a swarm of nearby transponders. Finally, the existing automotive radars have all the hardware needed to communicate with MMID transponders.

The field of RFID and backscattering communication has been studied for 60 years. A set of applications has reached maturity, but the field has not found its limits yet. The power efficiency and simple implementation of the backscattering modulation promise new applications in the future.

References

[1] RFID Journal, "Wal-Mart Tackles Out-of-Stocks", April 2005, www.rfidjournal.com/article/articleview/1551/1/1/, referenced September 5th 2008.

[2] K. Finkenzeller, *RFID Handbook*, 2nd edition, John Wiley & Sons, 2003.

[3] RFIDJournal, "Stealing Cars Will Get Tougher", July 2002, www.rfidjournal.com/article/articleview/33/1/1/, referenced September 14th 2008.

[4] RFIDJournal, "Passive Tags Track Cars", August 2004, www.rfidjournal.com/article/articleview/1078/1/1/, referenced September 14th 2008.

[5] RFIDJournal, "UHF Tags Enter the Timing Race", October 2007, www.rfidjournal.com/article/articleview/3691/1/1/, referenced September 4th 2008.

[6] RFID Gazette, "RFID Implants: 5 Amazing Stories", April 2007, www.rfidgazette.org/2007/04/rfid_implants_5.html, referenced September 4th 2008.

[7] Ekhau Inc., "Madrid Hospital Improves Employee Safety with Ekahau Wi-Fi RTLS", press release, June 2008, www.ekahau.com/?id=20089, referenced September 4th 2008.

[8] Nokia 6131 NFC, www.nokia.com, referenced September 5th 2008.

[9] C. S. Hartmann and L. T. Claiborne, "Fundamental Limitations on Reading Range of Passive IC-Based RFID and SAW-Based RFID", *IEEE International Conference on RFID*, Grapevine, Texas, USA, March 26 – 28, 2007, pp. 41 – 48.

[10] P. V. Nikitin, S. Lam, and K. V. S. Rao, "Low Cost Silver Ink RFID Tag Antennas", *IEEE Antennas and Propagation Society International Symposium*, Vol. 2B, July 3 – 8, 2005, pp. 353 – 356.

[11] V. Subramanian, J. M. J. Frchet, P. C. Chang, D. C. Huang, J. B. Lee, S. E. Molesa, A. R. Murphy, D. R. Redinger, and S. K. Volkman, "Progress Toward Development of All-Printed RFID Tags: Materials, Processes, and Devices", *Proceedings of IEEE*, Vol. 93, No. 7, pp. 1330 – 1338, July 2005.

[12] Kovio Inc., www.kovio.com; RFIDJournal, www.rfidjournal.com/article/articleview/4389/; and www.pennwellblogs.com/sst/eds_threads/2007/11/071123-printed-silicon-rf-ids-by-kovio.php?dcmp=WaferNEWS_ARCH, November 2007 – October 2008, referenced November 31st 2008.

[13] PolyIC GmbH & Co. KG, "The Revolution with Printed Electronics Begins – First Printed RFID and Smart Objects for the Market", press release, September 25, 2007, www.polyic.com/en/read.php?page=306, referenced September 4th 2008.

[14] P. F. Baude, D. A. Ender, T. W. Kelley, M. A. Haase, D. V. Muyres, and S. D. Theiss, "Organic Semiconductor RFID Transponders", *IEEE Electron Devices Meeting, IEDM '03 Technical Digest.*, 2003.

[15] J. C. Maxwell, "A Dynamical Theory of the Electromagnetic Field", *Philosophical Transactions of the Royal Society of London*, 1865.

[16] N. Tesla, "Apparatus for Transmission of Electrical Energy", *US Patent 649621*, May 1900.

[17] N. Tesla, "Art of Transmitting Electrical Energy Through the Natural Mediums", *US Patent 787412*, April 1905.

[18] H. T. Friis, "A Note on a Simple Transmission Formula", *Proceedings of the IRE*, Vol. 34, Issue 5, pp. 254 – 256, May 1946.

[19] W. C. Brown, "The History of Power Transmission by Radio Waves", *IEEE Transactions on Microwave Theory and Technology*, Vol. 32, Issue 9, pp. 1230 – 1242, September 1984.

[20] H. Stockman, "Communication by Means of Reflected Power", *Proceedings of the IRE*, pp. 1196 – 1204, October 1948.

[21] D. D. King, "Measurement and Interpretation of Antenna Scattering", *Proceedings of the IRE*, Vol. 37, pp. 770 – 777, July 1949.

[22] R. F. Harrington, "Theory of Loaded Scatterers", *Proceedings of the IEE*, Vol. 111, pp. 617 – 623, April 1964.

[23] R. F. Harrington, "Field Measurements Using Active Scatterers", *IEEE Transactions on Microwave Theory and Technology*, Vol. 11, p. 454, September 1963.

[24] J. Appel-Hansen, "Accurate Determination of Gain and Radiation Patterns by Radar Cross-Section Measurements", *IEEE Transactions*

on Antennas and Propagation, Vol. 27, pp. 640 – 646, September 1979.

[25] J. T. Mayhan, A. R. Dion, and A. J. Simmons, "A Technique for Measuring Antenna Drive Port Impedance Using Backscatter Data", *IEEE Transactions on Antennas and Propagation*, Vol. 42, pp. 526 – 532, April 1994.

[26] W. Wiesbeck and E. Heidrich, "Wide-Band Multiport Antenna Characterization by Polarimetric RCS Measurements", *IEEE Transactions on Antennas and Propagation*, Vol. 46, pp. 341 – 350, March 1998.

[27] "The Great Seal Bug Story", www.spybusters.com/Great_Seal_Bug .html, referenced August 14th 2008.

[28] Wikipedia, http://en.wikipedia.org/wiki/Identification_friend_or_foe; and http://en.wikipedia.org/wiki/Secondary_Surveillance_Radar, referenced August 14th 2008.

[29] A. R. Koelle, S. W. Depp, and R. W. Freyman, "Short-Range Radio-Telemetry for Electronic Identification, Using Modulated RF Backscatter", *Proceedings of the IEEE*, Vol. 63, Issue 8, pp. 1260 – 1261, August 1975.

[30] J. Landt, *Shrouds of Time: The History of RFID*, AIM, 2001, www.transcore.com/pdf/AIM shrouds_of_time.pdf, referenced August 14th 2008.

[31] K. V. S. Rao, "An Overview of Back Scattered Radio Frequency Identification System (RFID)", *IEEE Asia Pacific Microwave Conference*, Vol. 3, 1999, pp. 746 – 749.

[32] The Palomar Project, "Passive Long Distance Multiple Access UHF RFID System", Public Report, European Commission, Project Number IST1999-10339, November 2002.

[33] *ISO/IEC 18000-6: Information Technology — Radio Frequency Identification for Item Management — Part 6: Parameters for Air Interface Communications at 860 MHz to 960 MHz*, www.iso.org, ISO, 2004.

[34] *EPC Radio Frequency Identification Protocols: Class-1 Generation-2 UHF RFID, Protocol for Communications at 860 – 960 MHz, Version 1.1.0.*, www.epcglobalinc.org, EPCglobal, 2006.

[35] The European Telecommunications Standards Institute (ETSI), www.etsi.org.

[36] Federal Communications Commission (FCC), www.fcc.gov.

[37] RFID Journal, "China Approves Requirements for UHF Bandwidth", May 2007, www.rfidjournal.com/article/articleview/3318/, referenced August 14th 2008.

[38] K. V. S. Rao, D.-W. Duan, and H. Heinrich, "On the Read Zone Analysis of Radio Frequency Identification Systems with Transponders Oriented in Arbitrary Directions", *IEEE Asia Pacific Microwave Conference*, Vol. 3, 1999, pp. 758 – 761.

[39] U. Karthaus and M. Fischer, "Fully Integrated Passive UHF RFID Transponder IC with 16.7-μW Minimum RF Input Power", *IEEE Journal of Solid-State Circuits*, Vol. 38, pp. 1602 – 1608, October 2003.

[40] P. V. Nikitin and K. V. S. Rao, "Performance Limitations of Passive UHF RFID Systems", *IEEE Antennas and Propagation Society International Symposium*, July 9 – 14, 2006, pp. 1011 – 1014.

[41] P. V. Nikitin and K. V. S. Rao, "Antennas and Propagation in UHF RFID Systems", *IEEE International Conference on RFID 2008*, Las Vegas, NV, USA, April 16 – 17, 2008, pp. 277 – 288.

[42] F. Fuschini, C. Piersanti, F. Paolazzi, and G. Falciasecca, "Analytical Approach to the Backscattering from UHF RFID Transponder", *IEEE Antennas and Wireless Propagation Letters*, Vol. 7, pp. 33 – 35, 2008.

[43] J. D. Kraus, *Antennas*, McGraw-Hill, 1950.

[44] K. Kurokawa, "Power Waves and the Scattering Matrix", *IEEE Transactions on Microwave Theory and Techniques*, Vol. MTT-13, No. 3, pp. 194 – 202, March 1965.

[45] P. V. Nikitin, K. V. S. Rao, S. F. Lam, V. Pillai, R. Martinez, and H. Heinrich, "Power Reflection Coefficient Analysis for Complex Impedances in RFID Tag Design", *IEEE Transactions on Microwave Theory and Techniques*, Vol. 53, No. 9, pp. 2721 – 2725, September 2005.

[46] J.-P. Curty, M. Declercq, C. Dehollain, and N. Joehl, *Design and Optimization of Passive UHF RFID Systems*, Springer, 2007.

[47] J. Sondow and E. W. Weisstein, "Riemann Zeta Function", *MathWorld — A Wolfram Web Resource*, available at http://mathworld.wolfram.com/RiemannZetaFunction.html, referenced July 31st 2008.

[48] X. Q. Bao, W. Burkhard, V. V. Varadan, and V. K. Varadan, "SAW Temperature Sensor and Remote Reading System", *IEEE Ultrasonics Symposium*, 1987, pp. 583 – 586.

[49] A. D. DeHennis and K. D. Wise, "A Wireless Microsystem for the Remote Sensing of Pressure, Temperature, and Relative Humidity", *IEEE Journal of Microelectromechanical Systems*, Vol. 14, No. 1, pp. 12 – 22, February 2005.

[50] V. Pillai, H. Heinrich, D. Dieska, P. V. Nikitin, R. Martinez, and K. V. S. Rao, "An Ultra-Low-Power Long Range Battery/Passive RFID Tag for UHF and Microwave Bands With a Current Consumption of 700 nA at 1.5 V", *IEEE Transactions on Circuits And SystemsI: Regular Papers*, Vol. 54, No. 7, pp. 1500 – 1512, July 2007.

[51] N. Cho, S.-J. Song, S. Kim, S. Kim, and H.-J. Yoo,"A 5.1-μW UHF RFID Tag Chip Integrated with Sensors for Wireless Environmental Monitoring", *Proceedings of ESSCIRC*, September 12 – 16, 2005, pp. 279 – 282.

[52] J.-P. Curty, N. Joehl, C. Dehollain, and M. Declercq, "Remote Powered Addressable UHF RFID Integrated System", *IEEE Journal of Solid-State Circuits*, Vol. 40, pp. 2193 – 2202, November 2005.

[53] F. Kocer and M. P. Flynn, "A New Transponder Architecture with On-Chip ADC for Long-Range Telemetry Applications", *IEEE Journal of Solid-State Circuits*, Vol. 41, No. 5, pp. 1142 – 1148, May 2006.

[54] A. P. Sample, D. J. Yeager, P. S. Powledge, and J. R. Smith, "Design of a Passively-Powered, Programmable Sensing Platform for UHF RFID Systems", *IEEE International Conference on RFID*, Grapevine, Texas, USA, March 26 – 28, 2007, pp. 149 – 156.

[55] H. Nakamoto, D. Yamazaki, T. Yamamoto, H. Kurata, S. Yamada, K. Mukaida, T. Ninomiya, T. Ohkawa, S. Masui, and K. Gotoh, "A Passive UHF RF Identification CMOS Tag IC Using Ferroelectric RAM in 0.35-μm Technology", *IEEE Journal of Solid-State Circuits*, Vol. 42, No. 1, pp. 101 – 110, January 2007.

[56] Alien Technology, "Alien H3 EPC Class 1 Gen 2 RFID Tag IC, Product Overview", April 2008, www.alientechnology.com/docs/products/DS_H3.pdf, referenced July 2008.

[57] I. Kipnis, S. Chiu, M. Loyer, J. Carrigan, J. Rapp, P. Johansson, D. Westberg, and J. Johansson, "A 900MHz UHF RFID Reader Transceiver IC", *IEEE International Solid-State Circuit Conference*, February 13, 2007, pp. 214 – 215, 598.

[58] I. Kwon, Y. Eo, H. Bang, K. Choi, S. Jeon, S. Jung, D. Lee, and H. Lee, "A Single-Chip CMOS Transceiver for UHF Mobile RFID Reader", *IEEE Journal of Solid-State Circuits*, Vol. 43, No. 3, pp. 729 – 738, March 2008.

[59] AS3990 Preliminary Datasheet, Austria Microsystems corporation, www.austriamicrosystems.com/03products/products_detail/AS3990/download/AS3990_Features.pdf, referenced August 8th 2008.

[60] Elektrobit Company, "EB RFID Reader EB URP1000-ETSI Datasheet", www.elektrobit.com/file.php?110, referenced May 2008.

[61] D. Neculoiu, G. Konstantinidis, T. Vähä-Heikkilä, A. Müller, D. Vasilache, A. Stavinidris, L. Bary, M. Dragoman, I. Petrini, C. Buiculescu, Z. Hazoupulos, N. Kornilios, P. Pursula, R. Plana, and D. Dascalu, "GaAs Membrane-Supported 60 GHz Receiver with Yagi-Uda Antenna", *MEMSWAVE 2007, 8th International Symposium on RF MEMS and RF Microsystems*, Barcelona, Spain, June 26 – 29, 2007, pp. 15 – 18.

[62] E. M. Biebl,"RF Systems Based on Active Integrated Antennas", *(AEÜ) International Journal of Electronics and Communications*, Vol. 57, No. 3, pp. 173 – 180, 2003.

[63] A. Müller, D. Neculoiu, P. Pursula, T. Vähä-Heikkilä, F. Giacomozzi, and J. Tuovinen, "Hybrid Integrated Micromachined Receiver for 77 GHz Millimeter Wave Identification Systems", *37th European Microwave Conference 2007*, Munich, Germany, October 2007, pp. 1034 – 1037.

[64] D. Kim, M. A. Ingram, and W. W. Smith Jr., "Measurements of Small-Scale Fading and Path Loss for Long Range RF Tags", *IEEE Transactions on Antennas and Propagation*, Vol. 51, No. 8, pp. 1740 – 1749, August 2003.

[65] E. F. Knott, J. F. Schaeffer, and M. T. Tuley, *Radar Cross Section*, Artech House, 1993.

[66] E. Newman and D. Forrai, "Scattering from a Microstrip Patch", *IEEE Transactions on Antennas and Propagation*, Vol. 35, pp. 245 – 251, March 1987.

[67] R. E. Collin, "Limitations of the Thevenin and Norton Equivalent Circuits for a Receiving Antenna", *IEEE Antennas and Propagation Magazine*, Vol. 45, Issue 2, pp. 119 – 124, April 2003.

[68] P. V. Nikitin, K. V. S. Rao, and R. D. Martinez, "Differential RCS of RFID Tag", *IEE Electronic Letters*, Vol. 43, No. 8, pp. 431 – 432, April 2007.

[69] P. V. Nikitin and K. V. S. Rao, "Theory and Measurement of Backscattering from RFID Tags", *IEEE Antennas and Propagation Magazine*, Vol. 48, pp. 212 – 218, December 2006.

[70] M. Ritamäki, A. Ruhanen, V. Kukko, J. Miettinen, and L. H. Turner, "Contactless Radiation Pattern Measurement Method for UHF RFID Transponders", *IEE Electronic Letters*, Vol. 41, Issue 13, pp. 723 – 724, June 2005.

[71] Tagformance Lite, Voyantic Ltd, www.voyantic.com/index.php?trg =browse&id=64, referenced August 14th 2008.

[72] P. Pursula, T. Varpula, K. Jaakkola, and M. Hirvonen, "Antenna Radiation Characterization by Backscattering Modulation", *Proceedings of URSI/IEEE XXIX Convention on Radio Science*, Espoo, Finland, November 1 – 2, 2004, pp. 115 – 118.

[73] S.-J. Kim, B. Yu, Y.-S. Chung, F. J. Harackiewicz, and B. Lee, "Patch-Type Radio Frequency Identification Tag Antenna Mountable on Metallic Platforms, *Microwave and Optical Technology Letters*, Vol. 48, No. 12, pp. 2446 – 2448, December 2006.

[74] B. Yu, S.-J. Kim, B. Jung, F. J. Harackiewicz, and B. Lee, "RFID Tag Antenna Using Two-Shorted Microstrip Patches Mountable on Metallic Objects", *Microwave and Optical Technology Letters*, Vol. 49, Issue 2, pp. 414 – 416, February 2007.

[75] B. Lee and B. Yu, "Compact Structure of UHF Band RFID Tag Antenna Mountable on Metallic Objects", *Microwave and Optical Technology Letters*, Vol. 50, Issue 1, pp. 232 – 234, January 2008.

[76] C. Icheln, "The Construction and Application of a GTEM cell", *Master's Thesis*, Technical University of Hamburg, Hamburg, Faculty of Electrical Engineering and Helsinki University of Technology, Faculty of Electrical Engineering, November 1995.

[77] K. V. S. Rao, P. V. Nikitin, and S. F. Lam, "Antenna Design for UHF RFID Tags: A Review and a Practical Application", *IEEE Transactions on Antennas and Propagation*, Vol. 53, No. 12, pp. 3870 – 3876, December 2005.

[78] L. J. Chu, "Physical Limitations of Omni-Directional Antennas", *Journal of Applied Physics*, Vol. 19, pp. 1163 – 1175, December 1948.

[79] R. E. Collin and S. Rothchild, "Evaluation of Antenna Q", *IEEE Transactions on Antennas and Propagation*, Vol. 12, Issue 1, pp. 23 – 27, January 1964.

[80] J. T. Prothro, G. D. Durgin, and J. D. Griffin, "The Effects of a Metal Ground Plane on RFID Tag Antennas", *IEEE Antennas and Propagation Society International Symposium*, July 9 – 14, 2006, pp. 3241 – 3244.

[81] D. M. Dobkin and S. M. Weigand, "Environmental Effects on RFID Tag Antennas", *IEEE MTT-S International Microwave Symposium Digest*, June 12 – 17, 2005, pp. 135 – 138.

[82] P. Foster and R. Burberry, "Antenna Problems in RFID Systems", *IEE Colloquium on RFID Technology*, London, October 25, 1999, pp. 3/1 – 3/5.

[83] M. Hirvonen, J. C.-E. Sten, and P. Pursula, "Platform Tolerant Planar Inverted F-Antenna", *Proceedings of URSI/IEEE XXIX Convention on Radio Science*, Espoo, Finland, November 1 – 2, 2004, pp. 47 – 50.

[84] J. C.-E. Sten and M. Hirvonen, "Decay of Groundplane Currents of Small Antenna Elements", *IEEE Antennas and Wireless Propagation Letters*, Vol. 4, pp. 82 – 84, 2005.

[85] J. D. Griffin, G. D. Durgin, A. Haldi, and B. Kippelen, "RF Tag Antenna Performance on Various Materials Using Radio Link Budgets", *IEEE Antennas and Wireless Propagation Letters*, Vol. 5, Issue 1, pp. 247 – 250, December 2006.

[86] Confidex Ltd., "Survivor Brochure", Available at www.confidex.fi/fileadmin/user_upload/pdf/Survivor-small.pdf, referenced August 6th, 2008.

[87] H.-W. Son, G.-Y. Choi, and C.-S. Pyo, "Design of Wideband RFID Tag Antenna for Metallic Surfaces", *IEE Electronic Letters*, Vol. 42, No. 5, pp. 263 – 265, March 2006.

[88] K. V. S. Rao, S. F. Lam, and P. V. Nikitin, "Wideband Metal Mount UHF RFID Tag", *IEEE Antennas and Propagation Symposium*, San Diego, CA, June 2008.

[89] M. Hirvonen, K. Jaakkola, P. Pursula, and J. Säily, "Dual-Band Platform Tolerant Antennas for Radio-Frequency Identification", *IEEE Transactions on Antennas and Propagation*, Vol. 54, No. 9, pp. 2632 – 2637, September 2006.

[90] L. Ukkonen, L. Sydänheimo, and M. Kivikoski, "Patch Antenna with EBG Ground Plane and Two-Layer Substrate for Passive RFID of Metallic Objects", *IEEE Antennas and Propagation Society International Symposium*, June 20 – 25, 2004, pp. 93 – 96.

[91] M. Stupf, R. Mittra, J. Yeo, and J. R. Mosig, "Some Novel Design for RFID Antennas and Their Performance Enhancement with Metamaterials", *Microwave and Optical Technology Letters*, Vol. 49, No. 4, pp. 858 – 867, April 2007.

[92] D. Kim, J. Yeo, and J. I. Choi, "Low Profile Platform-Tolerant RFID Tag with Artificial Magnetic Conductor (AMC)", *Microwave and Optical Technology Letters*, Vol. 50, No. 9, pp. 2292 – 2294, September 2008.

[93] L. Ukkonen, L. Sydänheimo, and M. Kivikoski, "A Novel Tag Design Using Inverted-F Antenna for Radio Frequency Identification of Metallic Objects", *IEEE Symposium on Advances in Wired and Wireless Communication*, April 26 – 27, 2004, pp. 91 – 94.

[94] J.-H. Bae, J.-C. Kim, B.-W. Jeon, J.-W. Jung, J.-S. Park, B.-J. Jang, H.-R. Oh, Y.-J. Moon, and Y.-R. Seong, "Analysis of Phase Noise Requirements on Local Oscillator for RFID System Considering Range Correlation", *37th European Microwave Conference 2007*, Munich, Germany, October 2007, pp. 1664 – 1667.

[95] K. Penttilä, L. Sydänheimo, and M. Kivikoski,"Implementation of Tx/Rx Isolation in an RFID Reader", *International Journal of Radio*

Frequency Identification Technology and Applications, Vol. 1, No. 1, pp. 74 – 89, 2006.

[96] J.-W. Jung, K.-K. Nae, J. P. Thakur, H.-G. Cho, and J.-S. Park, "Directional Coupler for UHF Mobile RFID Reader", *Microwave and Optical Technology Letters*, Vol. 49, No. 7, pp. 1501 – 1505, July 2007.

[97] W.-K. Kim, M.-Q. Lee, J.-H. Kim, H.-S. Lim, J.-W. Yu, B.-J. Jang, and J.-S. Park, "A Passive Circulator with High Isolation Using a Directional Coupler for RFID", *IEEE MTT-S International Microwave Symposium*, San Francisco, CA, USA, June 11 – 16, 2006, pp. 1177 – 1180.

[98] F. Wei, X. W. Shi, Q. L. Huang, D. Z. Chen, and X. H. Wang, "A New Directional Coupler for UHF RFID Reader", *Microwave and Optical Technology Letters*, Vol. 50, No. 7, pp. 1973 – 1975, July 2008.

[99] W.-K. Kim, W. Na, J.-W. Yu, and M.-Q. Lee, "A High Isolated Coupled-Line Passive Circulator for UHF RFID Reader", *Microwave and Optical Technology Letters*, Vol. 50, No. 10, pp. 2597 – 2600, October 2008.

[100] J.-W. Jung, H.-H. Roh, H.-G. Kwak, M. S. Jeong, and J.-S. Park, "Adaptive TRX Isolation Scheme by Using TX Leakage Canceller at Variable Frequency", *Microwave and Optical Technology Letters*, Vol. 50, No. 8, pp. 2043 – 2045, August 2008.

[101] H.-W. Son, J.-N. Lee, and G.-Y. Choi, "Design of Compact RFID Reader Antenna with High Transmit/Receive Isolation", *Microwave and Optical Technology Letters*, Vol. 48, No. 12, pp. 2478 – 2481, December 2006.

[102] H. Seppä, T. Varpula, P. Pursula, and M. Kiviranta, "WO/2007/006840 RFID Reading Apparatus And Method", *International patent application*, Filed (National priority) July 2005, published January 2007.

[103] A. Safarian, A. Shameli, A. Rofougaran, and M. Rofougaran, "US/2008/0009258 Integrated Blocker Filtering RF Front End", *US patent application*, Filed February 2007, published January 2008.

[104] D. M. Pozar, *Microwave Engineering*, 2nd Edition, John Wiley & Sons, 1998.

[105] P. D. L. Beasley, A. G. Stove, B. J. Reits, and B.-O. As, "Solving the Problems of a Single Antenna Frequency Modulated CW Radar", *Proceedings of IEEE Radar Conference*, 1990, pp. 391 – 395.

[106] A. G. Stove, "Linear FMCW radar techniques", *IEE Proceedings-F*, Vol. 139, No. 5, pp. 343 – 350, October 1992.

[107] W.-T. Kang, I.-S. Chang, and M.-S. Kang, "Reflection-Type Low-Phase-Shift Attenuator", *IEEE Transactions on Microwave Theory Technology*, Vol. 46, No. 7, pp. 1019 – 1021, July 1998.

[108] L. Ukkonen, L. Sydänheimo, and M. Kivikoski, "Read Range Performance Comparison of Compact Reader Antennas for a Handheld UHF RFID Reader", *IEEE International Conference on RFID*, Grapevine, Texas, USA, March 26 – 28, 2007, pp. 63 – 70.

[109] Y. Kim, I.-J. Yoon, and Y. Kim, "Internal Antenna Design of 900 MHz-Band Mobile Radio Frequency Identification System", *Microwave and Optical Technology Letters*, Vol. 49, No. 9, pp. 2079 – 2082, September 2007.

[110] J.-J. Kang, D.-J. Lee, C.-C. Chen, J. F. Whitaker, and E. J. Rothwell, " Compact Mobile RFID Antenna Design and Analysis Using Photonic-assisted Vector Near-field Characterization", *IEEE International Conference on RFID*, Las Vegas, Nevada, USA, April 16 – 17, 2008, pp. 81 – 88.

[111] J. Savolainen, H. Hirvola, and S. Iraji, "Nokia integroi lukimen E61-malliin: EPC-tunnistus tulee pian kännykkään [Nokia Integrated a Reader into its E61 Model: EPC Identification Comes Soon to Mobile Phones]", *Prosessori*, pp. 42 – 43, August 2008.

Errata

In the published article [IV], in section IIB, the equation (14)

$$\sigma_1 = \frac{\lambda^2 G_A^2}{4\pi} \frac{16}{\pi^2} \frac{R_A^2 \Delta X^2}{(R^2 + X^2 + \Delta X^2)^2 + 4R^2 X^2},$$

should stand

$$\sigma_1 = \frac{\lambda^2 G_A^2}{4\pi} \frac{16}{\pi^2} \frac{R_A^2 \Delta X^2}{(R^2 - X^2 + \Delta X^2)^2 + 4R^2 X^2}.$$

In the published article [II], in section IIA, the equation (8)

$$P_{rx} = \sigma^m \frac{\lambda^2 G_{tx} P_{tx} G_{rx}}{(4\pi)^2 d^4}, \tag{5.1}$$

should stand

$$P_{rx} = \sigma^m \frac{\lambda^2 G_{tx} P_{tx} G_{rx}}{(4\pi)^3 d^4}. \tag{5.2}$$

This affects the Figures 4 – 6 in section IIB. The minor change in the Figures does not affect the analysis or the conclusion of the paper. The corrected Figures are printed here.

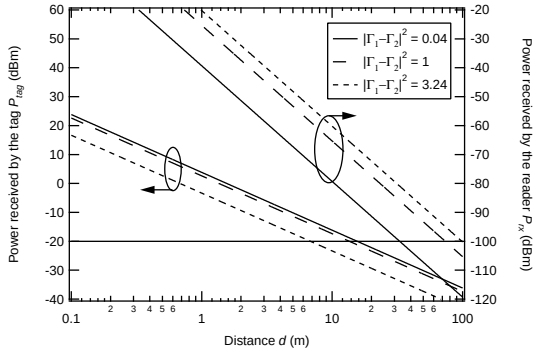

Figure 4. The limiting factors on the UHF RFID range.

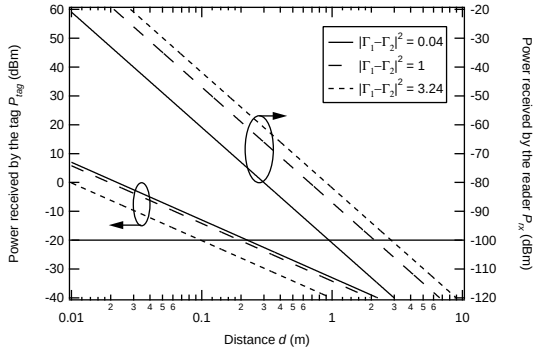

Figure 5. The limiting factors on the passive MMID range at 60 GHz.

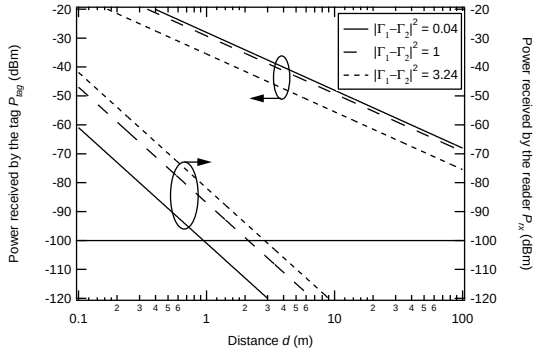

Figure 6. The limiting factors on the semipassive MMID range at 60 GHz.

Wirelessly Powered Sensor Transponder for UHF RFID

In: Proceedings of Transducers & Eurosensors'07 Conference.
Lyon, France, June 10–14, 2007, pp. 73–76.

WIRELESSLY POWERED SENSOR TRANSPONDER FOR UHF RFID

P. Pursula, J. Marjonen, H. Ronkainen and K. Jaakkola
VTT Technical Research Centre of Finland
Espoo, FINLAND
(email: pekka.pursula@vtt.fi)

Abstract: A transponder for UHF RFID with sensor interface for external capacitive sensors is described. The sensor interface consists of a capacitive voltage divider and a 10 bit successive approximation analog to digital converter. The power consumption is about 30 μW_{DC} and the transponder is wirelessly powered with RF waves from the reader device. Wireless measurement of capacitance is demonstrated at a distance of 30 cm with 0.5 W erp transmission power. Low operation distance is mostly due to low efficiency of the rectifying Schottky-diodes in the particular BiCMOS process.

Keywords: UHF RFID, sensor.

TRANSDUCERS & EUROSENSORS '07
The 14th International Conference on Solid-State Sensors, Actuators and Microsystems, Lyon, France, June 10-14, 2007

1. INTRODUCTION

One of the most modern applications of the RF technology is a radio frequency identification (RFID) transponder operating at ultra high frequencies (UHF). A passive transponder gets its power supply from the radiation field of the reading device by RF/DC rectification. Understandingly, the electronics of the transponder must consume power as little as possible, in order of microwatts.

Passive transponders have been used for sensing for a long time: In [1] a passive temperature sensor in the UHF with analog data transfer is described as early as 1987. Recently, more sophisticated sensor transponders with integrated sensors and digital communication have been reported (e.g. [2]). In this paper a passive sensor transponder with digital communication and an interface for an external capacitive sensor is described.

2. FUNCTIONAL DESCRIPTION

The transponder chip consists of three functional blocks: RF frontend, state machine and analog to digital converter (ADC). The chip was processed with MAS 1,5 µm BiCMOS process to an area of 2.5 * 3.0 mm^2. The chip schematic is presented in Fig. 1 and the photograph in Fig. 2.

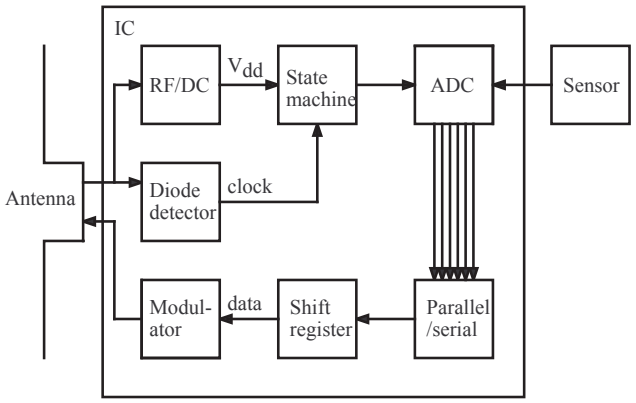

Figure 1: Block diagram of the wireless sensor transponder.

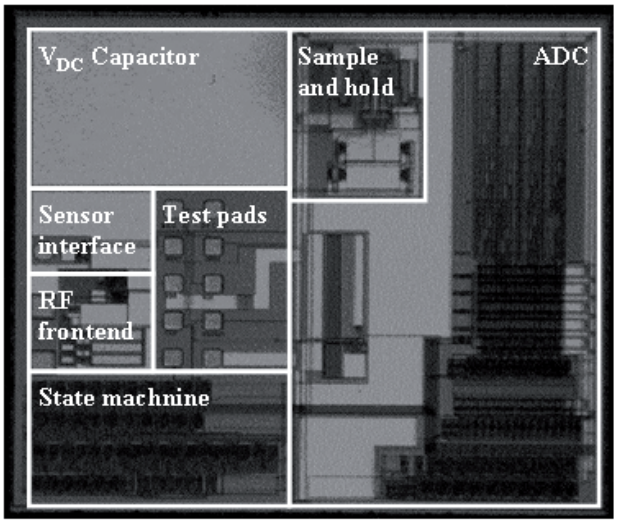

Figure 2: Photograph of the IC chip.

2.1 RF front end

The operating power for the chip is generated by a six diode Schottky ladder followed by a regulator. The RF frontend includes also a diode detector for reader-to-transponder communication. The reader sends clock to the transponder by pulse interval encoding and amplitude modulation, keeping the reader and transponder all the time synchronized [3]. A storage capacitor of several hundred pF is used to provide power for the chip for the short intervals (<10 μs), when RF power from the reader is off due to the modulation.

Communication from the tag to the reader is based on backscattering. The transponder IC modulates its input impedance with a switched capacitor to modulate the radiation scattered from the antenna. Phase modulation of about 35 degrees is achieved.

2.2. State machine

Communication protocol of the sensor system is extremely simplified. The transponder goes through a preprogrammed loop, whenever it gets enough power from the rectifier and a power-on-reset signal. The state machine creates control signals by counting the clock.

The transponder completes a new conversion approximately every 128 clock cycles, which means about 16 times a second with 10 kHz clock used when testing the system. While doing a new conversion, the previous conversion result is simultaneously transmitted to the reader.

2.3 Sensor interface

The analog to digital converter utilises a successive approximation register (SAR) architecture [4] with an offset voltage self-correction sample-and-hold circuit as a front-end [5]. The sensor interface is a capacitive voltage divider, which is charged for every sampling to avoid charge accumulation. The schematic of the ADC and the sensor interface is presented in Fig. 3.

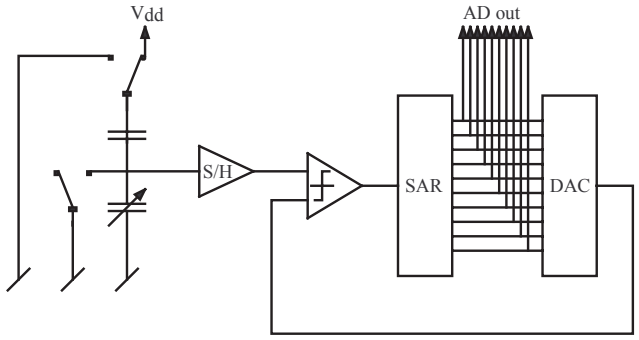

Figure 3. Block diagram of the sensor interface and the SAR based ADC.

3. MEASUREMENT RESULTS

3.1 RF front end

The rectifier power conversion efficiency η is defined as the ratio between output DC power P_{DC} and RF power P_{in} going into the rectifier

$$\eta = \frac{P_{DC}}{P_{in}} = \frac{V_{DC}^2 / R_{DC}}{(1-|\Gamma|^2)P_{RF}}, \qquad (1)$$

where V_{DC} is the output voltage, R_{DC} the load resistance, Γ reflection coefficient and P_{RF} input RF power from the analyser.

The rectifier in the chip has the power conversion efficiency of 0.7 % at output voltage of 1.8 V with a 1.1 MΩ load. In this chip aluminium metallisation was used for Schottky contact. A similar rectifier processed at VTT with Molybdenium Schottkies has efficiency of 12 %. The output voltages of the two rectifiers are presented as a function of ingoing RF power in Fig. 4.

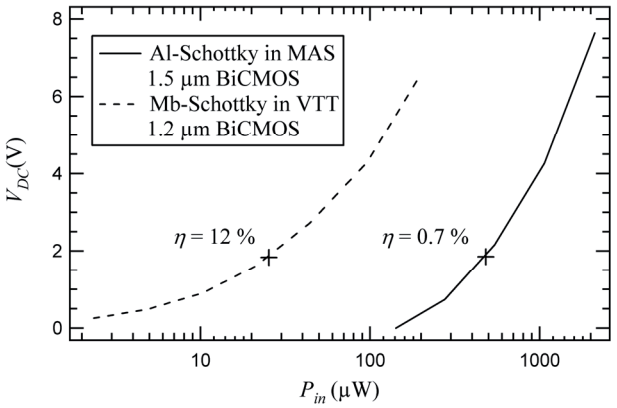

Figure 4. Output voltage V_{DC} of the rectifier as a function of ingoing RF power P_{in} with a 1.1 MΩ load. The rectifier power conversion efficiencies at 1.8 V output voltage are written out.

TRANSDUCERS & EUROSENSORS '07
The 14th International Conference on Solid-State Sensors, Actuators and Microsystems, Lyon, France, June 10-14, 2007

3.2 Analog to digital converter

A separate DC measurement of the ADC yielded the integral (INL) and differential (DNL) nonlinearities to be 3.3 LSB and 4 LSB at 1.8 V, respectively. The nonlinearity measurement results are presented in Figs. 5 and 6. The equivalent number of bits estimated from INL was 8.28 bits. Both static nonlinearities, INL and DNL, can be explained by the low open loop gain of the comparator and by the prevailing noise.

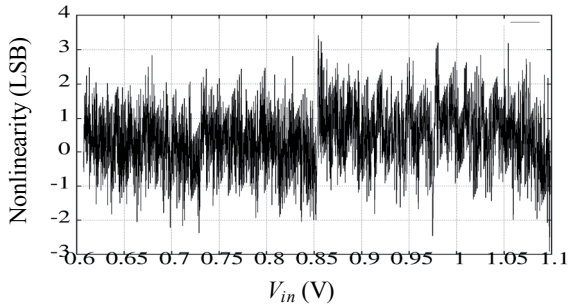

Figure 5. The integral nonlinearity of the ADC vs. input voltage V_{in} at V_{dd} = 1.8 V [6]. © IEEE 2006.

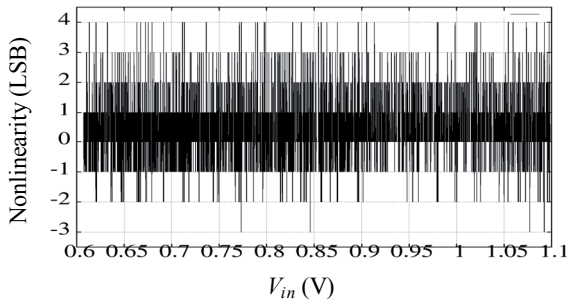

Figure 6. The differential nonlinearity of the ADC vs. input voltage V_{in} at V_{dd} = 1.8 V [6]. © IEEE 2006.

A dynamic measurement was done also, in which a full-range 2 Hz sinusoidal signal was applied into the sample-and-hold (S/H) circuit input. Sampling frequency was 75 Hz. In dynamic measurement the signal to noise ratio (SNR) was 40 dB, and spurious free dynamic range (SFDR) 30 dB for 8 Hz sine. The result of the dynamic measurement was to some extent invalid, because the used signal source was not spectrically pure either, i.e. there were frequency components produced by the signal source at higher frequencies with power levels -40 dBc or lower. The measured stand-by power consumption was 2.3 µW at 1.8 V, which met the specification.

3.3 Wireless measurement

To demonstrate the chip functionality wirelessly, the chip was connected by wire bonding and a matching circuit to a λ/2-dipole (Fig. 7). The measurement was carried out at 869 MHz with transmit power 0.5 W erp. The conversion result as a function of the measured capacitance in the wireless measurement is presented in Fig. 8.

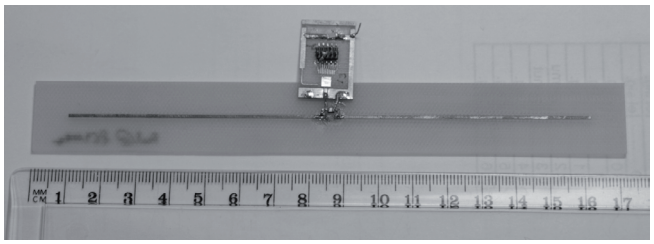

Figure 7. The demonstrator transponder. The IC chip (shiny rectangle) was wire bonded on a carrier, which was connected with a matching network to a λ/2-dipole. Above the chip, there is a connector for diagnostic outputs of the IC and a chip capacitor, which was measured.

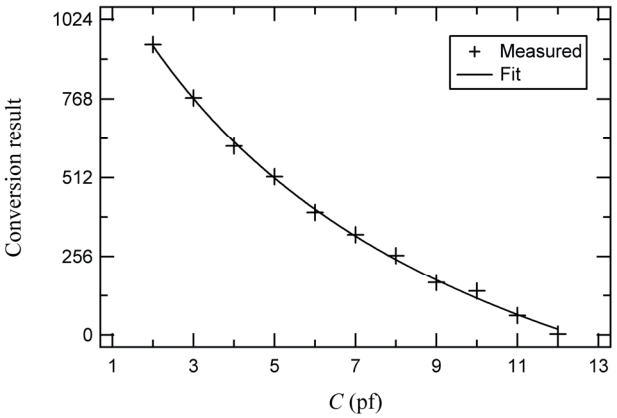

Figure 8. The conversion result and theoretical fit as a function of capacitance C in a wireless measurement.

The observed operating distance with transmit power 0.5 W erp was about 30 cm. The operating distance in this case is power transfer limited. This can be seen from Fig. 9, where communication in the system is demonstrated. The signal to noise ratio in the receiver is very good. Thus the operating distance is proportional to the square root of the rectifier efficiency η. Using the VTT process allows a considerable improvement in the operating distance.

1-4244-0842-3/07/$20.00©2007 IEEE

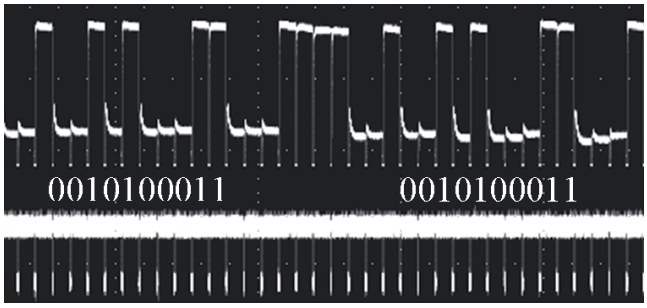

Figure 9. Communication in the wireless sensor system seen with an oscilloscope: The upper trace shows transponder response with conversion result written out. Between the conversion results a header is transmitted. The lower trace shows clock signal sent by the reader to the transponder.

4. CONCLUSIONS

In this paper a sensor transponder for UHF RFID was described. The chip includes a 10 bit analog to digital converter and is designed for external capacitive sensors. The chip power consumption is about 30 μW_{DC}.

Wirelessly powered measurement of capacitance was demonstrated at 869 MHz to a distance of 30 cm, which is short in comparison with the operating distances of several meters of the commercial UHF RFID transponders, but which only include memory. Furthermore, the short operating distance is mostly due to the low efficiency of the rectifier, which was realised using standard aluminium metallisation of the process.

Future and ongoing work of the authors includes realising a similar chip with the VTT process, which enables a better rectifier, as well as capacitive MEMS sensor integration on the same chip.

ACKNOWLEDGMENTS

This work has been financially supported by Tekes, the Finnish Funding Agency for Technology and Innovation, and EU under the sixth framework.

REFERENCES

[1] X. Q. Bao, W. Burkhard, V. V. Varadan, V. K. Varadan, "SAW temperature sensor and remote reading system," IEEE Ultrasonics Symposium, 1987, pp. 583-586.

[2] N. Cho, S.-J. Song, S. Kim, S. Kim, H.-J. Yoo, "A 5.1-μW UHF RFID tag chip integrated with sensors for wireless environmental monitoring", Proceedings of ESSCIRC, September 12-16, 2005, pp. 279-282.

[3] U. Karthaus, M. Fischer, "Fully integrated passive UHF RFID transponder IC with 16.7-μW minimum RF input power", IEEE J. Solid-State Circuits, volume 38, October 2003, pp. 1602-1608.

[4] J. Sauerbrey, D. Schmitt-Landsiedel, R. Thewes, "A 0.5V, 1mW successive approximation ADC", Proceedings of ESSCIRC, September 24-26, 2002, pp. 247-250.

[5] L. Ferreira, R. Moreno, T. Pimenta, C. Filho, "A precise sample-and-hold circuit topology in CMOS for low voltage applications with offset voltage self correction", IEEE International Conference on Communications, Circuits and Systems, volume 2, June 29-July 1, 2002, pp. 914-917.

[6] J. Marjonen, R. Alaoja, H. Ronkainen, M. Åberg, "Low power successive approximation A/D converter for passive RFID tag sensors", Proceedings of the 10th Biennial Baltic Electronics Conference, October 2-4, 2006, pp. 107-110.

Millimeter-Wave Identification

A New Short-Range Radio System for Low-Power High Data-Rate Applications

In: IEEE Transactions on Microwave Theory and Techniques 2008. Vol. 56, No. 10, pp. 2221–2228.

Millimeter-Wave Identification—A New Short-Range Radio System for Low-Power High Data-Rate Applications

Pekka Pursula, Tauno Vähä-Heikkilä, *Member, IEEE*, Alexandru Müller, *Member, IEEE*, Dan Neculoiu, *Member, IEEE*, George Konstantinidis, Aarne Oja, and Jussi Tuovinen

***Abstract*—The radio-frequency identification (RFID) concept is expanded to millimeter-wave frequencies and millimeter-wave identification (MMID) in this paper. The MMID concept and a comparison with UHF RFID are presented, showing the limitations and benefits of MMID. Three feasible applications are suggested for MMID, which are: 1) wireless mass memory; 2) an automatic identification system with pointing functionality; and 3) transponder communication with automotive radar. To demonstrate the feasibility of the MMID system, experimental results for both downlink and backscattering-based uplink are presented at 60 GHz.**

***Index Terms*—Backscattering, millimeter waves, millimeter-wave identification (MMID), RF identification (RFID).**

I. Introduction

TODAY, applications of radio-frequency identification (RFID) are widespread [1]. Inductive RFID systems, that operate at low-frequency (LF) and high-frequency (HF) bands are widely adopted, especially for access control, where short operational range and low data rate are sufficient, even desirable. In recent years, the ultra high-frequency (UHF) band has also been utilized for RFID. The UHF RFID systems are radiative, unlike the near-field-based systems at LF and HF, and they offer an operational range of a few meters with low-cost batteryless transponders. This makes UHF RFID tempting for logistics applications, e.g., for tracing postal packages. For some applications, such as tracking the location of transponders, microwave frequencies at the 2.45-GHz industrial–scientific–medical (ISM) band are used. These real-time locating systems (RTLSs) usually require an active transponder, i.e., a transponder with a battery.

Clearly, a tendency to move to ever higher frequencies is seen here. Herein, we propose using millimeter waves for identification applications. Here we call the millimeter RFID millimeter wave identification (MMID).

Manuscript received November 13, 2007; revised July 29, 2008. First published September 23, 2008; current version published October 8, 2008. This work was supported in part by the Amicom Network of Excellence under Grant EU FP6.

P. Pursula, T. Vähä-Heikkilä, A. Oja, and J. Tuovinen are with the VTT Technical Research Centre of Finland, 02044 Espoo, Finland (e-mail: pekka.pursula@vtt.fi.).

A. Müller and D. Neculoiu are with the Institute of Microtechnology (IMT)–Bucharest, 077190 Bucharest, Romania.

G. Konstantinidis is with the Microelectronics Research Group (MRG), Foundation for Research and Technology (FORTH), Institute of Electronic Structure and Laser (IESL), Heraklion, Crete, Greece.

Digital Object Identifier 10.1109/TMTT.2008.2004252

There are several advantages of MMID over RFID. At millimeter waves, e.g., 60 GHz, high data-rate communications with even gigabit data rates can be implemented. Here, an interesting application would be batteryless wireless mass memories that can be read in a few seconds with high data rates. Furthermore, at millimeter waves, directive antennas are small. A reader device with a small directive antenna would provide the possibility of selecting a transponder by pointing toward it. This is not possible in today's UHF RFID systems because directive antennas are too large. A directive reader antenna would help in locating transponders in high-density sensor networks or other places where transponders are densely located, e.g., in item level tagging. Finally, there are already applications where millimeter-wave radars are used, as in automotive radars. These radars could, in principle, be used as MMID reader devices that could communicate with the transponders. Imagine a transponder in a child's clothing that gives a warning to oncoming cars, thus preventing a fatal accident.

There has been some research on RFID at microwaves, at 24 GHz [2], and by the authors at millimeter waves, i.e., at 60 [3] and 77 GHz [4]. These papers, however, focus only on one component of the MMID system, namely, the design and fabrication of a transponder. In this paper, the possibilities and limitations of the MMID system are thoroughly presented.

This paper is organized as follows. In Section II, the overall characteristics of the system are explained and the basic equations for its operation are derived. These equations are then used to identify the three applications suggested. After a more detailed discussion on the system components, an experimental verification of backscattering communication at 60 GHz is presented.

II. General Characteristics

An MMID system consists of two main components, as presented in Fig. 1: a reader device and a transponder or tag.

The basic operation of the system is similar to that of any other RFID system. The transmitter in the reader sends out a modulated continuous wave signal (downlink). The transponder receives the signal, operates according to the detected command, and responds to the reader device (uplink). The response is detected by the receiver of the reader device. This description applies to almost every radio link, but it is the transponder powering and uplink realization that make the RFID and MMID systems unique.

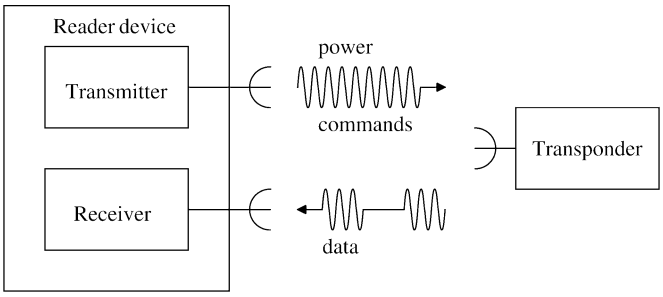

Fig. 1. Components of an MMID system.

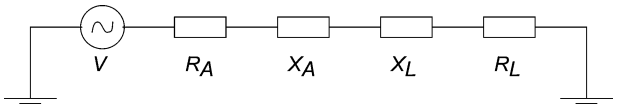

Fig. 2. Series model of a loaded antenna.

A transponder can be powered up in three ways. A passive transponder receives power from the reader transmission. In practice, a rectifier in parallel with the detector is used for generating dc power from the carrier sent by the reader. A semipassive transponder relies on a dc power source, such as a battery, but still uses backscattering for communication. This enables longer operational range than with a passive transponder, while providing a long battery lifetime, because the device does not draw any current from the battery in the absence of the reader. An active transponder is similar to an active radio: it uses a battery for powering an active detector and has an active radio for the uplink.

In RFID or MMID, the uplink is usually realized by modulation of backscattering. Lately, however, active radios have also been referred to as active RFID, when the link has been used for identification applications. This paper will concentrate on backscattering-based uplink.

The backscattering modulation is achieved by modulating the load of the transponder antenna. Thus, the reader receiver and transmitter must be operating simultaneously at the same frequency. The reader device can also be considered a radar: the uplink signal is a faint echo of the reader transmission.

A. Operation Principles

To understand the possibilities and limitations of an MMID system, one can shortly derive a few basic equations of the passive RFID with a backscattering uplink. The derivation is presented in more detail in [5] and [6]. Let us model the transponder as a series model of a reactive antenna (subscript A) and a reactive load (subscript L). The voltage source V in Fig. 2 presents the incoming RF radiation.

The current in the circuit is easily calculated from voltage and impedance. In a conjugate matched case, the power dissipated in load R_L is the transferred power in the Friis equation

$$\frac{V^2}{8R_A} = \frac{G_A\lambda^2}{4\pi}S \tag{1}$$

where S is the power intensity created by the reader device at the transponder and G_A is the transponder antenna gain. The power transfer to the transponder is described by the effective the aperture of the transponder A_e. The aperture A_e is defined as the ratio of power dissipated in the load to the power intensity S, i.e.,

$$A_e = \frac{\frac{1}{2}R_L|I|^2}{S}. \tag{2}$$

Similarly, the scattered power from the transponder is described by the radar cross section σ, which is the ratio of power dissipated in the antenna to the power intensity

$$\sigma = \frac{\frac{1}{2}G_A R_A|I|^2}{S} \tag{3}$$

where the gain G_A represents antenna losses and directivity as the scattered power is reradiated.

To combine (1)–(3), a reflection coefficient Γ is defined as [7]

$$\Gamma = \frac{Z_L - Z_A^*}{Z_L + Z_A} \tag{4}$$

where * denotes a complex conjugate. The equations for effective aperture and radar cross section can then be written as

$$\begin{aligned} A_e &= \frac{G_A\lambda^2}{4\pi}(1 - |\Gamma|^2) \\ \sigma &= \frac{G_A^2\lambda^2}{4\pi}|1 - \Gamma|^2. \end{aligned} \tag{5}$$

The equations are similar in form. They consist of almost similar terms describing the maximum aperture or cross section, multiplied by a distinct mismatch term.

From (5), it seems evident that minimizing the mismatch between the antenna and load gives the best results, but backscattering modulation for the uplink requires us to have two different load impedances at the transponder. Assuming a square wave modulation between two impedance states, namely, Γ_1 and Γ_2, another set of equations can be written as follows:

$$\begin{aligned} A_e^m &= \frac{G_A\lambda^2}{4\pi}\left(1 - \frac{1}{2}[|\Gamma_1|^2 + |\Gamma_2|^2]\right) \\ \sigma^m &= \sigma_0 + \sigma_m \\ &= \frac{G_A^2\lambda^2}{4\pi}\left|1 - \frac{1}{2}(\Gamma_1 + \Gamma_2)\right|^2 + \frac{G_A^2\lambda^2}{16\pi}|\Gamma_1 - \Gamma_2|^2 \end{aligned} \tag{6}$$

where a superscript m is added to denote the modulated state. The first term (σ_0) of the radar cross section describes scattering at the carrier frequency, and the other term (σ_m) describes scattering that carries information at the sideband frequencies. Now, the contradiction between good matching and high modulation is evident. The higher the difference between the modulation states, the higher the scattered power is, but the lower the power transferred to the load.

The power P_{tag} transferred from the reader to the transponder can be calculated from the Friis equation

$$P_{\text{tag}} = A_e^m\frac{G_{\text{tx}}P_{\text{tx}}}{4\pi d^2} \tag{7}$$

where subscript tx denotes reader transmitter and d is the distance between the transponder and reader. The minimum power

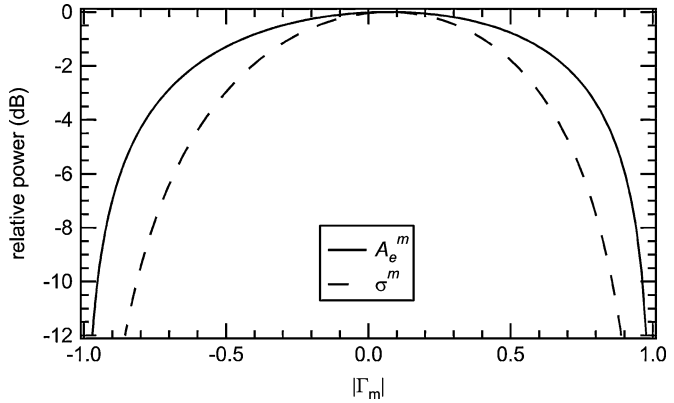

Fig. 3. Effect of mismatch Γ_m to the antenna aperture A_e^m and modulated radar cross section σ^m. Both are scaled to 0 dB at peak value. Values used in calculation: $R_A = R_L = 10\ \Omega$, modulation $\Delta Z = \pm 5\ \Omega$, mismatch purely resistive.

required by the transponder to operate is referred to as $P^0_{\rm tag}$. At UHF, $P^0_{\rm tag}$ can be as low as 10 μW [5], [8].

The power $P_{\rm rx}$ received by the reader is given by the radar equation

$$P_{\rm rx} = \sigma_m \frac{\lambda^2 G_{\rm tx} P_{\rm tx} G_{\rm rx}}{(4\pi)^2 d^4} \tag{8}$$

where subscript rx denotes the reader receiver.

There are, however, four real life phenomena that diminish the operational range from the theoretical limits given by these equations, which are: 1) transmitter noise; 2) mismatch; 3) fading; and 4) polarization.

1) Transmitter Noise: The sensitivity of a radio receiver is usually determined by the thermal, of Johnson noise, of the receiver. The noise is proportional to the noise figure F and bandwidth Δf of the receiver, i.e., $P_n = 4kT\Delta fF$.

In case of backscattering communication, the transmitted signal couples to the receiver through near-field effects in the reader and its antennas and other environment. The attenuation in the coupling can be as low as -30 dB. The transmitted signal carries amplitude and phase noise originating in the oscillator and power amplifier, which can then dominate over the Johnson noise of the receiver.

In the worst case, the order of magnitude of the RF noise can be estimated as follows: a typical phase-locked loop (PLL) oscillator gives a noise floor of -120 dBc/Hz. This signal is amplified to 30 dBm and then coupled to the receiver with -30-dB coupling. Hence, the noise level at the receiver is -120 dBm/Hz, even 50 dB over the Johnson noise. To eliminate this, high isolation between the transmitter and receiver should be achieved.

2) Mismatch: As seen from (6), a certain amount of mismatch is necessary to implement backscattering communication, although good matching is still required. In fact, matching is even more important than usual: the achieved modulation deteriorates faster with growing mismatch than power transfer. This is shown in Fig. 3, where a mismatch $\Gamma_m = \Gamma_m(Z_m)$ is added to (6): $Z_A = Z_L^* + Z_m(\Gamma_m)$.

A typical source of mismatch is a change in the environment within the antenna near field. In general, a change in the transponder antenna surroundings affects the antenna input port impedance. This can dramatically diminish the operational range of the system. This has led to the design of platform-tolerant antennas, especially antennas that can be mounted on dielectric or metal housing [10]. The design goal of these antennas is to minimize the effect of the antenna surroundings on the input impedance of the antenna.

3) Fading: Since the environment is full of reflectors and scatterers, signals arrive at the same point using different paths. This multipath propagation leads to interference. The signals can interfere destructively to create areas of diminished RF field. Measurements on fading in backscattering communication at 2.45 GHz can be found in [11].

4) Polarization: The signal and power transfer are affected by the transponder and reader antenna polarizations. At UHF, usually linearly polarized transponder antennas and circularly polarized reader antennas are used. This ensures operation regardless of polarization, but introduces a loss of -3 dB due to polarization mismatch. The effect of polarization is considered thoroughly in [7].

These four phenomena are highly dependent on the actual implementation of the MMID system. In this study, these phenomena are omitted to give theoretical upper limits to the RFID and MMID operational range. Thus, the Johnson noise is used as a limiting value for reception, and reader sensitivity is assumed to be $p^0_{\rm rx} = -150$ dBm/Hz, which is 20 dB higher than room-temperature Johnson noise. A more thorough treatment of required signal-to-noise (SNR) is presented in [12].

TABLE I
SYSTEM VARIABLES FOR UHF RFID AND MMID

Variable	UHF RFID passive	MMID passive	MMID semipassive
λ	347 mm	5.0 mm	5.0 mm
G_A	0 dBi	0 dBi	0 dBi
$G_{tx}P_{tx}$	33 dBm (erp)	33 dBm (erp)	33 dBm (erp)
G_{rx}	8 dBi	20 dBi	20 dBi
P^0_{tag}	-20 dBm	-20 dBm	-100 dBm
p^0_{rx}	-150 dBm/Hz	-150 dBm/Hz	-150 dBm/Hz
Δf	100 kHz	100 kHz	100 kHz
P^0_{rx}	-100 dBm	-100 dBm	-100 dBm

B. Comparison of MMID and UHF RFID

The carrier frequency of the system affects the components that can be used. Especially at millimeter waves, the small wavelength allows very directive antennas, but also diminishes the antenna effective aperture and radar cross section. This affects the modulation index that should be implemented in the transponder, as well as the feasible applications of the system. Hence a comparison of power transfer and backscattered power in widely adopted UHF RFID and MMID systems is presented. The typical system variables that are used in the comparison are presented in Table I. The main differences in the two systems are the wavelength and reader antenna gain.

The received power $P_{\rm rx}$ and power transferred to the transponder $P_{\rm tag}$ at UHF are presented in Fig. 4 as a function of distance d with several values of the modulation index $|\Gamma_1 - \Gamma_2|$. The horizontal line represents the theoretical limiting power level ($P^0_{\rm tag}$, $P^0_{\rm rx}$) for both of the scales. Thus, the maximum operational range is reached at the first point of intersection. The modulation is assumed to be ideal so that $\Gamma_1 = -\Gamma_2$.

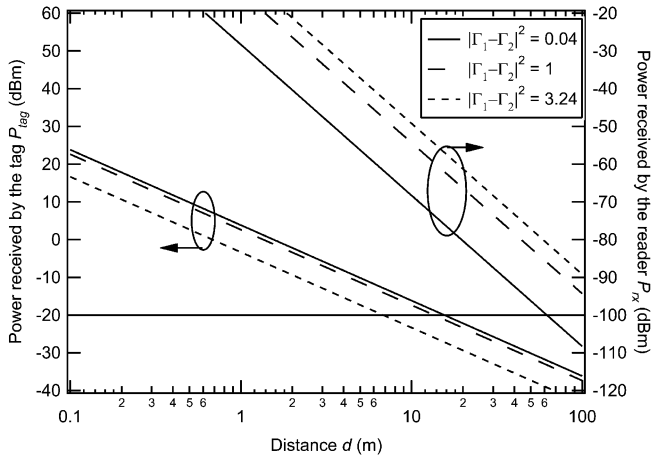

Fig. 4. Limiting factors on the UHF RFID range.

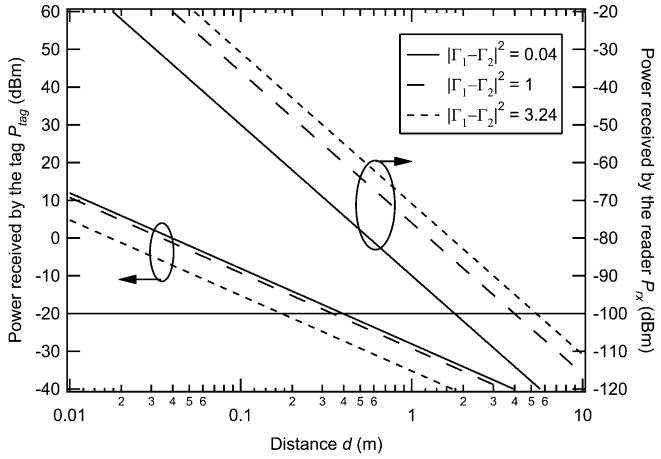

Fig. 5. Limiting factors on the passive MMID range at 60 GHz.

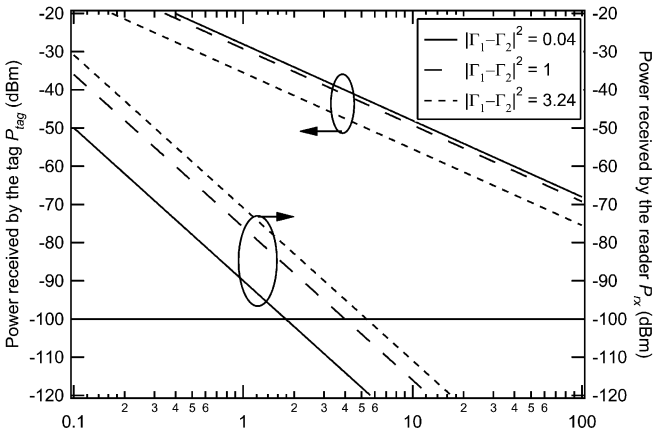

Fig. 6. Limiting factors on the semipassive MMID range at 60 GHz.

Clearly, the UHF RFID is power transfer limited, i.e., the transponder powering limits the operational range. The maximum range is approximately 5 m, and the passive operation of the transponders calls for a relatively shallow modulation.

A similar analysis for passive and semipassive MMID at 60 GHz is presented in Figs. 5 and 6, respectively. Three possible applications for MMID can be seen. A completely passive MMID is power transfer limited to a range of approximately 15 cm. To maximize the operational range of passive MMID, the modulation depth should be very shallow. At very short distances, i.e., at a few centimeters, the SNR of the received signal is very high. Excess SNR enables widening of the signal bandwidth. At a distance of a few centimeters, the SNR is over 10^4 with $\Delta f = 100$ kHz. This scales to a gigahertz bandwidth with unity SNR. However, smaller antennas with lower directivity are needed to satisfy the far-field criterion for the Friis and radar equations [see (7) and (8)] at short ranges. Since a wide bandwidth can be used at 60 GHz, a possible application of passive MMID could be a very short-range communication link, similar to near-field communication (NFC) with very high bandwidth, e.g., passive wireless mass memories.

In semipassive MMID, the transponder is powered by a battery, but the uplink is realized by backscattering. The downlink is limited only by the sensitivity of the transponder detector. A diode detector is efficiently Johnson noise limited, thus a sensitivity of $P^0_{\text{tag}} = -100$ dBm is used.

The limiting factor is the power received by the reader, which gives a maximum operational range of approximately 5 m in Fig. 6. For maximum range, the modulation depth should be maximized. The range could be extended by diminishing the signal bandwidth. This could provide an application similar to the UHF RFID of today—a short (today, typically 96 bit) ID code is transmitted over a distance of a few meters.

At UHF, the reader transmission cannot be efficiently directed and nearby transponders cannot be distinguished spatially. Here, MMID could provide pinpoint accuracy by high gain reader antennas, which provide narrow beam. The cost here is a battery in the transponder, but in sensor nodes or data loggers, the battery is needed for continuous operation also in the absence of the reader.

The operational range of an active MMID is only limited by signal detection at the transponder. Thus, a range of even a hundred meters is feasible, as seen from Fig. 6. This operation mode comes very close to a traditional radio link. This type of an active transponder could be used, for example, to communicate with automotive radars: the radar provides the location of the transponder and the transponder sends back additional information about the object. The system becomes almost symmetrical. The transponder is equipped with an active transmitter, which consumes a lot of power.

III. System Components

A. Transponder

A transponder has four main parts, which are: 1) an antenna; 2) a millimeter-wave front end; 3) a state machine; and 4) a functional block (such as a memory or sensor). The state machine controls the active block as commanded by the reader, e.g., accesses a memory address and streams its contents to the reader. The antenna can be very small in millimeter waves, and it would be tempting to use a high gain antenna in the transponder to increase the operational range. This, however, makes the transponder also directive, i.e., hard to access from any other direction than the main beam—and the direction of the main beam is seldom a fixed parameter in any application.

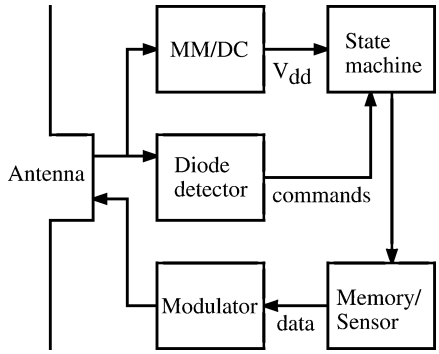

Fig. 7. Block diagram of a possible MMID transponder.

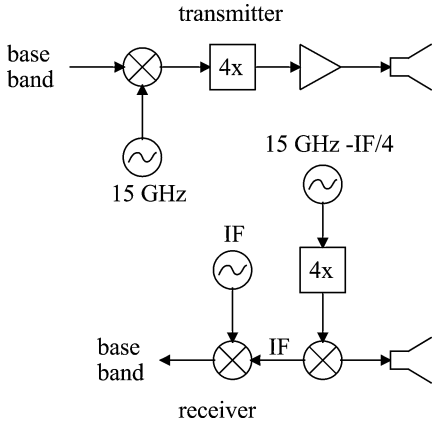

Fig. 8. Block diagram of a possible MMID reader at 60 GHz.

Thus, a relatively low gain antenna with a nearly uniform radiation pattern is preferred.

A passive transponder, as presented in Fig. 7, has the most complex millimeter front end since it requires a rectifier, detector, and modulator. When the incoming millimeter power is strong enough, the rectifier creates enough dc power from the field to power up a passive transponder. In a semipassive or an active transponder, a rectifier is not needed since a battery is used for dc power. At UHF, Schottky diodes and zero-bias transistors are used as rectifying elements. At millimeter waves, feasible elements could be Schottky and other diodes. The rectification is often quite inefficient because of low power and voltage levels. At UHF, the power conversion efficiency from RF to dc is in the order of 10% [13]. Similar efficiencies are to be expected also in MMID.

The modulator is used for changing the antenna load to achieve modulated backscattering for the uplink, as described earlier. This is used in passive and semipassive transponders, but not in active transponders, where an active radio sends the data to the reader. Best modulation depth can be acquired by switching between high- and low-impedance states. A fast switch, such as a diode or transistor-based switch, is required. A diode can also be applied as a modulator by changing the diode bias current. A microelectromechanical systems (MEMS) switch could deliver a very high on/off capacitance ratio, but tends to be quite slow [14].

The detector is required in all types of transponders. A diode is the optimal device because of its simplicity and low power consumption.

In fact, in a semipassive transponder, the front end can actually be simplified down to a single millimeter diode used for both detection and for uplink communication by implementing bias modulation. An optimal choice would be a zero-bias detector diode providing low power consumption while waiting for reader commands. In our proof-of-concept demonstration, we used a semipassive transponder with a Schottky diode [3], [4].

B. Reader Device

An UHF RFID reader usually uses a direct conversion architecture, where the same local oscillator is used for converting the baseband up in the transmitter and down in the receiver. This improves noise performance through noise correlation in down-conversion [15]. At millimeter waves, other solutions may also be useful and the actual reader architecture can vary depending on the MMID application. A possible architecture is presented in Fig. 8. The downlink utilizes amplitude modulation, but the uplink can also use phase modulation. Therefore, quadrature detection may be required.

The reader should have high isolation between the transmitter and receiver because the high-power transmission is present simultaneously at the same frequency as the weak received signal. The dynamic range is formidable: a typical transmission power could be several watts equivalent radiated power (erp). At the same time, the receiver should have as low a noise level as possible. Using the figures in Table I, we get dynamic range of 130 dB! Since this is clearly too much for any active circuit, high isolation between the transmitter and receiver is required.

An advantage of MMID over UHF RFID is the small size of directive antennas. A handheld reader at UHF typically has quite a big antenna, even as large as $(15\ \text{cm})^2$. This size can give approximately 6-dB gain. At millimeter waves, a small planar antenna of $(20\ \text{mm})^2$ can provide over 17-dBi gain (see, e.g., [16]). This enables smaller reader devices. Of course, transponders can also be similarly miniaturized.

IV. Measurement Results

To demonstrate the MMID concept at millimeter waves, both downlink and backscattering measurements are needed. The downlink experiment shows that data can be sent from a reader to a transponder. The backscattering measurement demonstrates the MMID concept itself, showing that a signal transmitted by the reader is modulated by a transponder and a modulated signal is received by the reader.

The measurements demonstrate a semipassive transponder, i.e., the transponder was not remotely powered, but had an external dc power source. The millimeter-wave front end of the transponder (see Fig. 9) consisted of a 60-GHz Yagi–Uda antenna with a monolithically integrated Schottky diode, both supported on a 2-μm-thick GaAs membrane [3]. The device is optimized for a receiver application, but lends itself to demonstrating the MMID operation principle. For a practical MMID application, a less directional antenna with the main lobe orthogonal to the tag plane would be preferable, as in [4].

The bondwires are long, and may operate as antennas at millimeter waves. A low-pass filter isolates the wires from the diode

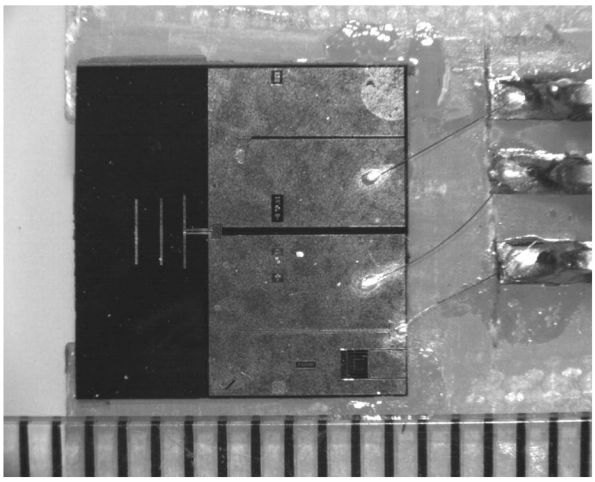

Fig. 9. Transponder used in measurements: on the left is the antenna. The Schottky diode is placed at the feed of the antenna, on the right side of which there is a low-pass filter. On the right, the baseband connector is seen. On the scale below, one tick is 1 mm.

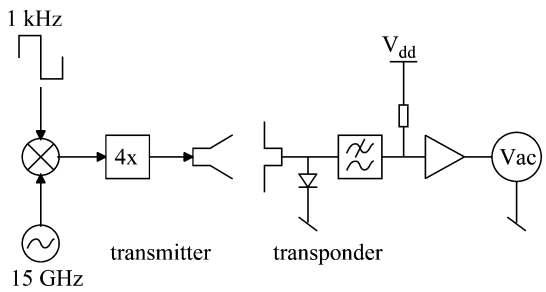

Fig. 10. Setup for downlink measurement.

at millimeter waves. The bondwires scatter, but this scattering is only at the carrier frequency, and does not affect the diode-related scattering at the information band.

A. Downlink

A modulated 60-GHz signal was transmitted to a transponder using a waveguide-based laboratory transmitter (see Fig. 10). The transmitter consisted of a modulated signal generator (Agilent E8257C), multiplier (HP83557A), and a horn antenna. The transmitted power at 60 GHz was 25-dBm erp.

An amplitude modulated signal was transmitted and it was received by the transponder. The detected voltage at the transponder and the transponder sensitivity are shown as a function of distance d between the transponder and the reader in Fig. 11. The detected voltage begins to saturate at low distance because the voltage is very high. This is seen as a drop in detector sensitivity.

The recorded waveforms can be seen in Fig. 12. The results show that downlink data transfer can be performed over a distance of at least 6 m with this measurement configuration. The range can be increased by transmitting more power, using a transponder with a more sensitive receiver and more antenna gain.

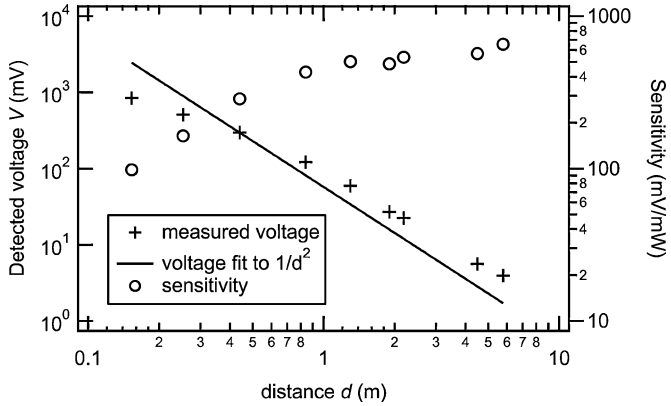

Fig. 11. Voltage detected by the transponder and transponder sensitivity.

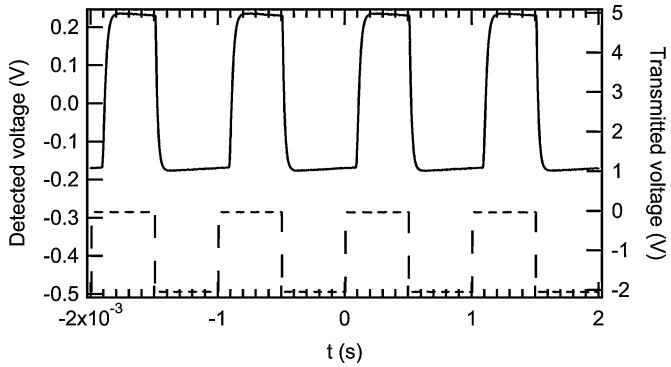

Fig. 12. Example of the waveforms in downlink measurement: detected voltage (solid line) and transmitted voltage (dashed line).

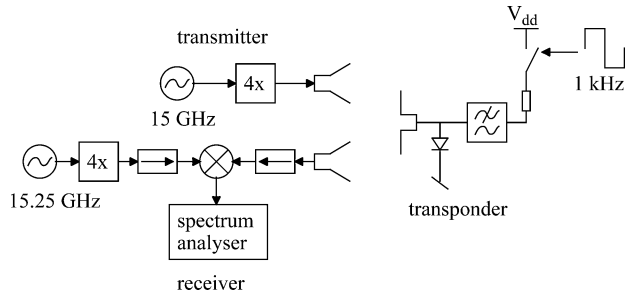

Fig. 13. Setup for uplink measurement.

B. Uplink

The uplink experiment has been used for demonstrating the MMID concept in a similar manner as illustrated in Fig. 1. The goal was to demonstrate modulated backscattering from the transponder. The reader consisted of a waveguide-based transmitter and receiver. The transmitter was the same as in the downlink experiment. The receiver consisted of a signal generator (HP83650A), a multiplier (Spacek Laboratories AV-4XW), a mixer (Spacek Laboratories PV-VB), isolators, and a horn antenna (Fig. 13).

A 60-GHz continuous wave signal transmitted by the reader was modulated with by transponder and the backscattered signal received again with the reader. The received signal was down-converted to 1 GHz and measured with the spectrum analyzer.

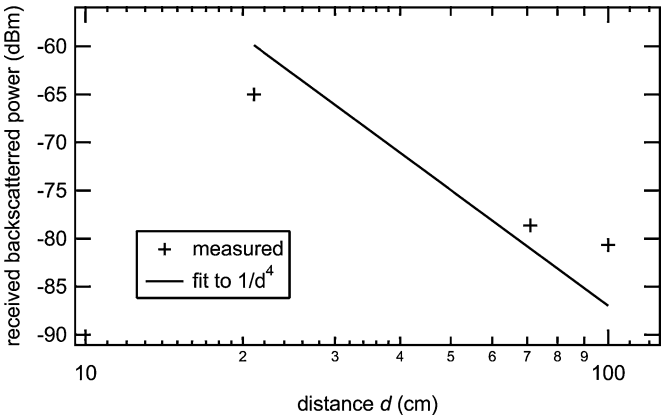

Fig. 14. Backscattered power received by the reader.

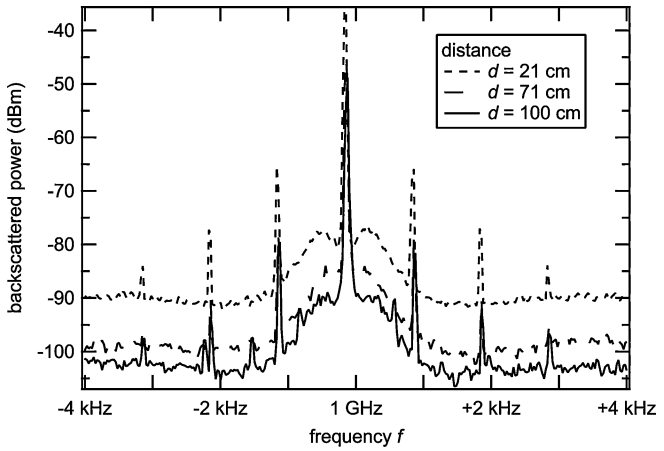

Fig. 15. Measured backscattered spectra. Resolution bandwidth was 100 Hz and averaging 100.

The received backscattered power as a function of distance d is shown in Fig. 14 and the measured spectrum is shown in Fig. 15.

The measurements prove that backscattered power can be used for data transmission at 60 GHz. The bandwidth used here, however, is inconveniently small, which is due to nonoptimal modulation and matching at the transponder. In our previous study related to 77-GHz transponder development, we have demonstrated a similar measurement in [4], where SNR of 20 dB was achieved with 330-kHz modulation, 10-kHz resolution bandwidth, and no averaging.

V. Conclusion

MMID, i.e., backscattering-based communication at millimeter waves, was studied. The general characteristics and limitations of MMID were illustrated: the theory of operation was explained by deriving fundamental equations for remote powering and backscattering-based communication.

A comparison between UHF RFID and MMID showed that MMID will not replace RFID: at UHF, remote powering is feasible to approximately 5 m, which suits today's RFID applications well. Remote powering is limited to tens of centimeters at millimeter waves, but at short range, very wide, even gigabit, data bandwidth can be realized.

Finally, experimental verification of the derived theory was provided at 60 GHz with laboratory equipment. Data transfer from reader to transponder was demonstrated at 6 m. Modulated backscattering was received with small bandwidth up to a of 1 m.

The presented theoretical and experimental considerations prove that backscattering can be used for data transmission at millimeter waves, and thus MMID is feasible.

References

[1] K. Finkenzeller, *RFID Handbook*, 2nd ed. New York: Wiley, 2003.

[2] E. M. Biebl, "RF systems based on active integrated antennas," *Int. J. Electron. Commun. (Arch. Elektr. Ubertragung)*, vol. 57, no. 3, pp. 173–180, 2003.

[3] D. Neculoiu, A. Müller, D. Vasilache, M. Dragoman, I. Petrini, C. Buiculescu, G. Konstantinidis, A. Stavinidris, Z. Hazoupulos, N. Kornilios, T. Vähä-Heikkilä, P. Pursula, L. Bary, R. Plana, and D. Dascalu, "GaAs membrane-supported 60 GHz receiver with Yagi–Uda antenna," in *Proc. 8th Int. RF MEMS RF Microsyst. Conf., MEMSWAVE 2007*, Barcelona, Spain, Jun. 26–29, 2007, pp. 15–18.

[4] A. Müller, D. Neculoiu, P. Pursula, T. Vähä-Heikkilä, F. Giacomozzi, and J. Tuovinen, "Hybrid integrated micromachined receiver for 77 GHz millimeter wave identification systems," in *37th Eur. Microw. Conf.*, Munich, Germany, Oct. 2007, pp. 1034–1037.

[5] U. Karthaus and M. Fischer, "Fully integrated passive UHF RFID transponder IC with 16.7-μW minimum RF input power," *IEEE J. Solid-State Circuits*, vol. 38, no. 10, pp. 1602–1608, Oct. 2003.

[6] P. Pursula, M. Hirvonen, K. Jaakkola, and T. Varpula, "Antenna effective aperture measurement with backscattering modulation," *IEEE Trans. Antennas Propag.*, vol. 55, no. 10, pp. 2836–2843, Oct. 2007.

[7] P. V. Nikitin and K. V. S. Rao, "Antennas and propagation in UHF RFID systems," in *IEEE Int. RFID Conf.*, Las Vegas, NV, Apr. 16–17, 2008, pp. 277–288.

[8] N. Cho, S.-J. Song, S. Kim, S. Kim, and H.-J. Yoo, "A 5.1-μW UHF RFID tag chip integrated with sensors for wireless environmental monitoring," in *Proc. ESSCIRC*, Sep. 12–16, 2005, pp. 279–282.

[9] K. Penttilä, L. Sydänheimo, and M. Kivikoski, "Implementation of Tx/Rx isolation in an RFID reader," *Int. J. Radio Freq. Identification Technol. Appl.*, vol. 1, no. 1, pp. 74–89, 2006.

[10] M. Hirvonen, P. Pursula, K. Jaakkola, and K. Laukkanen, "Planar inverted-F antenna for radio frequency identification," *Electron. Lett.*, vol. 40, no. 14, pp. 848–849, Jul. 2004.

[11] D. Kim, M. A. Ingram, and W. W. Smith, Jr., "Measurements of small-scale fading and path loss for long range RF tags," *IEEE Trans. Antennas Propag.*, vol. 51, no. 8, pp. 1740–1749, Aug. 2003.

[12] J.-P. Curty, M. Declercq, C. Dehollain, and N. Joehl, *Design and Optimization of Passive UHF RFID Systems*. Berlin, Germany: Springer, 2007.

[13] J. Zbitou, M. Latrach, and S. Toutain, "Hybrid rectenna and monolithic integrated zero-bias microwave rectifier," *IEEE Trans. Microw. Theory Tech.*, vol. 54, no. 1, pp. 147–152, Jan. 2006.

[14] G. M. Rebeiz, *RF MEMS: Theory, Design, and Technology*. New York: Wiley, 2003.

[15] J.-H. Bae, J.-C. Kim, B.-W. Jeon, J.-W. Jung, J.-S. Park, B.-J. Jang, H.-R. Oh, Y.-J. Moon, and Y.-R. Seong, "Analysis of phase noise requirements on local oscillator for RFID system considering range correlation," in *37th Eur. Microw. Conf.*, Munich, Germany, Oct. 2007, pp. 1664–1667.

[16] A. Lamminen, J. Säily, and A. Vimpari, "60 GHz patch antennas and arrays on LTCC with embedded-cavity substrates," *IEEE Trans. Antennas Propag.*, Jan. 2008, accepted for publication.

Pekka Pursula received the M.Sc. degree (with distinction) in technical physics from the Helsinki University of Technology (TKK), Helsinki, Finland, in 2002.

In 2002, he was with Philips Medical Systems Finland, where he developed RF systems in magnetic resonance imaging (MRI). Since 2003, he has been with the VTT Technical Research Centre of Finland, Espoo, Finland. He has authored or coauthored over ten refereed scientific publications. He has three patent applications pending. His current research interests include backscattering communication, RFID systems, and wireless sensors.

Mr. Pursula was the recipient of the 2004 Young Scientist Award presented at the URSI/IEEE 29th Convention on Radio Science, Espoo, Finland.

Tauno Vähä-Heikkilä (S'00–M'06) received the B.Sc. degree in space physics and M.Sc. degree in applied physics from the University of Turku, Turku, Finland, in 2000 and 2001, respectively, and the Dr. Tech. degree from the Helsinki University of Technology (TKK), Espoo, Finland, in 2006.

Since 2000, he has been with MilliLab, VTT Technical Research Centre of Finland, Espoo, Finland, where he is currently a Senior Research Scientist and Team Leader involved with adaptive radio systems. From 2002 to 2003, he was a Visiting Scholar with The University of Michigan at Ann Arbor. He has authored or coauthored over 50 scientific publications. His research interests include technology, circuit, and system development for reconfigurable radios from handsets to millimeter-wave applications.

Alexandru Müller (M'94) was born in Bucharest, Romania, in 1949. He received the Ph.D. degree in semiconductor physics from Bucharest University, Bucharest, Romania, in 1990.

He is the Head of the RF Microelectromechanical Systems (MEMS) Laboratory, National Institute of Research and Development in Microtechnologies (IMT)–Bucharest, Bucharest, Romania. He has authored or coauthored over 100 papers published in journals and conference proceedings. His main areas of expertise are microwave and millimeter-wave devices, micromachining of silicon and GaAs, manufacturing of membrane-supported microwave and millimeter-wave circuits based on silicon and GaAs micromachining, and acoustic devices on III-nitride semiconductors.

Dr. Müller and his team were involved in four European projects (in the programs FP4, FP6, and FP7). He coordinated one of the first European projects in RF MEMS "MEMSWAVE" (1998–2001). The MEMSWAVE project was nominated in 2002 as one of the ten finalists projects for the Descartes Prize.

Dan Neculoiu (M'06) received the M.Sc. degree in electronics and Ph.D. degree in electronic devices and circuits from the Polytechnic University of Bucharest, Bucharest, Romania, in 1985 and 1997, respectively.

Since 2005, he has been a Full Professor with the Electronics Department, Polytechnic University of Bucharest. His teaching interests focus on microwave devices and circuits, electronic devices and circuits, microsensors, and RF MEMS. Since 1996, he has been a Part-Time Research Scientist with the National Institute of Research and Development in Microtechnologies (IMT)–Bucharest, Bucharest, Romania. His current research interests are the design, modeling, and characterization of microwave and millimeter-wave circuits and systems based on semiconductor micromachining technologies. He has authored or coauthored over 60 refereed and invited technical papers.

Dr. Neculoiu has been a member of the European Microwave Association since 2004.

George Konstantinidis received the Ph.D. degree in solid-state electronics from the University of Salford, Salford, U.K., in 1987.

Since 1988, he has been a Researcher with the Microelectronics Research Group (MRG), Foundation for Research and Technology (FORTH), Heraklion, Crete, Greece. Since 1991, he has headed the processing research activities of the group and also coordinates research in micromachining technology. He was the Project Manager of the INCO–Copernicus MEMSWAVE Project in which novel nonsilicon RF MEMS components and circuits were fabricated at FORTH. He has authored or coauthored over 120 publications appearing in refereed journals and conference presentations. He has authored five book chapters. He holds one patent.

Dr. Konstantinidis was a runner-up of the 2002 Descartes Prize. He was the recipient of the 2003 Tudor Tanasescu Prize presented by the Romanian Academy of Sciences. In 2005, he was a key member of the EXEL team, which was among the recipients of the 2005 Descartes Prize.

Aarne Oja was born in Espoo, Finland, in 1960. He received the Dr.Tech. degree (with distinction) in technical physics from the Helsinki University of Technology (HUT), Helsinki, Finland, in 1988.

Until 1995, he investigated nuclear magnetism in metals at nanokelvin temperatures. Since 1995, he has been with the VTT Technical Research Centre of Finland, Espoo, Finland, where his research has focused on MEMS sensors and components, MEMS-based timing circuits, and remote sensors. Since 2000, he has been a Research Professor of sensor technology at the VTT Technical Research Centre of Finland. Since 2006, he has been the Vice President of the VTT Technical Research Centre of Finland.

Jussi Tuovinen received the Dipl.Eng., Lic.Tech., and Dr.Tech. degrees in electrical engineering from the Helsinki University of Technology (HUT), Espoo, Finland, in 1986, 1989, and 1991, respectively.

From 1986 to 1991, he was a Research Engineer with the Helsinki University of Technology (HUT) Radio Laboratory, where he was involved with millimeter-wave antenna testing for the European Space Agency (ESA), quasi-optical measurements, and Gaussian beam theory. From 1991 to 1994 he was with the Five College Radio Astronomy Observatory, University of Massachusetts at Amherst, as a Senior Post-Doctoral Researcher, where he studied holographic test methods for large telescopes and developed frequency multipliers up to 1 THz. From 1994 to 1995, he was a Project Manager with the HUT Radio Laboratory, where he was involved with hologram CATR and 119-GHz receiver development for the Odin satellite. From 1995 to 2004, he was the Director of the Millimetre Wave Laboratory of Finland (MilliLab), European Space Agency (ESA) External Laboratory. He is a co-investigator heading the development of 70-GHz receivers for the low-frequency instrument of the ESA Planck Mission. Since 1999, he has been a Research Professor with the VTT Technical Research Center of Finland, Espoo Finland. From 2001 to 2002, he was a Visiting Researcher with the University of Hawaii at Manoa, where he developed multipath communications methods using retrodirective antennas. From 2004 to 2005, he was the Research Director of VTT Information Technology. He is currently Vice President, Research and Development, Microtechnologies and Sensors, VTT Technical Research Center of Finland. He has authored or coauthored over 170 scientific papers. His research activities also include development of methods for on-wafer testing of integrated circuits and components, as well as imaging systems and MEMS at millimeter wave.

Dr. Tuovinen is a past secretary of the Finnish National Committee on Space Research (COSPAR) and the IEEE Finland Section. He was also the executive secretary of the Local Organizing Committee of the 27th Plenary Meeting of COSPAR, held in 1988. In 1998, he was the cochairman of the Second ESA Workshop on Millimeter Wave Technology and Applications. He has also served as a chairman of the IEEE Microwave Theory and Techniques (MTT)/Antennas and Propagation (AP) Finland Chapter. In 2003, he served as the chairman of the Third ESA Workshop on Millimeter Wave Technology and Applications. Since 2005, he has been the chairman of the Finnish Society of Electronics Engineers. He was the recipient of an ESA Fellowship for multiplier work at the University of Massachusetts at Amherst (1992 and 1993).

Planar Inverted-F Antenna for Radio Frequency Identification

In: IEE Electronics Letters 2004.
Vol. 40, No. 14, pp. 848–849.

Planar inverted-F antenna for radio frequency identification

M. Hirvonen, P. Pursula, K. Jaakkola and K. Laukkanen

A small and low-cost antenna solution for radio frequency identification (RFID) tags is presented. The impedance of the antenna is designed to match directly to the impedance of the RFID microchip. Also, the impedance of the antenna is immune to the platform. Thus, the antenna is applicable in many different environments. The design and measurement results are reported and discussed.

Introduction: Radio frequency identification has lately gained much interest in several service industries. Inductively coupled short-range RFID is already widely used, but demand is growing in the field of long-range identification, where electromagnetic waves and an antenna are used for coupling [1]. However, many challenging features are required from the antenna intended to be used in long-range RFID tags. First, the antenna has to be really small, preferably low-profile, in order to be usable. Secondly, the fabrication has to be inexpensive, since RFID tags are generally designed to be disposable. In passive systems the signal power received by the antenna supplies the microchip. Thus, a perfect impedance match between the antenna and the RFID microchip is essential in order to sustain the power supply of the chip. The impedance level of the chip usually differs from the common 50 Ω case, and the matching has to be direct, since matching networks cannot be used because of the cost and size limitations. More importantly, the matching has to hold in any environment. Since in RFID applications tags are attached directly to different kinds of objects, the impedance tolerance to the platform is a key issue.

Printed dipole antennas may be used in RFID tags, but their performance is highly platform dependent. Conversely, microstrip patch antennas are more tolerant to the effects of the platform, but are very large in size. By using a planar inverted-F antenna (PIFA) structure smaller size may be achieved, but generally at the cost of reduced tolerance to the environment [2]. To meet the challenging demands of long-range RFID, a platform-tolerant design of PIFA is presented in this Letter.

Antenna design: The geometry of the developed antenna is presented in Fig. 1. At the operation frequency of 869 MHz the antenna is only 3 mm (0.013λ) high and the patch is 45 mm (0.19λ) wide. The patch and the ground plane are square in shape. The antenna is filled with Teflon in the area under the patch. According to preliminary experiments cheaper polyethylene may also be used.

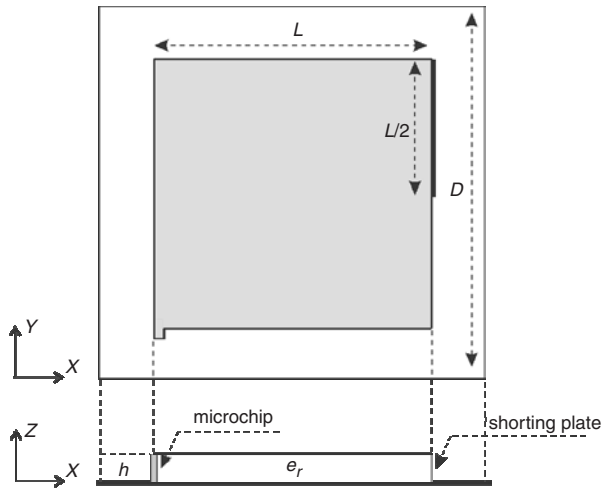

Fig. 1 *Antenna design*

The microchip feed is placed on one corner and the shorting plate is half the width of the patch edge. In this case the impedance of the antenna is matched to $(7-j170)$ Ω. With this design it is possible to achieve immunity to different platforms. The ground plane is optimised to be as small as possible (59 mm or 0.25λ), while still providing the impedance tolerance to the platform. However, the antenna is rather narrowband and the radiation is almost omnidirectional. Usually these features lead to platform-sensitive impedance behaviour, but in this case also the right radiation mode plays an important role. The main current flow is directed diagonally from the shorting plate to the feed. The patch is not in resonance and there is no dual-resonance with the ground plane near 869 MHz. In addition, it was discovered that with the presented design the radiation from the shorting plate is reduced, leading to better tolerance to different platforms.

Experimental results: The antenna performance was verified with a scattering measurement technique. A microchip with an input impedance of $(7-j170)$ Ω was attached as a feed of the antenna. The chip contains a 200 kHz oscillator which modulates the input reactance of the chip, causing a phase modulation of the backscattered signal. The modulation starts if the chip is fed at least with 10 μW of input RF power. As the limiting power is known, the transmitted power P_{tx} needed to wake up the chip is measured against the frequency to determine the antenna bandwidth, and against the antenna alignment to determine the antenna radiation pattern, i.e. the effective antenna aperture including mismatch is measured. Both the input impedance and the required power level of the chip are similar to that of the RFID chip in the passive long distance multiple access UHF RFID (PALOMAR) system [3].

The performance of the antenna has been studied with different platforms. The results of the bandwidth measurements are presented in Fig. 2 and in Table 1. In Fig. 2 all the peaks have been scaled to 0 dB. The bandwidth is defined as the half-power bandwidth of the antenna aperture, which is equivalent to +3 dB in required transmitted power P_{tx}. As seen from Fig. 2 and Table 1, the centre frequency varies only ±1 MHz around the operation frequency of 869 MHz. Also, the bandwidth varies only from 15 to 17 MHz. It is clear that the impedance and bandwidth variance against different platforms is minimal, indicating very good tolerance to different platforms.

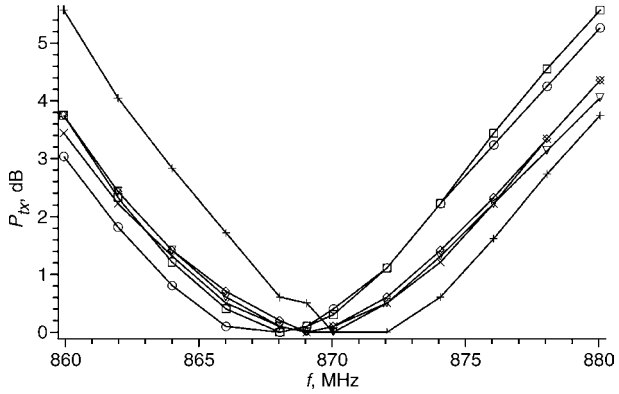

Fig. 2 *Results of bandwidth measurement*
— + — free-space
—◇— metal 150 × 150 mm
—▽— metal 600 × 600 mm
—○— wood
—□— PVC plastic
—×— water canister

Table 1: Measured centre frequencies and bandwidths

Platform	Centre frequency [MHz]	Half-power bandwidth [MHz]
Free-space	870	15
Metal 150 × 150 mm	869	17
Metal 600 × 600 mm	869	17
Wood	868	16
PVC plastic	868	15
Water canister	869	17

The co- and cross-polarisation radiation patterns measured with the scattering technique are presented in Fig. 3. It is evident that the antenna is rather omnidirectional with a simulated directivity of only 1.5 dBi. Also, the antenna has a rather high cross-polarisation level, which has to be considered in developing the reader device. Otherwise the orientation of the tag may have a major impact on the reading

reliability. Also, the three-dimensional radiation patterns were measured with a traditional far-field measurement system. From these results the radiation efficiency could be calculated exploiting the spherical wave expansion. The radiation efficiency of the antenna varied between 50 and 60% depending on the platform.

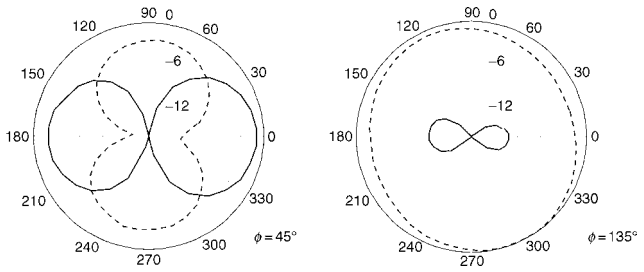

Fig. 3 *Measured radiation patterns*

—— E_ϕ
- - - - E_θ

Table 2: Maximum reading distances

Platform	Maximum reading distance, m
Free-space	2.0
Metal 150 × 150 mm	5.1
Metal 600 × 600 mm	4.3
Wood	3.9
PVC plastic	3.2
Water canister	2.0

The maximum reading distances were studied with the PALOMAR system, using the maximum allowed transmission power of 0.5 W ERP. The reading distances of the antenna on different platforms are presented in Table 2. Because of different directivity values on different platforms, the reading distances vary between 2 and 5 m. It is clear that the antenna operates satisfactorily on every tested platform, but the best performance is achieved on metal.

Conclusions: A compact and low-cost antenna applicable to RFID tags has been developed. By using a certain design an RFID microchip may be directly matched to the antenna. More importantly, a platform-independent impedance behaviour can be achieved. Also, the antenna has adequate bandwidth and radiation characteristics. Because of these features, the antenna is applicable in several RFID environments, e.g. on metal, wood and plastic surfaces or even on a water canister.

Acknowledgment: This work has been supported by Tekes, The National Technology Agency of Finland.

27 April 2004
Electronics Letters online no: 20045156
doi: 10.1049/el:20045156

M. Hirvonen, P. Pursula, K. Jaakkola and K. Laukkanen (*VTT Information Technology, PO Box 1202, FIN-02044 VTT, Finland*)

E-mail: mervi.hirvonen@vtt.fi

References

1 Finkenzeller, K.: 'RFID handbook' (John Wiley & Sons, Chichester, UK, 2003)
2 Huynh, M.C., and Stutzman, W.: 'Ground plane effects on planar inverted-F antenna (PIFA) performance', *IEE Proc., Microw. Antennas Propag.*, 2003, **140**, (4), pp. 209–213
3 The Palomar project: 'Passive long distance multiple access UHF RFID system', European Commission, Public Report, Project Number IST1999-10339, November 2002

Antenna Effective Aperture Measurement with Backscattering Modulation

In: IEEE Transactions on Antennas and Propagation 2007.
Vol. 55, No. 10, pp. 2836–2843.

Antenna Effective Aperture Measurement With Backscattering Modulation

Pekka Pursula, Mervi Hirvonen, Kaarle Jaakkola, and Timo Varpula

***Abstract*—A scattering measurement method for antenna characterization is described. The antenna backscattering is modulated by an oscillator circuit. The modulation begins, when a known RF power is transferred to the oscillator circuit from the antenna. This enables the measurement of the effective aperture of the antenna, from which the antenna bandwidth and radiation pattern are obtained. A theory for antenna aperture measurement is developed using a simple circuit model for the antenna—oscillator system. A dipole and a PIFA with a reactive input impedance at the application frequency were measured. The antenna aperture was measured to an accuracy of 9%, and the measurements complied with simulated and measured references. The method provides simple and accurate bandwidth and radiation pattern measurements with the reactive load the antenna is designed to work with.**

***Index Terms*—Antenna measurements, apertures, radar cross sections, scattering.**

I. Introduction

SINCE the pioneering work of King in 1949 [1], the study of antenna backscattering has developed into a very diverse field of study. The methods have developed far beyond the measurement of the radar cross section (RCS) of the antenna. Several authors have demonstrated backscattering-based methods for measuring the antenna gain (e.g., [2] and [3]) and the antenna input impedance (e.g., [3] and [4]). In most methods, the antenna under test is connected to known passive loads, but also negative resistance devices have been used [5]. Because the methods require the measurement of the power level of the scattered signal, environmental reflections limit the signal-to-noise ratio and accuracy of the measurement [4].

In this paper, a new approach to backscatter measurement is taken. The antenna under test is connected to an oscillator, which modulates the backscattered signal. This enables measuring the effective antenna aperture (also antenna aperture, or aperture, in this paper) and radar cross section associated with the modulated backscattering.

The oscillator circuit drives a small varactor in the input of the oscillator chip. The oscillator wakes up, when the antenna under test supplies it with enough power. If the RF power required by the oscillator chip is known, the effective antenna aperture can be measured. The method enables a fast and robust way to measure the center frequency, bandwidth and radiation pattern of the antenna under test as was shown, to some extent, in [6].

Manuscript received June 1, 2005; revised April 26, 2007. This work was supported by Tekes, The National Technology Agency of Finland.

The authors are with the VTT Technical Research Centre Finland, Espoo FI-02044, Finland (e-mail: pekka.pursula@vtt.fi).

Digital Object Identifier 10.1109/TAP.2007.905821

The method has been inspired by the need to characterize small radio frequency identification (RFID) antennas. In RFID applications, the antenna is usually directly matched to a capacitive IC chip. Hence the input impedance of the antenna is inductive, which makes it difficult to measure with conventional transmission techniques. The oscillator IC that is used in the measurements has same input impedance than the RFID chip, which the antenna will actually be used with. This is very important, because high mismatch in the antenna input can affect the current modes in an antenna.

In this paper, measurement results of a dipole and a small PIFA antenna at UHF frequencies are presented. The dipole, with well-known characteristics, is measured, even though its input impedance is nearly real at the application band. To demonstrate the method with a reactive antenna, a PIFA with direct matching to the oscillator chip is measured. The radiation pattern and frequency behavior of the both antennas are measured.

The scattering methods are commonly agreed to give better measurement results than the transmission measurements in the case of small antennas, because there is no feed line to disturb the near fields of the antenna, as is the case with transmission measurements. This is often referred to as a fact, but the effect is rarely demonstrated. The PIFA is designed to be mounted on metal surfaces. The disturbing effect of the feed line can be clearly seen, when the PIFA is measured on different sizes of metal platforms.

This paper proceeds as follows. In the Section II a theoretical model for the antenna—load system is developed and an expression for the effective antenna aperture is derived. The Section II also describes the basic idea of the measurements and considers the effect of different error sources. In Section III measurement results, as well as simulation and reference measurement results are presented.

II. Measurement Method

A. Theoretical Construction

To study the scattering effects on a loaded antenna, the model presented in Fig. 1 was used. The antenna and the load are described as impedances $Z_A = R_A + jX_A$ and $Z_L = R_L + jX_L$, respectively. The antenna resistance consists of the radiation resistance R_R and the dissipations in the antenna R_D, i.e., $R_A = R_R + R_D$. The voltage V is the equivalent voltage generated by the incident wave. This model assumes a reciprocal antenna: the current distributions, and thus antenna characteristics, should be identical for transmission and receiving.

Following the reasoning in [7] and [8] expressions for the effective aperture A_e and the radar cross section σ of the antenna

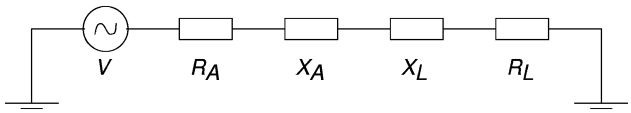

Fig. 1. Series model of a loaded antenna.

can be derived. The RF current I in the circuit can be calculated as

$$I = \frac{V}{Z} = \frac{V}{(R_A + R_L) + j(X_A + X_L)} \tag{1}$$

where Z is the impedance of the circuit. The effective aperture A_e is defined as the ratio of the power dissipated in the load resistance R_L and the power density S of the incident wave, i.e.

$$A_e = \frac{R_L I_{\rm rms}^2}{S} \tag{2}$$

where $I_{\rm rms}$ is the effective RF-current in the circuit. Similarly the radar cross section σ is defined as the power the antenna radiates, i.e., power dissipated in the radiation resistance R_R times the directivity D of the antenna, divided by the power density S

$$\begin{aligned}\sigma &= \frac{DR_R I_{\rm rms}^2}{S} = \frac{\eta D R_A I_{\rm rms}^2}{S} \\ &= \frac{G_A R_A I_{\rm rms}^2}{S}.\end{aligned} \tag{3}$$

Here, η is the radiation efficiency and G_A is the gain of the antenna.

Assuming conjugate matching between the antenna and the load, where $Z_A = Z_L^\dagger$, the maximum power $P_{\rm max}$ transferred from the antenna to the load can be expressed as

$$P_{\rm max} = \frac{V_{\rm rms}^2}{4R_A}. \tag{4}$$

The power $P_{\rm max}$ can be identified with the transferred power of the Friis transmission equation

$$P_{\rm max} = \frac{G_A \lambda^2}{4\pi} S. \tag{5}$$

Combining (1)–(5), expressions for the effective aperture A_e and the radar cross section σ become

$$\begin{aligned}A_e &= \frac{G_A \lambda^2}{4\pi} \frac{4R_A R_L}{(R_A + R_L)^2 + (X_A + X_L)^2} \\ \sigma &= \frac{G_A^2 \lambda^2}{4\pi} \frac{4R_A^2}{(R_A + R_L)^2 + (X_A + X_L)^2}.\end{aligned} \tag{6}$$

The equations consist of a maximum aperture (first fraction) and a second fraction describing the mismatch between the antenna and the load. Equation (6) can be also expressed with a reflection coefficient

$$\begin{aligned}A_e &= \frac{G_A \lambda^2}{4\pi} \left(1 - |\Gamma|^2\right) \\ \sigma &= \frac{G_A^2 \lambda^2}{4\pi} |1 - \Gamma|^2\end{aligned} \tag{7}$$

where the reflection coefficient is defined as

$$\Gamma = \frac{Z_L - Z_A^\dagger}{Z_L + Z_A} \tag{8}$$

and † stands for a complex conjugate.

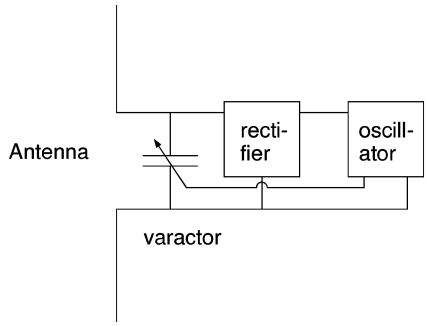

Fig. 2. Block diagram of the antenna—chip system.

In previous studies, the measurement methods have been based on measuring the radar cross section. The antenna can also be characterized by measuring the antenna aperture. To do this, the antenna is connected to an oscillator chip, whose input impedance is known. The chip includes a rectifier, a low-frequency oscillator and a varactor, as sketched in Fig. 2. The chip has no battery, but it extracts all the power it needs from the RF power transmitted by an illuminating antenna. The critical RF power $P_{rf,0}$ the chip requires for the modulation to start, is known.

In this study, two kinds of resonator chips were used, which are described in [8] and [9]. The input impedance of the chips is about $(7 - \mathrm{j}180)\ \Omega$.

When the oscillator drives the varactor at the input of the chip, the input reactance X_L of the chip varies a small amount of ΔX. As seen from (1), a change in chip input reactance modulates the phase of the current in the antenna—chip system. Thus the field scattered from the antenna—chip system is also phase modulated, which is seen as sidebands in the scattered signal. The scattered power is not measured, but only used to indicate the power transferred to the load. Only the transmitted power is measured. This simplifies the measurement apparatus considerably, and enables the center frequency, bandwidth and normalized radiation pattern measurements even in normal laboratory conditions.

Even though it is not necessary to measure the backscattered power, it is interesting to calculate also the radar cross section of the first sideband of the antenna.

B. Effects of Modulation

The analysis in Section II-A was based on the assumption that the input impedance of the oscillator chip is constant. Actually the reactance of the chip is modulated by an amount ΔX. What is the effective impedance of the chip, that is actually seen in the measurements?

If the varactor was in the same state all the time, one would measure the antenna aperture given in (6). If the varactor was switched to the other state, one would measure a similar aperture curve, which was shifted to a new center frequency. At a certain frequency, one of the varactor states induces more mismatch to the antenna—chip boundary than the other state. In the higher mismatch state, less RF power is transferred into the chip than in the other varactor state. The oscillator has to get enough DC power to function in the both states of the varactor, for the modulation to function properly.

Without DC capacitors, the chip has to get enough RF power for the oscillator to function in the higher mismatch state of the varactor. In this case, the limiting power $P_{rf,0}$ would refer to different states of the varactor, and hence to different input impedances of the chip, on different sides of the aperture peak.

But, because the chip has relatively big DC capacitors, the energy charged in the capacitors can be used to drive the oscillator over the higher mismatch state of the varactor. Of course, in the lower mismatch state the chip has to get some extra RF power to charge the capacitors. This averaging behavior leads to a situation, where the critical power $P_{\mathrm{rf},0}$ refers to neither of the varactor states, but to a state, which corresponds to the rms-current in the antenna—chip system.

To calculate the rms-current the modulation has to be fixed. For a square wave modulation, the impedance of the antenna—chip system is

$$Z(t) = \begin{cases} R + j(X + \Delta X) & -T/2 < t < 0 \\ R + j(X - \Delta X) & 0 < t < T/2 \end{cases} \tag{9}$$

where $R = (R_A + R_L)$, $X = (X_A + X_L)$ and T is the period of the modulation. Now the effective current can be expressed as an integral

$$\begin{aligned} I_{\mathrm{rms}}^2 &= \frac{V^2}{T} \int_{-T/2}^{T/2} \frac{\sin^2(\omega_0 t)}{|Z(t)|^2} dt \\ &= \frac{V_{\mathrm{rms}}^2}{2} \left(\frac{1}{R^2 + (X + \Delta X)^2} \right. \\ &\qquad \left. + \frac{1}{R^2 + (X - \Delta X)^2} \right) \end{aligned} \tag{10}$$

where $\omega_0 \gg 1/T$ is the RF frequency. Now the aperture becomes

$$A_e = \frac{\lambda^2 G_A}{4\pi} \left(\frac{2R_A R_L}{R^2 + (X + \Delta X)^2} + \frac{2R_A R_L}{R^2 + (X - \Delta X)^2} \right). \tag{11}$$

Especially interesting are the two limits of the mismatch reactance X

$$A_e = \begin{cases} \frac{\lambda^2 G_A}{4\pi} \frac{4R_A R_L}{R^2 + \Delta X^2} & X \ll \Delta X \\ \frac{\lambda^2 G_A}{4\pi} \frac{4R_A R_L}{R^2 + X^2} & X \gg \Delta X. \end{cases} \tag{12}$$

At the sides of the peak, where $|X|$ is big, the modulation does not affect the aperture. But in the middle of the peak, where $X = 0$, the aperture is reduced due to the modulation. In other words, the modulation flattens the aperture peak.

Measuring the aperture requires only the measurement of the critical transmit power $P_{tx,0}$, but it is interesting to study the scattered power also. To derive a theoretical expression for the power in the sidebands, the baseband current in the antenna—chip system is expressed as a Fourier series $I = 1/2 I_0 + \Sigma_n (I_{n,\sin} \sin(n\omega_m t) + I_{n,\cos} \cos(n\omega_m t))$, where ω_m is the modulation frequency. The Fourier coefficients are

$$\begin{aligned} I_0 &= \frac{2V}{T} \int_{-T/2}^{T/2} \frac{dt}{Z(t)} \\ &= 4V \frac{R + jX}{(R + jX)^2 + \Delta X^2} \\ I_{n,\sin} &= \frac{2V}{T} \int_{-T/2}^{T/2} \frac{\sin(n\omega_m t)}{Z(t)} dt \\ &= \begin{cases} \frac{4V}{n\pi} \frac{j\Delta X}{(R + jX)^2 + \Delta X^2} & n \text{ odd} \\ 0 & n \text{ even} \end{cases} \\ I_{n,\cos} &= \frac{2V}{T} \int_{-T/2}^{T/2} \frac{\cos(n\omega_m t)}{Z(t)} dt \\ &= 0. \end{aligned} \tag{13}$$

The effective RF current corresponding to one of the first sidebands is $I_{\mathrm{rms}}^2 = 1/8 I_{1,\sin}^2$. Two factors of 1/2 arise because of baseband and RF "root-mean-squaring." The third factor discards power in the other of the first sidebands. Thus the effective current describes power in only one of the symmetric first sidebands. The power in the sideband can also be described by a radar cross section σ_1, which can be calculated from the effective current using (3)–(5)

$$\sigma_1 = \frac{\lambda^2 G_A^2}{4\pi} \frac{16}{\pi^2} \frac{R_A^2 \Delta X^2}{\left(R^2 + X^2 + \Delta X^2\right)^2 + 4R^2 X^2}. \tag{14}$$

C. Measurement Procedure

The measurement setup is shown in Fig. 3. It consists of a continuous wave transmitter and a receiver with a spectrum analyzer. The oscillator IC chip is connected to the antenna under test (AUT), which is attached to a rotating mount.

The loaded antenna is illuminated with the transmitter, which creates a power intensity S at the antenna under test. In each

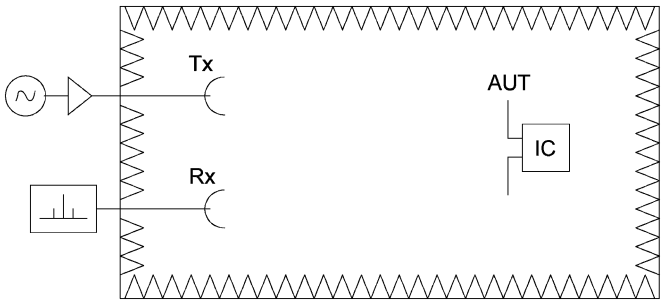

Fig. 3. Measurement setup.

measurement point, the transmitted power P_{tx} is increased until the modulation wakes up, i.e., the sidebands are detected at the receiver. At this critical transmission power $P_{tx,0}$, the IC chip gets just enough power to function, i.e., the rf power $P_{\rm rf}$ coupled to the oscillator chip is the known critical power $P_{\rm rf,0}$, which the chip needs to function. The critical transmission power $P_{tx,0}$ is recorded to calculate the antenna aperture. The received power at the sideband frequency $P_{rx,1}$ was recorded to test (14).

The effective aperture A_e and the radar cross section of the first sideband σ_1 are defined as

$$A_e = \frac{P_{\rm rf}}{S}$$
$$\sigma_1 = \frac{P_{\rm sc,1}}{S} \tag{15}$$

where $P_{\rm sc,1}$ is the power scattered from the antenna at sideband frequency.

Because the power intensity S is proportional to the transmitted power P_{tx}, it can be measured at a single reference power level $P_{tx,\rm ref}$, and then scaled

$$S = \frac{P_{tx}}{P_{tx,\rm ref}} S_{\rm ref} \tag{16}$$

where $S_{\rm ref} = S(P_{tx,\rm ref})$. The transmitted power is increased until the modulation wakes up. At this power level, the IC chip gets just enough power to function. In other words $P_{\rm tx} = P_{tx,0}$ and $P_{\rm rf} = P_{\rm rf,0}$. Now the antenna aperture and the radar cross section can be expressed as

$$A_e = \frac{P_{\rm rf,0}}{S_{\rm ref}} \frac{P_{tx,\rm ref}}{P_{tx,0}}$$
$$\sigma_1 = \frac{(4\pi d)^2}{\lambda^2 G_{rx}} \frac{P_{rx,1}}{S_{\rm ref}} \frac{P_{tx,\rm ref}}{P_{tx,0}} \tag{17}$$

where d is the distance between antenna under test and receiver antenna. The power propagation from the antenna under test to the receiver has been calculated with Friis equation. The reference power intensity $S_{\rm ref}$ can be measured to quite a high accuracy with the same equipment used in the actual measurement.

D. Error Analysis

Most antenna scattering measurement methods require the power level measurement of the scattered field. Usually the antenna is connected to a passive load and the scattered field is at the same frequency than the transmitted field. In this kind of a measurements, the transmitted field connects through environment or directly to the receiver, which severely impairs the receiver sensitivity. Thus complicated decoupling and background cancellation systems (e.g., [3]) has been used. In the aperture method described here, the power level of the scattered field is not measured, but only the transmission power, which is much easier to do with high accuracy.

Even if one measures the scattered power, direct coupling is not a problem, because the scattered signal is transferred to sidebands.

On the other hand, the aperture method requires exact knowledge of the required RF power of the oscillator chip. This is not trivial to measure with high accuracy due to the reactive input impedance of the chip. There is also some hysteresis in the rectifier as a function of incoming power. Thus care has to be taken in the measurements, to sweep the transmission power always in the same direction.

Another common error source is the repositioning error in scattering methods, that require antenna under test to be measured with different loads (for example, [3] and [4]). In the aperture method, only one load is used, but the measurement of the reference power intensity at AUT is required. This introduces some repositioning error. But repositioning error gives rise much faster to phase than power level errors [4]. Because in aperture method only power level is measured, repositioning error is not a major problem.

The aperture measurement suffer of course from environmental reflections, which effect the power intensity at antenna under test. But this is taken care of by the reference power intensity measurement.

A quantitative analysis in measurement error can be calculated by using a total differential of the antenna aperture in (17). This yields a relative error of the form

$$\frac{\Delta A_e}{A_e} = \frac{\Delta P_{\rm rf,0}}{P_{\rm rf,0}} + \frac{\Delta P_{tx,\rm ref}}{P_{tx,\rm ref}} + \frac{\Delta P_{tx,0}}{P_{tx,0}} + \frac{\Delta S_{\rm ref}}{S_{\rm ref}} \tag{18}$$

where prefix Δ refers to the uncertainty of the quantity.

The power levels can be measured to an accuracy of 0.1 dB with basic measurement equipment, except the required RF power $P_{\rm rf,0}$. This was measured to an accuracy of 6%. Adding up the terms, a relative error of 9% is acquired.

Similar error analysis can be carried out for the radar cross section of the first sideband in (17). Now there are more error sources, but they can be measured to an accuracy on 0.1 dB, or 1% quite easily, for required RF power $P_{\rm rf,0}$ is not included. Thus, the estimated error is 7%.

III. Measurement Results

In this section measurements of two antennas are described. First, a dipole antenna is measured due to its well-known characteristics. The oscillator chip used in the measurements has a capacitive input impedance, and thus an external matching circuit is needed. The dipole was measured in an ordinary laboratory environment, to demonstrate the robustness of the measurement system.

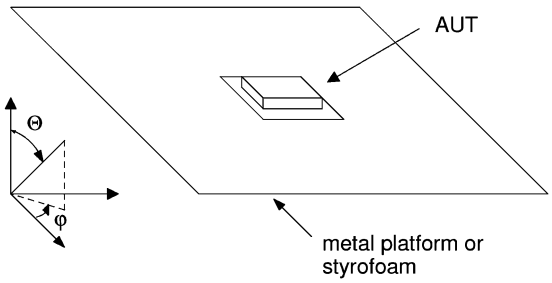

Fig. 4. PIFA (AUT) attached to platform.

The measurement method is well suited for measuring antennas with reactive input impedance. Thus a modified planar inverted antenna (PIFA), with direct impedance matching to the oscillator chip, is measured. The antenna under test is a PIFA that has been designed for RFID applications at 869 MHz band [10]. The antenna is designed to be attached on metal platforms. Hence the measurements were carried out on metal platforms of different sizes, and on a styrofoam support, to simulate the free space condition. The PIFA on an platform is presented in Fig. 4. The PIFA measurements were carried out in an anechoic chamber.

Two kinds of measurements were carried out. In bandwidth measurement, the critical transmitted power $P_{tx,0}$ was measured at different frequencies. In radiation pattern measurement, the critical power was measured as a function of antenna alignment. First the radiation pattern measurement is considered.

A. Radiation Pattern Measurements

To measure the normalized power radiation pattern P_n, one does not have know the reference power intensity S_{ref} or the critical rf power $P_{\mathrm{rf},0}$ in (17). If the measurement setup is stable, these quantities remains constant through the measurement. Because the antenna aperture is the measure of the power transfer between the antenna and the load, the radiation pattern can be calculated as

$$P_n(\varphi,\Theta) = \frac{A_e(\varphi,\Theta)}{A_{e,\max}} = \frac{P_{tx,0,\min}}{P_{tx,0}(\varphi,\Theta)} \tag{19}$$

where the $A_{e,\max} = \max(A_e(\varphi,\Theta))$ is the maximum aperture, which corresponds to the minimum critical transmitted power $P_{tx,0,\min} = \min(P_{tx,0}(\varphi,\Theta))$. Note that (19) holds exactly only, if the frequency remains constant, as is the case when measuring the radiation pattern.

The error analysis is quite straightforward taking total differential of (19). The uncertainty in the measured power levels was 0.1 dB, which leads approximately to an overall error $\Delta P_n = 0.2\ \mathrm{dB}$.

The dipole antenna is 15 cm in length, and resonating at about 870 MHz as such. The antenna is a little shorter than a $\lambda/2$-dipole, as real implementations of the dipole antenna tend to be. The dipole antenna was connected to the oscillator chip with a Π-type LC matching circuit. The matching was best at 850 MHz, at which frequency the radiation pattern was measured. The measured radiation pattern of the dipole is presented in Fig. 5, as well as theoretical radiation pattern of a $\lambda/2$ -dipole from [7]. As can be seen from the figure, the patterns are almost identical.

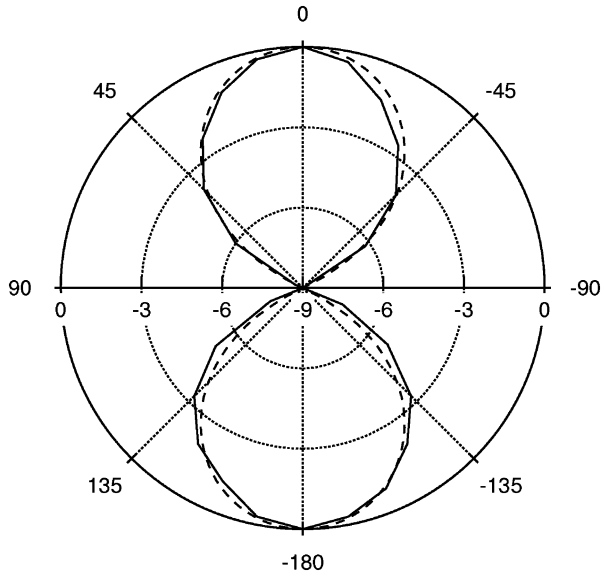

Fig. 5. Measured (—) and theoretical (- -) radiation patterns in decibels of the dipole antenna.

The measured radiation patterns of both polarizations in a main plane ($\phi = 135°$) of the PIFA are presented in Fig. 6. Both polarizations are scaled to main polarization main beam value. These results can be compared to simulated radiation patterns in Fig. 7 and transmission measurement results in Fig. 8. In the transmission measurements the AUT was fitted to a 50 Ω feed line with a strip line fitting network. To reduce the amount of metallic feed line near the antenna, the fitting network was connected to other measurement apparatus through an optical link. The antenna mounting, including the platform, was identical to the aperture measurement. The antenna was fed through the metal platform.

The results of the transmission measurements differ from the other results significantly, especially in free space, where there is no metal plane to screen the feed line from the antenna. As the radiation patterns become more similar when the size of the metal platform grows, it seems that the feed line and the fitting network disturb the antenna radiation. Thus the transmission measurement results cannot be used as a absolute reference for the aperture method.

The simulated and aperture method radiation patterns are almost identical. Only on the biggest metal platform a difference is seen. The biggest measured metal platform was only $(600\ \mathrm{mm})^2$ in area, but simulations were performed on an infinite platform, which explains the difference.

B. Bandwidth Measurements

The critical power was measured as a function of frequency with a step of a few MHz. The measurements were carried out for the dipole antenna and for the PIFA on different platforms. The antenna aperture was calculated using (17) and the relative error was approximated in Section II-C to be about 10%, mainly from the uncertainty in $P_{\mathrm{rf},0}$.

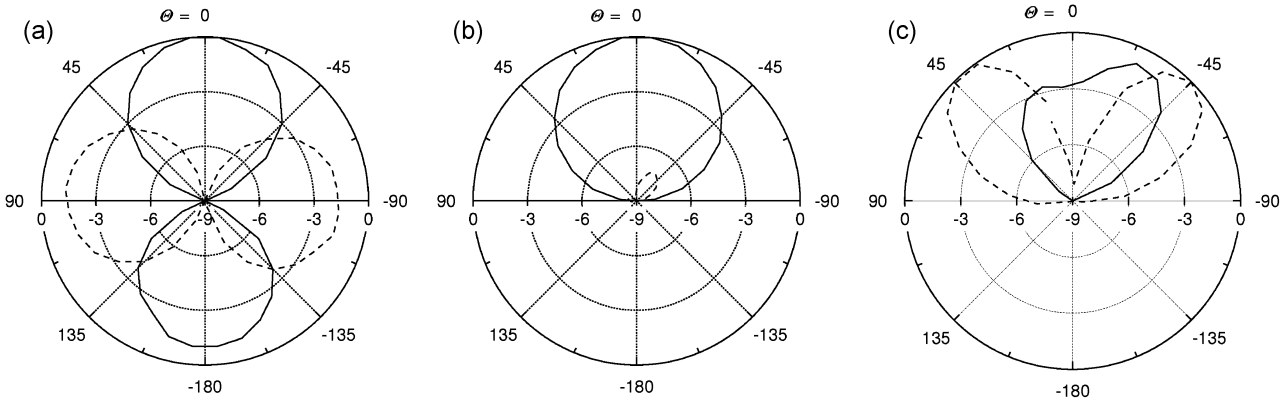

Fig. 6. Radiation patterns in decibels of the PIFA measured with the aperture method: (a) in free space, (b) on $(150\ \mathrm{mm})^2$ metal, and (c) on $(600\ \mathrm{mm})^2$ metal. Solid line (—) present the co-polarization and dashed line (- -) the cross-polarization radiation pattern.

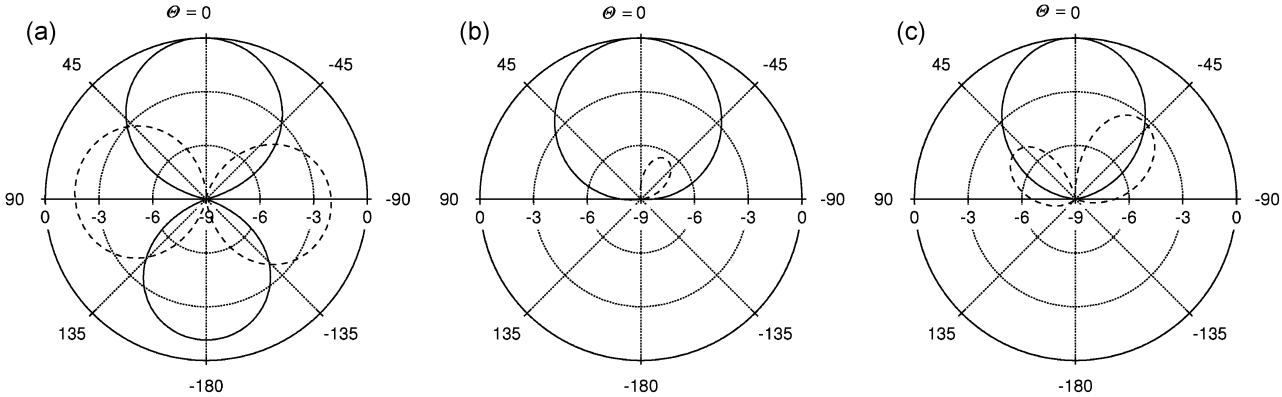

Fig. 7. Radiation patterns in decibels of the PIFA simulated with HFSS: (a) in free space, (b) on $(150\ \mathrm{mm})^2$ metal, and (c) on infinite metal. Solid line (—) present the co-polarization and dashed line (- -) the cross-polarization radiation pattern.

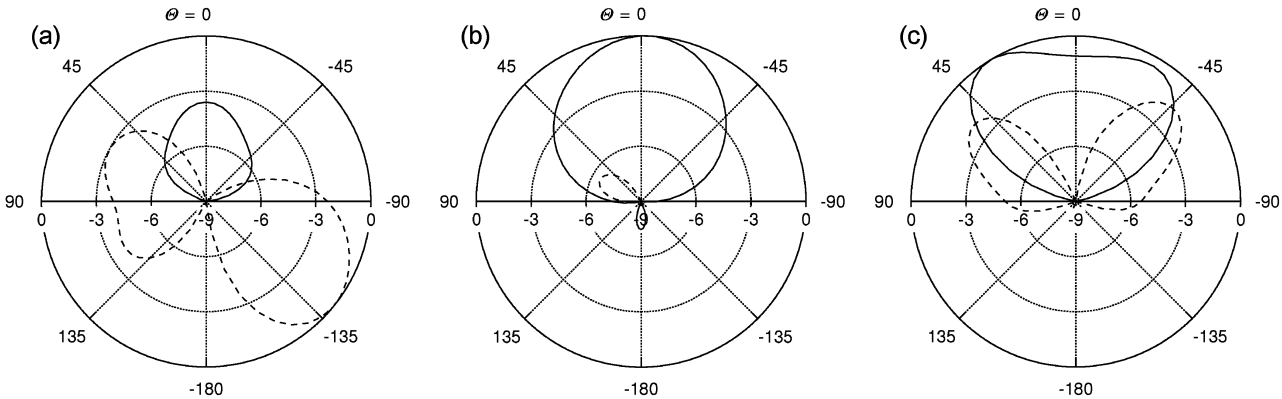

Fig. 8. Radiation patterns in decibels of the PIFA measured with the transmission method: (a) in free space, (b) on $(150\ \mathrm{mm})^2$ metal, and (c) on $(600\ \mathrm{mm})^2$ metal. Solid line (—) present the co-polarization and dashed line (- -) the cross-polarization radiation pattern.

To calculate the absolute value of the aperture, the RF power required by the chip has to be known. The required RF power was measured in a test fixture with a network analyzer (VNA). The required power of the oscillator chip used in PIFA measurements was measured to be $P_{\mathrm{rf},0} = (16 \pm 1)\ \mu\mathrm{W}$. This is in line with [8], which describes the chip used.

In the case of the dipole, the oscillator was connected to the VNA with the LC matching circuit used with the antenna. The required power of the chip connected to the matching circuit was measured to be $P_{\mathrm{rf},0} = (25 \pm 1)\ \mu\mathrm{W}$. The input impedance $Z_{\mathrm{in,osc}}$ of the oscillator chip connected to the matching circuit was measured to calculate a reference. The dipole input impedance $Z_{\mathrm{in,dip}}$ is well known, and can be calculated for example from a circuit model presented in [11]. Now the antenna aperture of the dipole can be calculated with (7) and theoretical dipole gain. The measured antenna aperture of the dipole and the calculated reference are presented in Fig. 9.

The matching circuit has a strong effect to the measured peak shape: The matching was designed for an average state of the chip, but the reference does not take into account the modulation. Nevertheless, the curves are almost identical in magnitude and in shape for about −3 dB from the aperture maximum. When comparing the curves, one must remember that the relative error in the circuit model is 6%, which is almost enough

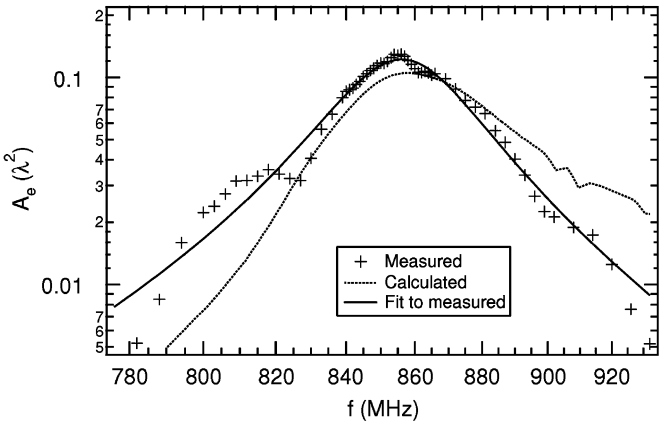

Fig. 9. Measured aperture of the dipole and a calculated reference.

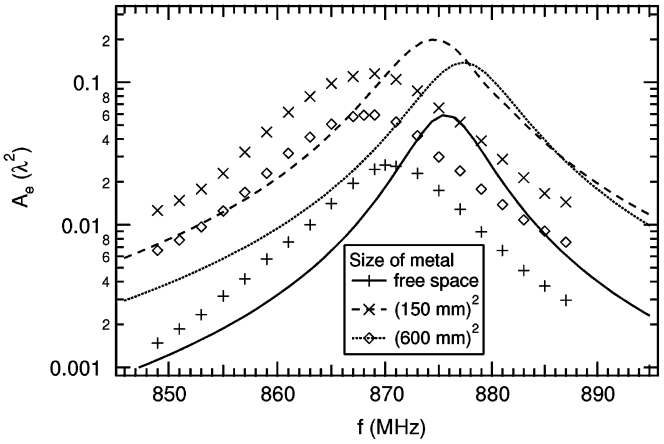

Fig. 10. Measured (markers) and calculated (lines) apertures of the PIFA on different platforms as a function of frequency.

to explain the difference in the curves. The measured maximum aperture at 854 MHz is $0.13\lambda^2$, which is almost exactly the theoretical maximum [$\Gamma = 0$ in (6)].

For the PIFA, a reference was calculated in similar way. Values for antenna gain and impedance were simulated with HFSS and measured values of the oscillator chip input impedance were used. The measured and calculated apertures for the PIFA is presented in Fig. 10.

The calculated and measured curves are similar in shape, but shifted in frequency. This can be either a simulator or a measurement error. The simulated peaks are narrower, and about 3 dB higher than measured ones. This is due to the flattening effect of the modulation, as seen from (12). As the chip reactance is modulated by $\Delta X \approx R_L$, a flattening of about 3 dB is only to be expected.

Also the radar cross section of the first sideband was measured. In Fig. 11 the measured aperture and radar cross section of the PIFA in free space are presented. The uncertainty was estimated in Section II-C, giving $\Delta\sigma_1/\sigma_1 = 7\%$.

The figure illustrates the fact that the effect of mismatch at the antenna—chip interface has a stronger effect to the radar cross section than the aperture. This is also seen in the expressions of A_e and σ_1 [(11) and (14)]: the aperture $A_e \propto X^{-2}$, but the radar cross section $\sigma_1 \propto X^{-4}$.

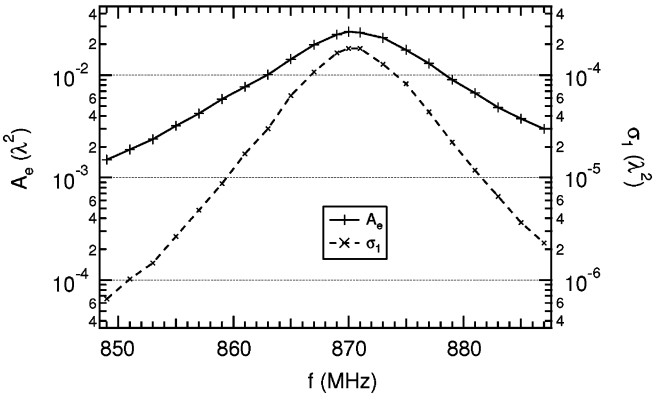

Fig. 11. Measured aperture A_e and radar cross section σ_1 of the PIFA in free space.

IV. Summary and Conclusion

A new method utilizing backscatter data to characterize antenna was presented. The method is based on backscattering modulation, which is achieved by connecting the antenna to a IC chip that consists of an oscillator driven modulator. The method enables the measurement of the antenna aperture and radar cross section of the modulated signal. Because carrier signal coupling from transmitter to receiver does not disturb the measurement, the measurement apparatus is very simple and quite accurate results can be acquired even in normal laboratory conditions.

The method was justified theoretically, and expressions for the antenna aperture and the radar cross section were derived with and without backscattering modulation. It was shown, that the modulator in the antenna load flattens the measured antenna aperture peak.

Radiation pattern and bandwidth measurements are simple and accurate with the introduced method. One reference measurement for the power intensity S is required for determining the absolute value of the antenna aperture, which essentially describes the antenna gain including mismatch at antenna input. From bandwidth measurements, the center frequency and bandwidth can be accurately determined.

A dipole antenna was measured near 869 MHz with the aperture method to demonstrate the method with a well known antenna. The measured radiation pattern was almost identical to the theoretical dipole radiation pattern. The measured frequency behavior was compared to a calculated frequency behavior. In the middle of the peak the curves differed less than 10% in value, and were of identical shape.

Because the method is well suited for measuring also antennas with reactive input impedance, a reactive RFID antenna with direct impedance matching was measured. The radiation pattern measurement results were similar to simulations and traditional transmission method measurement results, except that the disturbing effect of the feed line when measuring small antennas with transmission measurement technique was clearly seen. The measured center frequency of the PIFA differed from simulated values about 5 MHz. The simulated peaks were narrower and higher, which was only to be expected, because of the load modulation.

In general, the introduced method complied very well with the calculated and measured references.

ACKNOWLEDGMENT

The authors would like to thank Mr. O. Jaakkola for his contribution to the concept of the study. The IC chips were manufactured by Atmel Germany GmbH.

REFERENCES

[1] D. D. King, "Measurement and interpretation of antenna scattering," *Proc. IRE*, vol. 37, pp. 770–777, Jul. 1949.
[2] W. Wiesbeck and E. Heidrich, "Wide-band multiport antenna characterization by polarimetric RCS measurements," *IEEE Trans. Antennas Propag.*, vol. 46, pp. 341–350, Mar. 1998.
[3] J. Appel-Hansen, "Accurate determination of gain and radiation patterns by radar cross-section measurements," *IEEE Trans. Antennas Propag.*, vol. AP-27, pp. 640–646, Sep. 1979.
[4] J. T. Mayhan, A. R. Dion, and A. J. Simmons, "A technique for measuring antenna drive port impedance using backscatter data," *IEEE Trans. Antennas Propag.*, vol. 42, pp. 526–532, Apr. 1994.
[5] R. F. Harrington, "Field measurements using active scatterers," *IEEE Trans. Microw. Theory Tech.*, vol. MTT-11, p. 454, Sep. 1963.
[6] P. Pursula, T. Varpula, K. Jaakkola, and M. Hirvonen, "Antenna radiation characterization by backscattering modulation," in *Proc. URSI/IEEE XXIX Nat. Convention on Radio Science, VTT Symp. 235*, Nov. 2004, pp. 115–118 [Online]. Available: http://www.vtt.fi/inf/pdf/symposiums/2004/S235.pdf
[7] J. D. Kraus, *Antennas*. New York: McCraw-Hill, 1950, pp. 41–56.
[8] U. Karthaus and M. Fischer, "Fully integrated passive UHF RFID transponder IC with 16.7- μW minimum RF input power," *IEEE J. Solid-State Circuits*, vol. 38, pp. 1602–1608, Oct. 2003.
[9] Application note, ATA5590 Tag Antenna Matching [Online]. Available: http://www.atmel.com/dyn/resources/prod_documents/doc4843.pdf cited Sep. 4, 2006
[10] M. Hirvonen, P. Pursula, K. Jaakkola, and K. Laukkanen, "Planar inverted-F antenna for radio frequency identification," *Electron. Lett.*, vol. 40, pp. 848–850, Jul. 2004.
[11] T. G. Tang, Q. M. Tieng, and M. W. Gunn, "Equivalent circuit of a dipole antenna using frequency-independent lumped elements," *IEEE Trans. Antennas Propag.*, vol. 41, pp. 100–103, Jan. 1993.

Pekka Pursula was born in Vantaa, Finland, in 1978. He received the Master of Science (Tech.) degree (with distinction) in technical physics from Helsinki University of Technology (TKK), Espoo, Finland, in 2002.

In 2002, he was with Philips Medical Systems Finland developing RF systems in magnetic resonance imaging. Since 2003, he has been with the VTT Technical Research Centre of Finland, Espoo. His present research interests include RFID systems and wireless sensors.

Mr. Pursula received the Young Scientist Award at the URSI/IEEE XXIX Convention on Radio Science, Espoo, Finland, in November 2004.

Mervi Hirvonen received the Master of Science (Tech.) and Licentiate of Science (Tech.) degrees in electrical engineering from Helsinki University of Technology (TKK), Espoo, Finland, in 2004 and 2006, respectively.

Since 2002, she has been with the VTT Technical Research Centre of Finland, Espoo, initially as a Research Trainee and, since 2004, as a Research Scientist. Her current research interests include antennas and electromagnetics related to wireless sensors, RFID systems and mobile communications.

Kaarle Jaakkola was born in Helsinki, Finland, in 1976. He received the Master of Science (Tech.) degree in electrical engineering from Helsinki University of Technology (TKK), Espoo, Finland, in 2003.

Since 2000, he has been working with the VTT Technical Research Centre of Finland, Espoo, first as a Research Trainee and, since 2003, as a Research Scientist. From 2000 to 2002, he participated in the Palomar (EC IST) project developing RF parts for a new RFID system. His current research interests include RFID systems, wireless and applied sensors, antennas, electromagnetic modelling, and RF electronics.

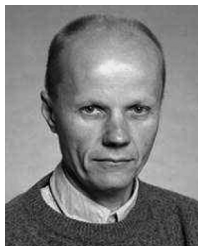

Timo Varpula was born in Seinjoki, Finland, in 1954. He received the Doctor degree from Helsinki University of Technology (TKK), Espoo, Finland, in 1982.

At TKK, he conducted research on weak magnetic fields produced by the human brain, eye, and heart. He also developed superconducting magnetometers and data analysis for biomagnetic signals. From 1983 to 1986, he worked as a Project Manager at Instrumentarium Corporation, Ltd., where he developed whole-body nuclear magnetic resonance imaging systems. After joining the VTT Technical Research Centre of Finland, Espoo, he was Section Leader from 1986 to 1994 and conducted research on measurement devices for metrological and industrial purposes. In 1994 to 2004, he worked as a Group Manager at VTT Automation and VTT Information Technology. In 2004 to 2006, he was the Research Manager at VTT Microsensing. He is presently Technology Manager at VTT Sensors. His research interests include radiofrequency identification, RF, microwave, and wireless sensors for scientific and industrial applications. He has coauthored 32 scientific publications and holds seven patents.

Backscattering-Based Measurement of Reactive Antenna Input Impedance

In: IEEE Transactions on Antennas and Propagation 2008.
Vol. 56, No. 2, pp. 469–474.

Backscattering-Based Measurement of Reactive Antenna Input Impedance

Pekka Pursula, Dan Sandström, and Kaarle Jaakkola

***Abstract*—A scattering technique for measuring reactive antenna input impedance is described. The antenna scattering is measured with three different loads: an open circuit, a conjugate match, and a reactive match. The load reactances tune the antenna into resonance at the measurement band. Theory and error considerations are presented, as well as measurement results of two ultra high frequency radio frequency identification antennas. The measurements were performed in a gigahertz transverse electromagnetic mode cell. The measured impedances are within about 10% of the simulated values for a dipole-like antenna. The results of a planar inverted-F antenna are somewhat more complex, but also supported by the presented simulations and the coaxial impedance measurement results.**

***Index Terms*—Antenna impedance, backscattering, radio frequency identification (RFID), ultra high frequency (UHF).**

I. Introduction

BACKSCATTERING-based antenna input impedance measurement techniques have been studied for decades [1], [2]. These techniques are not widely adopted, even though simple procedures with accurate results, like [3] and [4], have been reported. There are probably two reasons for this: 1) the scattering measurement in general requires sensitive instruments, and 2) in many cases, a feed-line connection to the antenna is needed to obtain results with sufficient accuracy. Recently, however, interest in backscattering measurements have increased, especially with radio frequency identification (RFID)-antennas, where the feed line connection to the antenna port is difficult to obtain. A backscattering-based radar cross-section measurement has been studied recently in [5], but the analysis was not developed far enough to extract the antenna input impedance from the backscattered signal.

In ultra high frequency RFID (UHF RFID), a capacitive integrated circuit (IC) is connected directly to an antenna. Optimizing the efficiency of the RF rectifier of the RFID chip has lead to highly reactive input impedances of the IC. Optimal operation of the transponder, or the tag, requires conjugate matching between the antenna and the IC, resulting in inductive antenna input impedances. The magnitude of reactance of the IC and the antenna can be even ten times higher than the resistance. Antennas like this cannot be simply connected to a 50 Ω feed line for input impedance measurement. A matching circuit could be used, but this does not remove the feed line, which affects the antenna behavior. In addition, the frequency behavior of the matching circuit differs from the behavior of the capacitive IC chip.

In the technique introduced in [3], the antenna scattering is measured with three resistive loads. The antenna input impedance is then calculated based on a linear three port model. The technique will be expanded for reactive load impedances, to measure the input impedance of an inductive antenna with a capacitive load. The technique perfectly fits to the measurement of UHF RFID antennas, because the capacitive loads are almost identical in frequency behavior to the load introduced by the RFID IC chip.

The advantage of proper loading cannot be overemphasized for two reasons: 1) since the antenna is tuned to resonance with the load, signal to noise ratio is optimized; and 2) the load of the antenna affects the antenna scattering in many unexpected ways, as will be seen later in this paper.

A scattering measurement is needed to measure the input impedance of a small reactive antenna; feed line measurements do not give accurate results, since the feed line couples strongly to the antenna and radiates as a part of the antenna. Especially this is a problem with small antennas, like RFID antennas, and with antennas whose feedpoint is not single-ended, e.g., planar inverted-F antennas (PIFAs) with small ground plane [6]. In the case of the technique to be introduced, no instrumentation other than a vector network analyzer is needed.

In the next section, the theory of the measurements is extended for reactive loads. After that, error analysis is presented. As an experimental verification, two reactive antennas are measured near 869 MHz in a gigahertz transverse electromagnetic mode (GTEM) cell. The measured antennas are specially designed RFID tag antennas for various applications. It is of great importance to be able to measure these antennas wirelessly in order to obtain information on their operation in different environments, and for a basis of their optimization. In Section V the measurement results are compared with simulations and coaxial feed line measurements.

II. Theory

In this paper, we rely on the formulation developed by Harrington [2] and use the method described by Mayhan [3], with some exceptions. Harrington described the antenna under test (AUT), the receiving and transmitting antenna, as a linear three port network, which can be characterized with three impedance or admittance parameters. In this paper, the calculations are based on impedances, so these parameters are z_{rt}, z_{at} and Z_D. Subscript

Manuscript received November 16, 2006; revised October 2, 2007. This work was supported in part by Tekes, the Finnish Funding Agency for Technology and Innovation and in part by the EU under the sixth framework.

P. Pursula and K. Jaakkola are with the Technical Research Centre of Finland (VTT), Espoo, FIN 02044, Finland (e-mail: pekka.pursula@vtt.fi).

D. Sandström was with the Technical Research Centre of Finland (VTT), Espoo, FIN 02044, Finland. He is now with the Electronic Circuit Design Laboratory, Helsinki University of Technology, Espoo, FI 02150, Finland.

Digital Object Identifier 10.1109/TAP.2007.915425

r is for receiving and t for transmitting antenna respectively; z_{rt} describes coupling between receiving and transmitting antenna, and z_{at} coupling between transmitter and the AUT.

When the AUT is in the electric field of the transmitting antenna, it backscatters part of the incoming field. This scattered field is then received causing an excitation voltage at the receiving antenna. This relationship is, according to [2]

$$v_t \propto \left(z_{rt} - \frac{z_{at}^2}{Z_D + Z_L} \right) i_r \tag{1}$$

where Z_D is the antenna input, or drive port, impedance of AUT and Z_L is the load impedance attached to the terminals of AUT.

To obtain Z_D from (1), which consists of three unknown parameters Z_D, z_{rt} and z_{at}, it is evident that three measurements with three different loads are needed. Mayhan [3] used a short circuit, an open circuit and a resistive load. Because of the reactive nature of RFID antennas, the short circuit was replaced with a capacitive load in order to achieve resonance at the desired frequency. For the same reason, the resistive load was replaced with a capacitor and resistor connected in series. These three different load are denoted by Z_c, Z_o and Z_m. Subscript c is for capacitive load, o for open circuit and m for matched load. The same subscripts are used for the measured scattered fields, denoted by V_c, V_o and V_m. They can be solved by substituting different load impedances into (1), resulting in

$$KV_o = z_{rt} \tag{2}$$

$$KV_c = z_{rt} - \frac{z_{at}^2}{Z_D + Zc} \tag{3}$$

$$KV_m = z_{rt} - \frac{z_{at}^2}{Z_D + Zm} \tag{4}$$

where K is a dimensional constant. Substituting (2) into (3) and (4), results in a new set of equations

$$K(V_c - V_o) = \frac{-z_{at}^2}{Z_D + Z_c} \tag{5}$$

$$K(V_m - V_o) = \frac{-z_{at}^2}{Z_D + Z_m}. \tag{6}$$

Dividing (5) with (6) and solving for Z_D gives

$$Z_D = \frac{Z_m - AZ_c}{A - 1} \tag{7}$$

where A contains the measured scattered fields, which can be associated with a relevant scattering parameter; in this paper a monostatic case is considered and thus S_{11} is used. Now A can be expressed as

$$A = \frac{S_c - S_o}{S_m - S_o}. \tag{8}$$

III. Error Analysis

The technique gives accurate results when the antenna mode scattering dominates over the structural mode scattering, which holds for the rod antennas measured in [3] for a very wide band. In (1), the first term describes the structural mode scattering and the second term the antenna mode scattering [7]. The structural mode scattering neither depends on the load of the antenna nor the antenna input impedance, but the antenna structure, e.g., metal plates in PIFAs, scatter nevertheless. The other term describes antenna mode scattering, that depends on the antenna input impedance and load. The antenna mode scattering arises, because the structure works as an antenna, feeding power to the load. Hence, it is natural that the signal to noise ratio of the antenna input impedance measurement is at its maximum when the antenna mode dominates the scattering.

In Section II, the three different loads were chosen to be an open circuit, a capacitive load and a matched load. The value of the capacitor is based on the simulated antenna input impedance and is determined in Section V. The resistor value should be chosen so that it contributes to the total error as little as possible. Mayhan [3] listed various error sources in his article, but our interest is to find the optimal value for the resistor. When attaching different loads to the AUT, physical displacement errors occur. This error type is dominating in higher frequencies. The error is calculated using partial differentiation. Taking into account the phase shift when the AUT is removed for load attachments, we get

$$\begin{aligned} \Delta Z_D &= \sum_i \left| \frac{\partial Z_D}{\partial S_i} \right| \Delta_i \\ &= \sum_i \left| \frac{\partial Z_D}{\partial S_i} \right| \left(\frac{\partial S_i}{\partial |S_i|} \Delta_{|S_i|} + \frac{\partial S_i}{\partial \phi_i} \Delta_{\varphi_i} \right) \end{aligned} \tag{9}$$

where i refers to c, m and o. $\Delta_{|S_i|}$ stands for the residual background level after background cancellation methods have been used and Δ_{φ_i} is the phase shift caused by displacement. The background level can be estimated from the undulation of the S-parameter magnitude curves.

By denoting the displacement error as Δ_L, (9) takes the following form:

$$\Delta Z_D = \sum_i \left| \frac{\partial Z_D}{\partial S_i} \right| \left(\Delta_{|S_i|} + j4\pi \frac{\Delta_L}{\lambda} |S_i| \right) e^{j\varphi}. \tag{10}$$

After some manipulation, an expression for the error as a function of measured scattering parameters is obtained

$$\begin{aligned} \Delta Z_D = &\frac{(S_o - S_m)(Z_m - Z_c)}{(S_m - S_c)^2} \Delta_c + \frac{(S_o - S_c)(Z_m - Z_c)}{(S_m - S_c)^2} \Delta_m \\ &+ \frac{(S_m - S_c)(Z_m - Z_c)}{(S_m - S_c)^2} \Delta_o. \end{aligned} \tag{11}$$

Assuming that the Δ-variables are uncorrelated, summation in (11) can be done quadratically. It is also assumed that the Δ-variables are equal and denote them as σ_B. The final form of the error estimate, denoted by σ_D^2, is thus

$$\sigma_D^2 = \sigma_B^2 |Z_m - Z_c|^2 \cdot \frac{|S_o - S_m|^2 + |S_o - S_c|^2 + |S_m - S_c|^2}{|S_m - S_c|^4}. \tag{12}$$

In (12), σ_B^2 stands for the residual background level [see (9)]. The equation consists of differences between two S_{11}-parame-

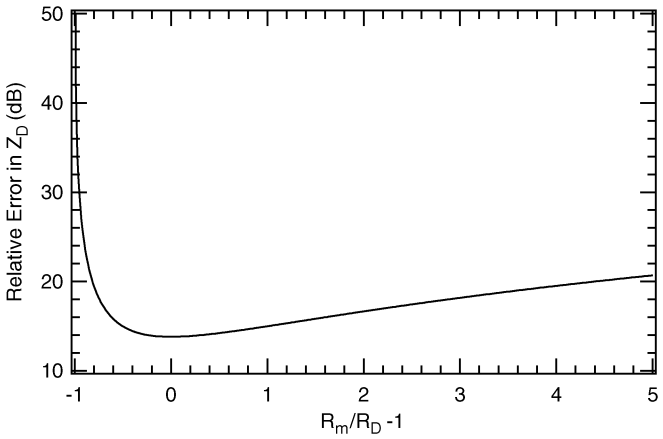

Fig. 1. Relative error in Z_D as a function of the load resistance R_m. Reactive matching is assumed perfect, and resistances $R_c = 0$ and $R_o = \infty$.

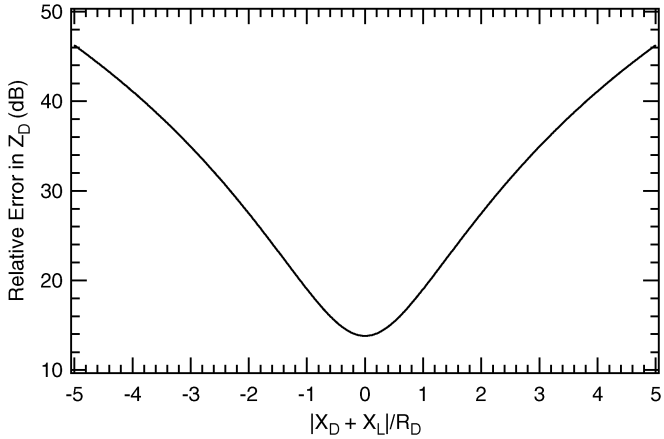

Fig. 2. Relative error in Z_D as a function of the reactive mismatch $|X_D + X_L|$, where load reactances $X_c = X_m = X_L$. Resistances $R_c = 0$, $R_m = R_D$ and $R_o = \infty$.

ters. Using (2)–(4), an expression can be derived for σ_D^2, that includes the different load impedances Z_c and Z_m

$$\sigma_D^2 = \frac{K^2\sigma_B^2 R_D^4}{|z_{at}^2|^2}\left[\frac{|Z_D+Z_m|^2|Z_D+Z_c|^2}{R_D^4} \cdot \frac{|Z_D+Z_c|^2+|Z_D+Z_m|^2+|Z_m-Z_c|^2}{|Z_m-Z_c|^2}\right]. \quad (13)$$

The input resistance R_D has been introduced into the equation to make the bracketed term that describes the error as a function of the impedances unitless.

In order to determine the optimum choice for the load resistor in Z_m, the bracketed part of (13) was calculated at the resonant frequency by substituting different resistor values to the load Z_m. For simplicity, the reactive match is assumed to be perfect. The result is in Fig. 1. The smallest contribution to total error is achieved when the resistor value is chosen to be the same as the antenna input resistance.

The same kind of calculation can be made for reactive mismatch of Z_m and Z_c with respect to Z_D. Denoting the reactive part of Z_D as X_D and X_L as the reactive part of $Z_i, i = c, m$, we can use (13) and vary X_L. The result is in Fig. 2, from which we can see that the error related to reactive mismatch is at its minimum when the reactive part of Z_m and Z_c equals the reactive part of Z_D.

The error grows with increasing reactive and resistive mismatch. The loads can only be fully matched to the antenna at one frequency point. Hence, the error grows when leaving the antenna center frequency.

IV. Antennas Under Test

The transponder antenna is the most critical part of the system in many applications of passive UHF RFID. This is mostly because the performance of the antenna, realized as the maximum reading distance of the tag, tends to be affected by the mounting platform as well as the whole near environment of the tag. The two antennas measured, shown in Fig. 3, represent two types of UHF RFID tags.

The Palomar antenna [11] is a single-layer structure especially designed to be compact in size and to provide an almost isotropic radiation pattern. This is due to its operation both as an electric and a magnetic dipole. The prototype measured has been fabricated by cut milling on a single-layer FR4 board. Because the antenna is a single-layer structure, it can also be manufactured inexpensively as a label using the most common technology of today's tag manufacturing.

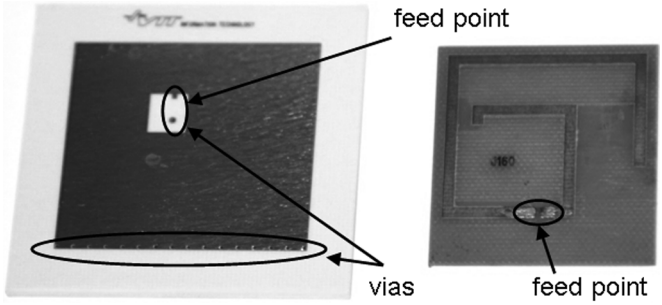

Fig. 3. The measured antennas: on the left the PIFA and on the right the Palomar antenna.

The PIFA antenna [12] has been designed to be mounted on any surface, especially on metal that is practically impossible for direct mounting of a dipole-based label antenna. This antenna prototype has been realized using printed circuit board technology on a two-metal-layer panel of low-loss microwave material (RO4003). The size of the antenna is $60 * 60 * 3\ \mathrm{mm}^3$. The short-circuiting contact between the layers of the antenna, which is required for the PIFA structure, has been implemented by a set of vias at one edge of the antenna patch. There is also a via connection at the feed point of the antenna. This type of tag antenna is more expensive to produce than the more common labels. Such antennas are typically used for recyclable tags in harsh environments, e.g., pallets and containers.

In the case of the Palomar antenna and similar structures, the measurement method concerned is of special importance. Because of its omnidirectional radiation pattern, the operation of the antenna is easily disturbed by any cable connected to it; thus the impedance reading would be inaccurate in such measurement. Theoretically, a PIFA-type antenna radiates in half-space and its feed impedance can be measured using a coaxial cable

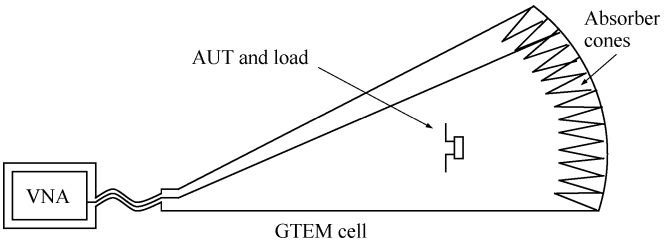

Fig. 4. Measurement setup. The scattering parameter S_{11} is measured with the vector network analyzer (VNA).

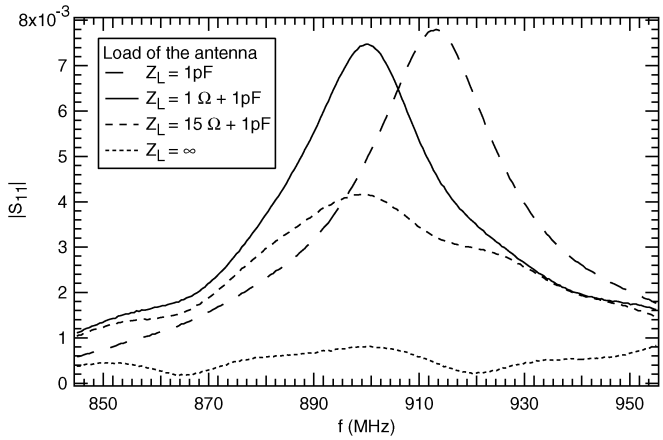

Fig. 5. Measured scattering parameters S_{11} of the Palomar antenna with different loads.

and tapped feed through the ground plane of the antenna. This has been done to the PIFA concerned for comparison, and the results are examined in the next section. Practical PIFA antennas have non-infinite ground plane, especially RFID tag antennas that have to be compact in size. Therefore, the coaxial cable feed does disturb the antenna.

V. Measurement Results

To verify the theoretical results, the two antennas introduced in the previous section were measured with the technique. Both are designed for direct matching to a UHF RFID IC chip. The designed input impedance of the antennas is $(10 + j160)\ \Omega$ at 869 MHz. The inductive input impedance is matched by a capacitive load of 1 pF, i.e., a reactance of $-183\,\Omega$ at 869 MHz. A resistive load of 15 Ω for R_m was chosen because the relative error quickly rises, if $R_m < R_D$.

The measurements were carried out in a GTEM cell, described in [8]. GTEM cells have been used to measure radiation patterns [9] and gain of small antennas [10]. The GTEM cell is a waveguide, in which a plane wave propagates with TEM-mode. Thus the wave propagating in the cell is similar to a wave in free space. However, mismatch in wave and characteristic impedances has to be considered if absolute values of the scattered signals need to be determined, i.e., when measuring the antenna gain [10]. But, in our case, the input impedance of the antenna is calculated from relative scattered signals. In other words, the coupling constant K in (2)–(4) is not needed in (7) to calculate the input impedance.

The schematic of the measurement setup is presented in Fig. 4. The antenna under test (AUT) was positioned in the GTEM cell and the scattering parameter S_{11} measured with the vector network analyzer (VNA), which was connected to the feed point of the GTEM cell. The measurement was repeated with the three different loads connected to the AUT. The S_{11} of the empty GTEM cell was also measured; this was not needed to calculate the input impedance Z_D of the antenna, but only to present the change in S_{11} due to the different loads with the background subtracted.

Fig. 5 presents the measured magnitudes of the scattering parameter S_{11} of the Palomar antenna with four different loads. The load $Z_L = \infty$ describes the antenna structural mode. The capacitive and matching loads give rise to antenna mode, which dominates the structural mode in the application band.

An interesting phenomenon is observed with the capacitive load: if no series resistance is present, the antenna center frequency is shifted to higher frequencies and, more important, the S_{11} of the capacitive load and the matching load cross. This leads to evident error in the input impedances, for Z_D diverges, when S_c equals S_m as seen from the (7).

The reason for this behavior was beyond the resources of the study but was probably due to the series inductance of the chip resistor. An empirical solution for the problem was found: By adding a small series resistance to the capacitive load, the center frequency remained at the center frequency of the matched load. Hence, loads $Z_o = \infty$, $Z_m = 15\,\Omega{+}1$ pF and $Z_c = 1\,\Omega{+}1$ pF were used.

Figs. 6 and 7, present the results of the Palomar antenna input impedance, as well as simulations with the HFSS software. In the case of the reactance, the opposite reactance of 1 pF at the center frequency of the scattering peaks in Fig. 5 is presented as this should be the antenna reactance at the frequency.

The error is smallest in the middle of the scattering peak, where the measured scattering parameters differ the most, as seen from (9). The error sources of the measurement setup were estimated as follows: The error in scattering parameter magnitude, or $\Delta_{|S_i|}$, was approximated as the ripple in the measured curves in Fig. 5. The repositioning error was approximated as 1 mm. In this case, the effect of the repositioning error was over an order of magnitude higher than the effect of the residual background. The resulting errors are presented in Figs. 6 and 7 as the gray area surrounding the measured value. As expected, the error grows as the difference between matched and shorted scattering parameters in Fig. 5 diminishes. Very accurate results are acquired at the resonance peak frequency.

The PIFA antenna was also measured with four loads, as seen in Fig. 8. In the open-circuited case the antenna self-resonance is seen at 910 MHz. Also here the resonance peak shift to higher frequencies with zero load resistance, and a series resistance of 1 Ω was added to the load Z_c. The resonance seems to have slightly different characteristics here than in the case of the Palomar antenna: the antenna mode scattering seems to add to the structural mode in anti-phase at frequencies below the resonance peak, resulting in scattering parameter amplitudes below the structural mode.

Figs. 9 and 10, present the results of the PIFA antenna input impedance, as well as simulations and a reference measurement:

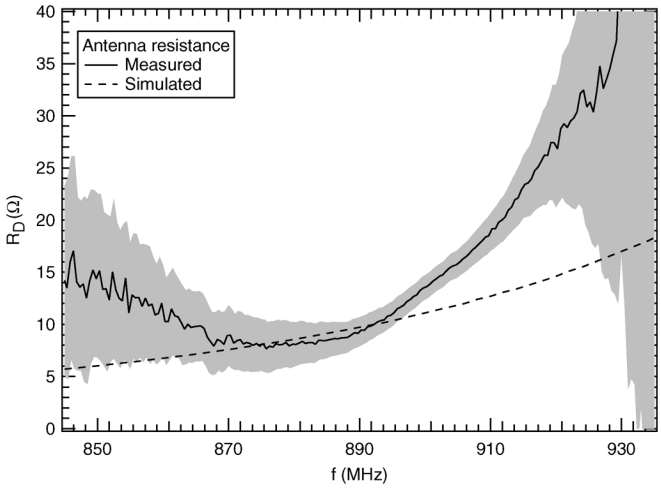

Fig. 6. Measured and simulated input resistances of the Palomar antenna. The gray area represents the error in the measured value.

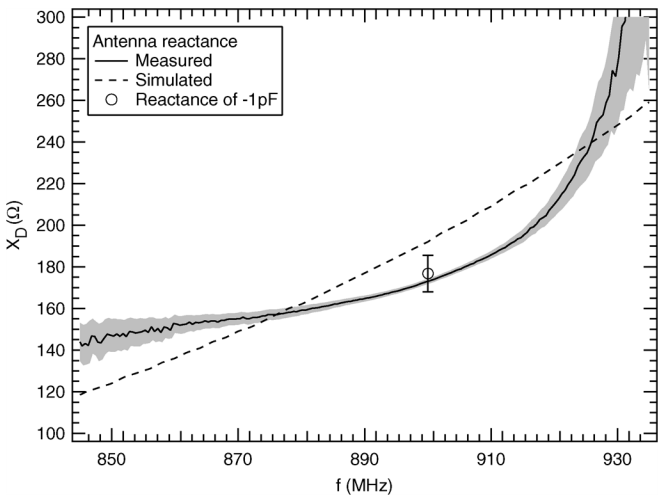

Fig. 7. Measured and simulated input reactances of the Palomar antenna. The gray area represents the error in the measured value.

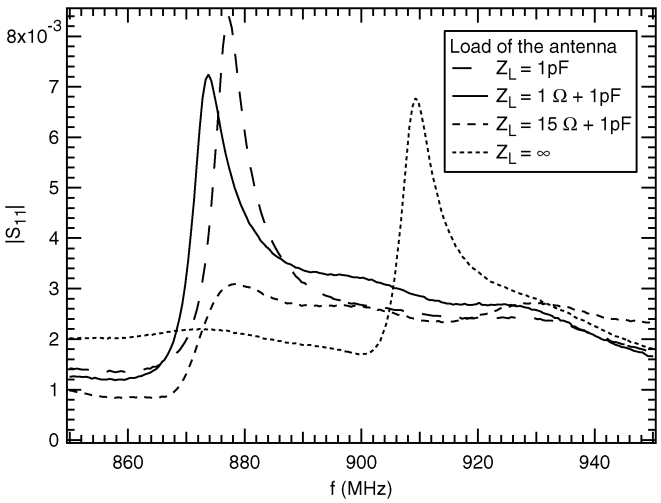

Fig. 8. Measured scattering parameters S_{11} of the PIFA antenna with different loads.

A coaxial feed line was attached to the antenna feed point and the scattering parameter S_{11} measured with a VNA. The opposite reactance of 1 pF at the center frequency of the scattering peaks in Fig. 8 is also presented.

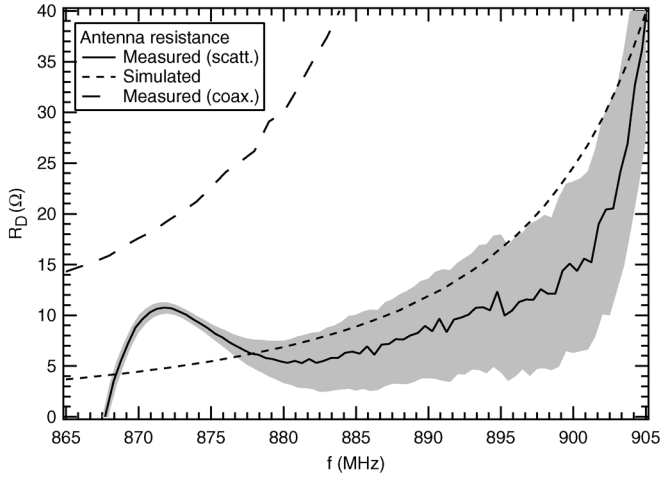

Fig. 9. Measured and simulated input resistances of the PIFA antenna. The gray area represents the error in the measured value.

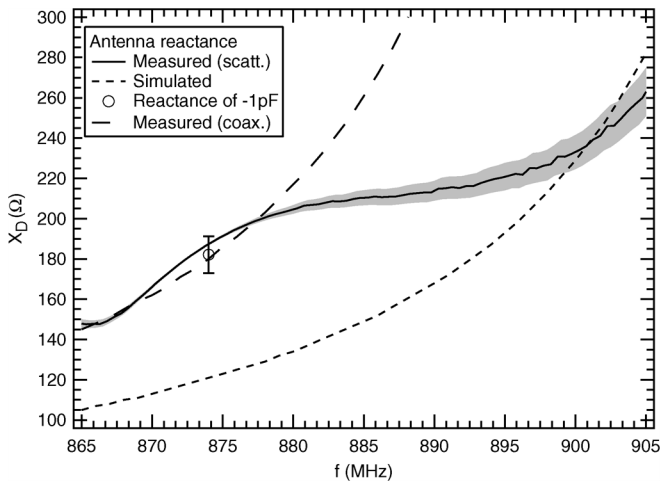

Fig. 10. Measured and simulated input reactances of the PIFA antenna. The gray area represents the error in the measured value.

Immediately it is seen that the measurement result of the antenna resistance cannot be right at low frequencies, where negative values are obtained. This happens as shorted and matched scattering parameters sink below the structural mode scattering. However, reasonable results are obtained from 875 to 900 MHz, where the antenna mode scattering dominates: the resistance follows the simulated value in magnitude and shape. On the other hand, the coaxial measurement does not give similar results. Because the PIFA does not have an infinite ground plane, it is not ideally a single-ended structure: connecting the feed line outer conductor to the ground plane induces currents to the outer conductor, which leads to higher dissipation, and thus higher measured antenna resistance.

The reactance hits almost exactly the opposite reactance of 1 pF, and the coaxial measurement results. The simulated value is further away from the measured values, but the simulated value cannot be considered a perfect reference for the scattering measurement: the reactances of 3D antenna structures calculated with HFSS often differ from results of other simulators (e.g., [13]). However, HFSS allows true 3D modelling without infinite layers, which allows the study of ground plane size in small PIFA antennas.

In the measurement of the PIFA antenna, the scattering technique evidently has two problems: First, the PIFA is a complicated three-dimensional system, which is probably not described well enough by a simple series resistance and reactance model, as is supposed in [1] and [2] as the theory of scattering is developed. The structural mode is also high in magnitude (by a factor of four in the scattering parameter higher than with the Palomar antenna), and complex in frequency, as with patches [14]. Taking into account the polarization coupling in the antenna, like in [4], would probably give better results. Second, the error estimates cannot describe the error due to too simple an antenna model. Thus only a small value of error is presented, even if the resistance is negative.

VI. Conclusion

This paper presented a scattering technique for antenna input impedance measurements of reactive antennas. Theory was developed and sources of measurement error considered. Two reactive antennas were measured at UHF frequencies. From the error analysis and the measurements, it was seen that the technique gives the best results when the antenna mode dominates the structural mode scattering.

The measurements of the Palomar antenna, a modified dipole, justified the theoretical construction; the results of the measurements and the simulations of the antenna coincided well. The results of the PIFA antenna were more complicated. The structural mode of the PIFA antenna is high in magnitude, and the used model is too simple to describe the scattering of this three-dimensional antenna accurately. Nevertheless, reasonable results were acquired, where the antenna mode scattering dominated the structural mode.

The measurement technique proved to be valid in a narrow band, about three times the half-power bandwidth of the antenna. However, this was achieved with very simple apparatus: a vector signal analyzer and a GTEM cell, which could be replaced with an antenna and an anechoic chamber. No compensation or background elimination techniques other than averaging and scattering parameter reduction in the VNA were used. The simplicity of the apparatus and the measurements makes the technique advantageous in narrow band measurements.

Acknowledgment

The authors wish to thank M. Hirvonen for many useful discussions on antenna scattering, and C. Icheln and the Radio Laboratory of Helsinki University of Technology for cooperation and the opportunity to use the GTEM cell

References

[1] D. D. King, "Measurement and interpretation of antenna scattering," *Proc. IRE*, vol. 37, pp. 770–777, Jul. 1949.
[2] R. F. Harrington, "Theory of loaded scatterers," *Proc. Inst. Elect. Eng.*, vol. 111, pp. 617–623, Apr. 1964.
[3] J. T. Mayhan, A. R. Dion, and A. J. Simmons, "A technique for measuring antenna drive port impedance using backscatter data," *IEEE Trans. Antennas Propag.*, vol. 42, pp. 526–532, Apr. 1994.
[4] W. Wiesbeck and E. Heidrich, "Wide-band multiport antenna characterization by polarimetric RCS measurements," *IEEE Trans. Antennas Propag.*, vol. 46, pp. 341–350, Mar. 1998.
[5] P. V. Nikitin and K. V. S. Rao, "Theory and measurement of backscattering from RFID tags," *IEEE Antennas Propag. Mag.*, vol. 48, pp. 212–218, Dec. 2006.
[6] P. Pursula, M. Hirvonen, K. Jaakkola, and T. Varpula, "Antenna effective aperture measurement with backscattering modulation," *IEEE Trans. Antennas Propag.*, vol. 55, no. 10, pp. 2836–2843, Oct. 2007.
[7] E. F. Knott, J. F. Schaeffer, and M. T. Tuley, *Radar Cross Section*. Boston, MA: Artech House, 1993, pp. 407–407.
[8] C. Icheln, "The construction and application of a GTEM cell," Master's thesis, Faculty of Electrical Engineering, Technical Univ. Hamburg, Hamburg, Germany, Nov. 1995.
[9] C. Icheln, P. Haapala, and P. Vainikainen, "Application of a GTEM cell to small antenna measurements," in *IEEE AP-S Int. Symp. Digest*, Montreal, Canada, Jul. 1997, vol. 1, pp. 546–549.
[10] P. Hui, "Small antenna measurements using a GTEM cell," in *Proc. IEEE Antennas and Propagation Society Int. Symp.*, Jun. 2003, vol. 4, pp. 715–718.
[11] The Palomar Project, Passive Long Distance Multiple Access UHF RFID System Public Rep., European Commission, Project IST1999-10339, Nov. 2002.
[12] M. Hirvonen, P. Pursula, K. Jaakkola, and K. Laukkanen, "Planar inverted-F antenna for radio frequency identification," *Electron. Lett.*, vol. 40, pp. 848–850, Jul. 2004.
[13] W. Yu, J. Yeo, and R. Mittra, "Application of non-uniform and conformal FDTD techniques to the analysis of a class of planar antennas," in *Proc. IEEE Antennas and Propagation Society Int. Symp.*, Jun. 2002, vol. 2, p. 675, Fig 1.
[14] E. Newman and D. Forrai, "Scattering from a microstrip patch," *IEEE Trans. Antennas Propag.*, vol. 35, pp. 245–251, Mar. 1987.

Pekka Pursula was born in Vantaa, Finland, in 1978. He received the Master of Science (Tech.) degree (with distinction) in technical physics from Helsinki University of Technology (TKK), Espoo, Finland, in 2002.

In 2002, he was with Philips Medical Systems Finland developing RF systems in magnetic resonance imaging. Since 2003, he has been with the Technical Research Centre of Finland (VTT), Espoo. He is co-inventor of two international patent applications. His present research interests include RFID systems and wireless sensors.

Mr. Pursula received the Young Scientist Award at the URSI/IEEE XXIX Convention on Radio Science, Espoo, in November 2004.

Dan Sandström is working toward the M.Sc. degree in electrical engineering at Helsinki University of Technology (TKK), Espoo, Finland.

From 2005 to 2007, he was a Research Assistant in the Technical Research Centre of Finland (VTT), Espoo. He is currently with the Electronic Circuit Design Laboratory, TKK. His research interests involve millimeter-wave integrated circuit design in CMOS.

Kaarle Jaakkola was born in Helsinki, Finland, in 1976. He received the Master of Science (Tech.) degree in electrical engineering from Helsinki University of Technology (TKK), Espoo, Finland, in 2003.

Since 2000, he has been working with the Technical Research Centre of Finland (VTT), Espoo, first as a Research Trainee and from 2003 on as a Research Scientist. From 2000 to 2002, he participated in the Palomar (EC IST) project developing RF parts for a new RFID system. His current research interests include RFID systems, wireless and applied sensors, antennas, electromagnetic modelling, and RF electronics.

UHF RFID Reader with Reflected Power Canceller

Accepted in: IEEE Microwave and Wireless Component Letters, to be published in January 2009.

UHF RFID Reader with Reflected Power Canceller

Pekka Pursula, Mikko Kiviranta, and Heikki Seppä

***Abstract*—Reflected power imposes severe linearity problems to the receiver in RFID readers. In this paper, the design and realization of a UHF RFID reader with a reflected power canceller circuit (RPC) based on quadrature feedback are presented. Theory and measurements of the signal and noise in the receiver are presented as a function of incident carrier power. The receiver sensitivity is even better with high incident carrier power than without the canceller: A noise spectral density at the data band is -140 dBm/Hz at +12 dBm incident carrier power. At the same time, input compression point of +15 dBm is achieved. The dynamic range of the receiver is improved by 10 dB.**

***Index Terms*—UHF, RFID, carrier suppression, reflection canceller, high-Q active filter.**

I. Introduction

A KNOWN problem in a ultra high frequency radio frequency identification (UHF RFID) reader is carrier power leakage from the transmitter to the receiver [1]. This creates high linearity requirements for the receiver. Similar problems have been encountered in frequency modulated continuous wave (FMCW) radars, where several solutions have been documented: a reflected power canceller (RPC) circuit with PIN diodes [2], [3] and a balanced topology front end [4].

A similar approach can be used in UHF RFID. The idea has been described by the authors [5] and others [6]. However, these patents include several possible RPC circuits without presenting thorough analysis of the circuits.

In this paper, a UHF RFID reader with a RPC circuit is analysed theoretically, and measurement results are presented, clearly showing the benefit of the chosen topology, especially the usage of PIN diodes. The authors have also presented another approach to achieve these goals in RFID readers [7].

In the next section, the signal and noise in the electronics is analysed. Then measurement results from a prototype are presented, and the paper is concluded.

II. Theory

The quadrature, or Cartesian, feedback is known from many applications, e.g. PA linearization [8] and FMCW radar [3]. The principle is most concisely expressed for complex-valued signals. Referring to Fig. 1, the received signal has the complex amplitude c_R. Complex amplitude c_F is assumed for the compensating feedback signal. The open-loop feedback signal c_{FO} can be calculated as done in Fig. 1 and equated with assumed feedback signal c_F. Solving c_F gives the amplitude of the signal fed to the downmixer, when the feedback loop is closed:

The authors are with VTT, Technical Research Centre Finland. Correspondence to pekka.pursula@vtt.fi.

The work has been partly financed by European Union through FP6 and Tekes, Finnish Funding Agency for Technology and Innovation.

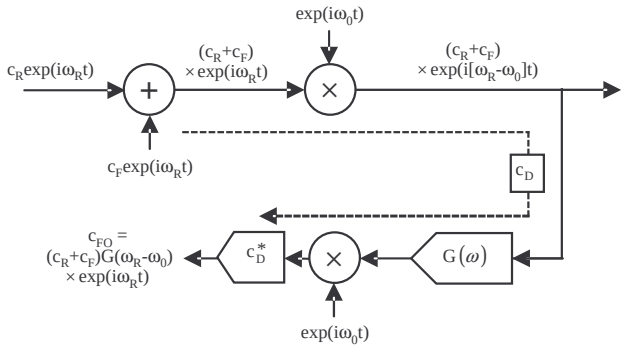

Fig. 1. Signal flow of the quadrature feedback in the case of complex-valued signals.

$$c_R + c_F = c_R \frac{1}{1 - c_D^* c_D G\left(\omega_R - \omega_0\right)}. \qquad (1)$$

Here $c_D = \exp\left(i\theta\right)$ is the phase shift due to the delay and parasitics in the signal path, compensated by the c_D^* term designed into the circuit. When a single-pole low-pass loop filter $G\left(\omega\right) = -G_0/(1 + i\omega/\omega_C)$ is chosen and perfect delay compensation $c_D^* c_D = 1$ is assumed, the downmixer signal becomes

$$c_R + c_F = c_R \left(1 + G_0 \frac{\omega_C}{\omega_C + i\left(\omega_R - \omega_0\right)}\right)^{-1}, \qquad (2)$$

which is equivalent to applying a notch filter with bandwidth ω_C and center frequency ω_0 to the received signal. Because the ω_0 is determined by the local oscillator, which is independent of the ω_C-determining loop filter, tremendously effective Q-values can be obtained. In the context of RFID such a steep notch can be used to filter away the carrier power, and still pass the tag-backscattered side bands to the downmixer. In this manner the downmixer and the low noise amplifier (LNA) associated with it can be kept from saturating.

Without the quadrature feedback, the dynamic range of a RFID receiver is typically determined as the difference between the noise floor and high-power compression point of the downmixer or LNA. In the compensator-equipped circuit in Fig. 1, the dynamic range of the upmixer in the feedback path becomes the bottleneck, and nothing is gained if the upmixer is fabricated using the same technology as the downmixer, because the two then tend to have the same dynamic range limitation. Fortunately PIN-diodes offer a very large dynamic range and can be used as upmixers. Their noise floor is effectively thermally limited and power handling capacity exceeds +20 dBm. Because their reaction speed to the control

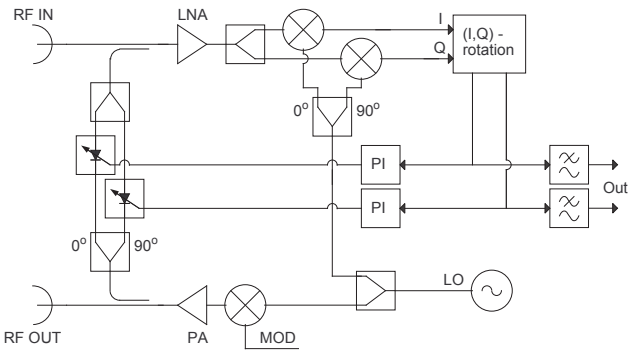

Fig. 2. Block diagram of the reader.

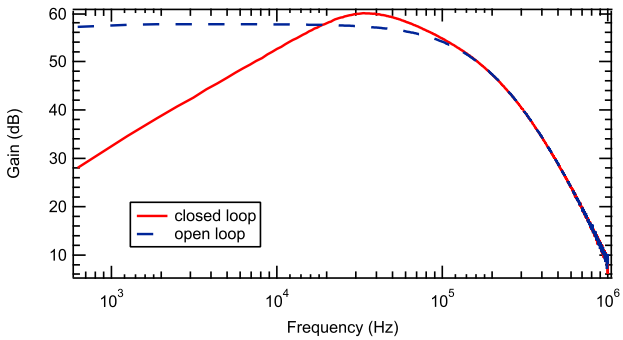

Fig. 4. Measured gain from RF input single side band to base band output as a function of offset frequency from the carrier.

current is typically limited to below 100 kHz, they cannot be used directly as downmixers.

The proposed circuit for two real-valued quadrature signals rather than one complex-valued signal is presented in Fig. 2. The feedback includes two parallel analog loops, that are orthogonalised at the base band. The electronics can also be implemented with a single antenna and a circulator.

The sensitivity of the receiver is described by the input referred noise power spectral density S. The LNA and downmixer noise contributions are lumped into S_{RX}. The noise power radiated by the transmitter is a constant fraction α_O of the radiated carrier power, so that the noise contribution at the receiver due to the reflection from the environment $S_{TX} = \alpha_O P_{in}$ can be expressed in terms of the received carrier power P_{in}. When the RPC loop is closed, the baseband circuitry add a constant noise term S_F caused by base band amplifiers and a power-dependent noise term $\alpha_F P_{in}$ caused by PIN diode shot noise and downmixer-to-upmixer leakage at data band. The input referred noise can then be expressed as

$$S = S_{RX} + \alpha_O P_{in}, \tag{3}$$

when the RPC is inactive, and as

$$S = S_{RX} + S_F + \frac{\alpha_O P_{in}}{G_0} + \alpha_F P_{in}, \tag{4}$$

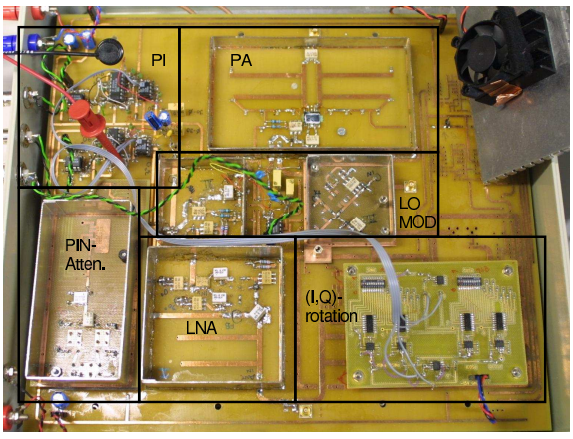

Fig. 3. Photograph of the 865 MHz electronics.

when the RPC is functioning. The RPC suppresses the S_{TX} by carrier frequency loop gain G_0, because the compensating and received signals are derived from the same source, so that noise of the compensating signal is correlated with S_{TX}. In the case $G_0 \gg 1$, the ratio α_F/α_O determines whether activation of the RPC circuit increases or decreases the noise power at the data band, given a received carrier power level P_{in}.

The feedback limits the dynamic range: The LNA stays linear as far as the incident carrier power is less than the maximum output power of the feedback path, and the noise level is determined by the feedback noises S_F and α_F. Especially, if diode ring mixer is used as the feedback mixer, the noise floor can be thermally limited, but their maximum output power is limited to around 0 dBm. Adding an RF amplifier after the mixer improves output power by the amplifier gain, but also raises S_F by the same gain. Thus dynamic range cannot be improved with such a device. The PIN diode attenuator provides both low noise and high output power without an additional amplifier, and dynamic range is improved.

III. Prototype and Measurements

Two prototype systems have been realized; one at the 865 MHz band for the European UHF RFID, and another for the 2.4 GHz ISM band. The 2.4 GHz version was built using the Maxim MAX2701/2721 chipset and the I/Q compensation control implemented digitally in an Altera Cyclone II FPGA.

The measurement results from the 865 MHz reader are presented here. The electronics was made of discrete components,

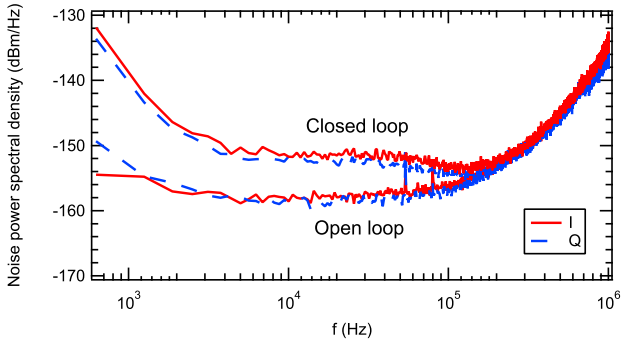

Fig. 5. Measured input referred noise spectral density as a function of offset frequency from the carrier.

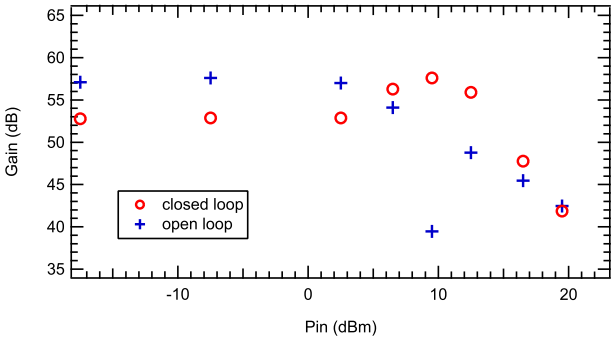

Fig. 6. Measured gain from RF input single side band to base band output at data band (offset 20 kHz) as a function of incident carrier power. Signal power is kept constant throughout the measurement, and only carrier power is altered.

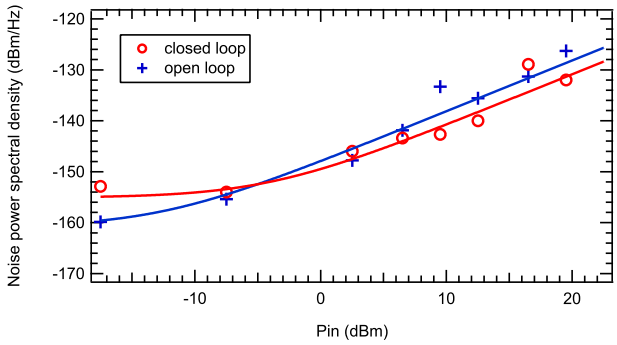

Fig. 7. Measured input referred noise spectral density at data band (offset 50 kHz) as a function of received carrier power.

and all the base band components used analog electronics: The (I,Q)–rotation circuit was realized using multiplying D/A–converters. Loop filters are analog PI controllers. PIN-diode attenuators similar to [9] were used as upmixers. A photograph of the prototype is presented in Fig. 3. The maximum RF power of the transmitter is 0.5 W.

The system was measured with a FFT analyzer. The side band signal gain was measured to see the carrier suppression. The stop band near the carrier is seen from Fig. 4. The upper cutoff is realised by a low pass filter in the base band output. The input referred noise of the receiver is presented in Fig. 5. The measurements show that the reflected power canceller (RPC) presented here suppresses the carrier, yet leaves data band at 10–100 kHz intact. The overshoot in the closed loop gain is due to insufficient phase margin in the feedback loop.

The input compression point and the noise spectral density of the receiver as a function of incident carrier power was measured by routing the transmitter output through an attenuator to the receiver. A mixer was connected parallel to the attenuator to add a CW side band signal to the data band with a constant amplitude to simulate the transponder backscattering. The incident carrier power was swept but the power of the CW signal at data band was unaltered. The gain from the RF single side band to base band output as a function of the incident carrier power is presented in Fig. 6. The figure shows that the reflected power canceller raises the compression point of the receiver by about 10 dB. The limiting factor is the power driving capability of the RPC. The overshoot in the closed loop signal level is due to a change in the controller loop gain, which is power-dependent due to the power-law response of the PIN diode to the control current.

The input referred noise spectral density at the data band as a function of received carrier power is presented in Fig. 7, as well as a fit according to (3) and (4). The feedback increases noise of the receiver by about 5 dB at low incident carrier power. At high incident carrier power the feedback reduces the noise by about 3 dB. Better noise reduction is to be expected, if the feedback loop gain cutoff is moved nearer to the carrier, because this diminishes leakage from the downmixer. The achieved noise spectral density of -140 dBm/Hz at +12 dBm incident carrier power converts to total sensitivity of about -90 dBm with 100 kHz bandwidth, but comparison to commercial products is not straightforward. For example, in [10] a reader sensitivity of -80 dBm is promised, but no comment on incident carrier power is given.

IV. Conclusion

We have suggested a reflected power canceller (RPC) based on quadrature feedback for UHF RFID reader. The RPC suppresses the incident carrier at the receiver input. Hence the carrier cannot saturate the receiver, and high sensitivity of the receiver can be preserved even with high reflected carrier power.

The measurements show that the reflected power canceller presented here suppresses the carrier, yet leaves the data band intact. The noise performance of the receiver is not compromised by the feedback: In fact, the noise spectral density of the receiver is even less than without the RPC with high incident carrier power, because of the noise compensation behaviour of the system. The input compression point of the receiver is about +15 dBm. The receiver sensitivity of -140 dBm/Hz at +12 dBm incident carrier power is achieved. Overall, the reader dynamic range is increased by 10 dB.

References

[1] J.-P. Curty, M. Declercq, C. Dehollain, N. Joehl, *Design and Optimization of Passive UHF RFID Systems*, Springer, 2007.

[2] P. D. L. Beasley, A. G. Stove, B. J. Reits, B-O. As, “Solving the Problems of a Single Antenna Frequency Modulated CW Radar”, *Proc. IEEE Radar Conf.*, 1990, pp. 391–395.

[3] A. G. Stove, “Linear FMCW radar techniques”, *IEE Proceedings-F*, Vol. 139, No. 5, Oct. 1992, pp. 343–350.

[4] J-G. Kim, S. Ko, S. Jeon, J-W. Park, S. Hong, “Balanced Topology to Cancel Tx Leakage in CW Radar”, *IEEE Microwave and wireless components letters*, Vol. 14, No. 9, Sep. 2004, pp. 443–445.

[5] H. Seppä, T. Varpula, P. Pursula, M. Kiviranta, “WO/2007/006840 RFID Reading Apparatus And Method”, *International patent application*, Jan. 2007.

[6] A. Safarian, A. Shameli, A. Rofougaran, M. Rofougaran, “US/2008/0009258 Integrated Blocker Filtering RF Front End”, *US patent application*, Jan. 2008.

[7] P. Pursula, H. Seppä, “Hybrid Transformer Based Adaptive RF Front End for UHF RFID Mobile Phone Readers”, *IEEE International Conference on RFID 2008*, Las Vegas, USA, Apr. 16-17, 2008, pp. 150–155.

[8] J. L. Dawson and T. H. Lee, “Cartesian feedback for RF power amplifier linearization”, *Proc. 2004 American Control Conf.*, Vol. 1 , pp. 361–366.

[9] W-T. Kang, I-S. Chang, M-S. Kang, “Reflection-Type Low-Phase-Shift Attenuator”, *IEEE Trans. Microwave Theory Tech.*, Vol. 46, No. 7, Jul. 1998, pp. 1019–1021.

[10] Elektrobit Company, *EB RFID Reader EB URP1000-ETSI Datasheet*, available at www.elektrobit.com/file.php?110, referenced May 2008.

Hybrid Transformer-Based Adaptive RF Front End for UHF RFID Mobile Phone Readers

In: Proceedings of IEEE International Conference on RFID.
Las Vegas, USA, April 16–17, 2008, pp. 150–155.

2008 IEEE International Conference on RFID
The Venetian, Las Vegas, Nevada, USA
April 16-17, 2008

Hybrid Transformer-Based Adaptive RF Front End for UHF RFID Mobile Phone Readers

Pekka Pursula and Heikki Seppä

Abstract— **We introduce hybrid transformer-based adaptive RF front end for UHF RFID readers. Small, narrow band antennas with high radiation efficiency can be utilised with an adaptive tuning of the antenna. The adaptivity also increases immunity to environmental changes, like detuning of the antenna by user hand. The hybrid transformer-based front end provides high isolation from TX to RX and eliminates the need for a cumbersome and expensive circulator. The small size of the module including the antenna enables integration to mobile phones.**

I. Introduction

In UHF RFID readers the linearity of the receiver is of high importance [1]. The high transmitted power, even up to 33 dBm, should be isolated from the receiver still keeping the sensitivity reasonably high. The received signal power from the tag can be as low as -60 dBm. In addition to designing the receiver sensitive for the signal, also high carrier power level has to be taken into account.

In addition to the requirement of the high receiver linearity, the total power consumption should be as low as possible in handset devices. The complete system including the electronics and the antenna should also be very limited in size and mass productable with extremely low price. The size problem has been addressed by integrating as much as possible of the transmitter and receiver in integrated circuits [2], and designing small antennas for mobile phone readers [3].

There are two design alternatives: The active components in the receiver can be designed to tolerate high input power, but this is near impossible without degrading the sensitivity of the receiver too much. The other possibility is to introduce high isolation between the transmitter output and receiver active components. The latter solution is often realised with circulators or directional couplers, which provide 20 – 30 dB isolation. The problem with circulators, in addition to high price and large size, is incapability to eliminate the reflected power from the environment. This is not very important in the gate readers but highly important in the handsets.

Reflected power changes in time, especially in handsets, where user hand may be very near the antenna. This reflection can be eliminated by measuring it through receiver and adding a signal in antiphase to the input of the receiver. This kind of a reflection canceller circuits have been used for example within frequency modulated continuous wave (FMCW) radars [4], [5].

In this paper we introduce an UHF RFID reader front end, which offers low power consumption and high power isolation from the TX output to RX input. The system eliminates the reflected power even from the nearby objects, and it is based on the reactive hybrid transformer dividing the power into two branches. One of the branches feeds the antenna, and other feeds an adjustable load. The ratio of the currents in the branches can be changed by varying the transformer coil inductances in the branches. The modulated signal from the tag is detected with an external coil in the transformer. The antenna is kept in resonance by tuning it with a varactor. In order to optimise the power consumption, the power amplifier is operated in the saturated mode and its output is connected directly to the antenna.

The authors are with VTT Technical Research Centre of Finland, P.O. Box 1000, 02044 VTT, Espoo, Finland. Correspondence to pekka.pursula@vtt.fi

II. RFID Reader Based on the Reactive Hybrid Transformer

The basic concept of the reader is given in Fig. 1. The power amplifier (PA) having a low output impedance is directly connected via a series resonance circuit to the antenna. Neglecting the parasitic elements, the radiated power depends on the output voltage of the PA, the real part of the antenna feeding point impedance and the radiation efficiency of the antenna. The antenna is kept in resonance, i.e. its imaginary part is zero, by adjusting the varactor diode in the antenna.

If the power amplifier is operated in the saturated mode, the transmitted power can be give as

$$P_{TX} = \eta \left(1 + \frac{R_{PA} + R_{lc}}{R_{ant}}\right)^{-2} \frac{V_{PA}^2}{R_{ant}} \qquad (1)$$

where η is the antenna radiation efficiency, R_{PA} is the output resistance of the PA, R_{lc} describes the losses of the series resonance, R_{ant} is the antenna input resistance, and V_{PA} is the PA output voltage.

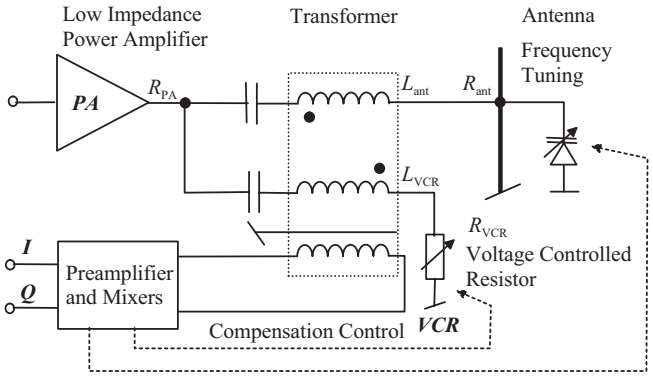

Fig. 1. Schematic of the RF front end module.

978-1-4244-1712-4/08/$25.00 ©2008 IEEE

The idea here is not to maximise the output power by matching the PA into the antenna but optimizing the total power efficiency of the system. Equation 1 shows that the efficiency can be optimised by maximising the antenna input resistance and minimising the PA output resistance. To keep the series losses as low as possible, the wiring from the PA to the antenna should be minimised and low inductance values in the transformer should be used.

In addition to the varactor for frequency tuning, the system includes a voltage control resistor (VCR), which is used to compensate for the changes of the real part of the antenna input impedance. If the ratio of the currents in the antenna and VCR branches is n, i.e. $n = I_1/I_2$, and the signal are in phase, the resistance of the VCR has to be n times that of the antenna including the other losses feeding the antenna. In the ideal case the loss in power is $1/n$. This means that in practice n has to be 3 - 6 in order keep the total power consumption as low as possible. There is no reason to make the ratio too high, since then the losses of in the power amplifier and the antenna will definitely dominate. In practice the maximum efficiency of the power amplifier could be 80 % and the efficiency of the small antenna 60 %. This means that we loose at least half of the power because of the PA and the antenna only. Consequently, the power ratio in the power divider more than 4 cannot be justified.

The VCR can be realised in different ways. We have tested here a FET and a PIN diode here as a tunable resistor. The VCR requires a sophisticated design to keep it real across the whole RFID bandwidth and for all resistance values. A PIN diode is an easiest component for this purpose but it dissipates more power than a FET.

To keep the currents in phase and in right ratio, the system has to be controlled. The outputs of the dual mixer stage control both the VCR and the varactor in the antenna. In principle, the imaginary part controls the varactor and the real part the resistance. Of course, the phase could be disturbed by the bridge and the delays from transmission lines and thus the controller has to be designed to combine *I* and *Q* signals for the right control. The bandwidth of the control has to be fast enough to compensate for the reflections but slow enough not to deteriorate the modulation from the tag. In practice, an ordinary PI controller providing feedback gain up to 1 kHz is sufficient.

The dynamic range of the compensation depends on the application. The most difficult situation is in a handset where a hand may cover the antenna or a large metallic object can be close to it. The retuning of the antenna by the nearby objects can be minimised by a proper antenna design. Since the whole UHF frequency band is so wide that the tuning range covering this is also sufficient to keep an antenna real near all the circumstances. This is, of course, valid only for antennas not too sensitive to nearby objects, e.g. electric dipole close to the cover is extremely sensitive to dielectric objects. The real part of the input impedance of a well designed antenna with a high radiation efficiency (e.g., 60 %) is hardly never halved and thus an octave is sufficient for VCR tuning range. As seen from Eq. 1, the lowered antenna impedance leads to the higher radiation power. This is a good feature, since it helps to track a tag even with a hand touching the antenna.

III. Analysis of Hybrid Transformer

In this chapter, the hybrid transformer is studied theoretically by solving network equations. The model of the transformer is shown in Fig. 2. Port 0 stands for TX output, Port 1 is the antenna, Port 2 is the voltage controlled resistor (VCR) and Port 3 the RX input.

The network equations for the model are presented in Eq. 2. Here we have used standard definition for mutual inductance $M_{ab} = k_{ab}\sqrt{L_a L_b}$.

A. Isolation and TX attenuation

Solving Eq. 2 for isolation between TX and RX ports, i.e. $I_3 = 0$ with $V_1 = V_2 = V_3 = 0$, we get

$$\begin{aligned} -\omega^2 M_{23}\left(L_1 - M_{12} - \frac{1}{\omega^2 C_1}\right) \\ +\omega^2 M_{13}\left(L_2 - M_{12} - \frac{1}{\omega^2 C_2}\right) \\ +j\omega\left(R_1 M_{23} - R_2 M_{13}\right) &= 0, \end{aligned} \tag{3}$$

which includes two requirements for the isolation, one for real part and one for imaginary part. The equation for the real part includes two resonance relations, which can be individually tuned to zero.

The imaginary part of Eq. 3 gives a rather intuitive condition for the load resistances

$$\frac{R_1}{R_2} = \frac{M_{13}}{M_{23}} = \frac{k_{13}}{k_{23}}\sqrt{\frac{L_1}{L_2}}. \tag{4}$$

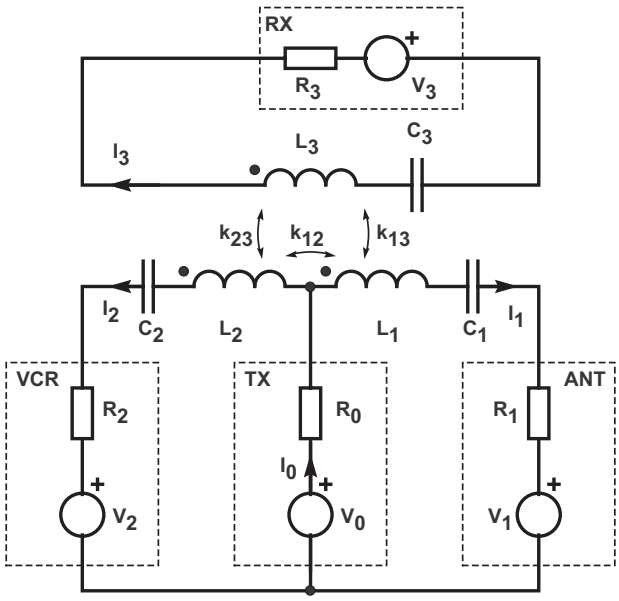

Fig. 2. The model of the hybrid transformer.

$$\begin{bmatrix} R_0+R_1+j\omega L_1+\frac{1}{j\omega C_1} & R_0+j\omega M_{12} & j\omega M_{13} \\ R_0+j\omega M_{12} & R_0+R_2+j\omega L_2+\frac{1}{j\omega C_2} & -j\omega M_{23} \\ j\omega M_{13} & -j\omega M_{23} & R_3+j\omega L_3+\frac{1}{j\omega C_3} \end{bmatrix} \begin{bmatrix} I_1 \\ I_2 \\ I_3 \end{bmatrix} = \begin{bmatrix} V_0-V_1 \\ V_0-V_2 \\ V_3 \end{bmatrix} \quad (2)$$

This gives also the ratio of the currents I_1 and I_2. Hence we define the current division ratio $n = R_2/R_1$. This is also roughly proportional to the the ratio of turns in coils L_2 and L_1, because the inductance of a tightly wound coil is proportional to the square of the turns.

In resonance and isolation, the current distribution is determined by the load resistances, which leads to power ratio

$$\frac{P_1}{P_2} = \frac{R_2}{R_1} = n. \quad (5)$$

Hence the current division ratio can also be named as the power division ratio.

It can be seen from the above equations that hybrid transformer can deliver isolation between the TX output and the RX input. The power ratio scales as the load resistances, in the square root of hybrid coil inductance. The power ratio can also be expressed as gain G_{TX} from TX output to the antenna. The TX gain is

$$G_{TX} = \frac{P_1}{P_0} = \left(1+\frac{R_1}{R_2}\right)^{-1} = \left(1+\frac{1}{n}\right)^{-1}. \quad (6)$$

B. RX gain and noise figure

The gain from antenna to RX port, or the RX gain G_{RX}, can be calculated in a similar manner. To simplify the equations, we use we use Q-values of the series resonators: $Q_a = \omega L_a/R_a$. An interesting relation for the Q_1 and Q_2 holds in isolation:

$$\frac{Q_2}{Q_1} = \left(\frac{k_{23}}{k_{13}}\right)^2 n. \quad (7)$$

With incoming power $P_1 = V_1^2/R_1$ at port 1 in the network equation, we get for $n \gg 1$

$$G_{RX} = \frac{P_3}{P_1} \approx \frac{1}{Q_1 Q_3}\left(\frac{k_{23}}{k_{13}}\right)^4 \frac{1}{n^2}. \quad (8)$$

The RX gain degrades in the square of ratio n, and the TX gain increases directly proportional to n ratio. For high n, the loss in RX power is significant and in this respect very high values of n should not be used.

Let us also derive an equation for the sensitivity, i.e. the degrading in signal-to-noise ratio inherent to the hybrid. The signal-to-noise ratio for powers can be written as

$$\begin{aligned} SNR_{Out} &= \frac{I_3^2(V_1 = V_{signal})}{I_3^2(V_1 = V_{noise,1}) + I_3^2(V_2 = V_{noise,2})} \\ &= \frac{P_1}{4k_bT\Delta B}(1+n)^{-1} \\ &= (1+n)^{-1} SNR_{In}. \end{aligned} \quad (9)$$

Here we have used $P_1 = V_{signal}^2/R_1$ as the signal power, and thermal noise of the resistors as noise sources. It is to be noticed, that SNR degrades directly proportional to the ratio n.

To calculate the noise figure NF of the hybrid, we need to take into account also the loss of signal, which was showed to be proportional to n^2. Thus the noise figure becomes

$$NF \propto n^3 \quad (10)$$

As noise figure rapidly increases with n, very high value for n is not feasible. For low read range, $n = 4$ can still be feasible, if a good LNA is used. Numerical values for the attenuation as a function n of are presented in chapter IV.

C. Bandwidth

We have shown that the reactive bridge with a PA directly connected to an antenna provides an attractive UHF RFID reader concept. The drawback, however, is that the reactive arms limit the bandwidth. The bandwidth of the VCR arm is simply the ratio between its resistance and the impedance of the transformer stray inductance. Thus the relative bandwidth ΔB of the VCR arm can be approximated from the Q-value to be

$$\frac{1}{Q} = \frac{\Delta B}{\omega_0} = \frac{R_1}{n\omega_0 L_1(1-k_{12}^2)} \quad (11)$$

To keep the coupling constant high enough we easily end up with a rather high inductance. The total power efficiency of the system increases with increasing n, but the bandwidth may become too narrow. The compromise has to be done. If assuming $n = 4$, R_1 =10 Ω, L_1 = 6 nH, and $k_{12} = 0.7$, we get $\Delta B \approx 0.15\omega_0$. Using the above values the bandwidth could be about 150 MHz which is just enough covering all the UHF frequencies used for RFID applications around the world. The lowest frequency is 865 MHz used in Europe and the highest 950 MHz used in Japan. The inductance can be lowered by using a planar coil where the loops are set in parallel. In this way, a coil having diameter of 4 mm and 4 loops in parallel could have an inductance of the order of 3 nH or even less. The third coil used for detecting the modulation can also limit the bandwidth.

If the reactive hybrid with loading enables high enough bandwidth for all UHF RFID bands, the antenna bandwidth has to cover the information bandwidth only. The maximum information bandwidth is in USA being 1 MHz and thus the quality factor of the antenna has to be smaller than 100 without deteriorating the modulation. If aiming at highly efficient small sized antenna, the *Q*- value becomes easily very high. Since the reflection is compensated for by using the varactor in the antenna, it enables us to work with a narrow banded antenna.

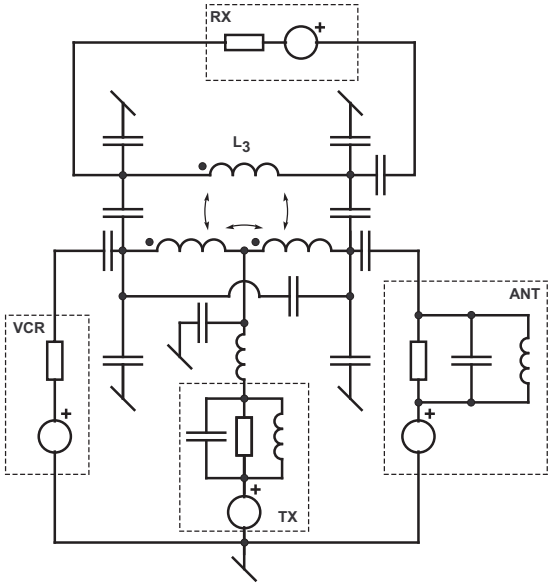

Fig. 3. Simulation model of the hybrid transformer: Antenna is modelled as a parallel resonator, PA matching and biasing circuits are added to the TX port and capacitive coupling and parasitics are modelled within the hybrid.

IV. Simulations

As seen in the previous chapter, analytical solution of three-mesh network leads to complicated equations. In this chapter, commercial simulator software Aplac has been used to study the hybrid RF front end further. With this powerful tool, a more precise model of the actual realised front end can be used. The model is presented in Fig. 3.

The model has two main differences to the analytically examined model. First, all ports have been loaded with more realistic loads: The antenna is presented as a parallel resonator, and the TX input port takes into account the PA matching circuit. Second, the hybrid model has a lot of parasitic components, both capacitive and inductive, which have been derived from measurements.

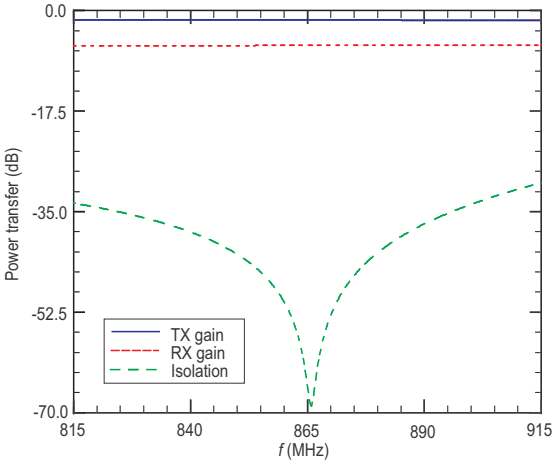

Fig. 4. Simulation results of the isolation, power transfer to antenna, and sensitivity with $n \approx 3$.

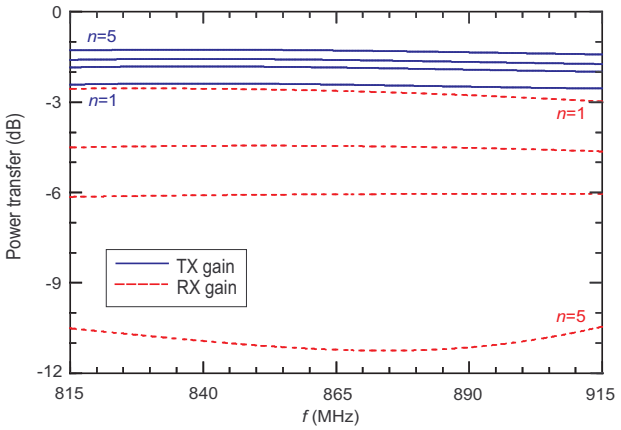

Fig. 5. Simulation results of the power efficiency and sensitivity with several values of the current ratio n.

The basic functionality of the hybrid is presented in Fig. 4. The isolation forms now a negative peak. At the same time, TX and RX gains are at maximum, but they are very wide band compared to the isolation.

To optimise the sensitivity and power efficiency of the hybrid, one would like to see the effect of power ratio n to TX and RX gains. The simulation results of the system with several values of the ratio n are presented in Fig. 5.

Clearly the dependence of sensitivity and power efficiency are against each other and the theoretically solved relations hold approximately: Sensitivity degrades twice the amount power is saved through the increasing of R_2. The optimum ratio of the load resistances is a compromise that may vary in different applications.

Another interesting thing is to show, how the varactor tuned antenna can be used to tune the whole RF front end in frequency. In this case, the antenna parallel capacitor is varied to emulate parallel varactor. As seen in Fig. 6, the isolation is tuned smoothly over the European RFID band of 862-869 MHz by changing the antenna varactor capacitance.

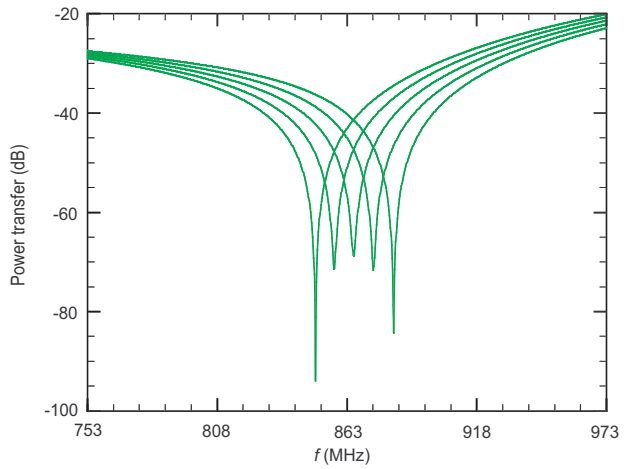

Fig. 6. Simulated isolation with different capacitance values of the antenna tuning varactor.

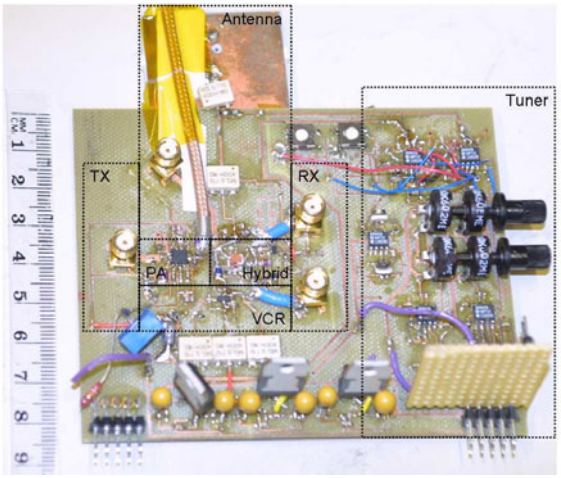

Fig. 7. First prototype of the RF front end.

V. Measurement Results

After excessive analysis and simulations, a prototype of the hybrid RF front end was fabricated. The prototype consists of the hybrid transformer with ratio $n \approx 3$, a commercial power amplifier (PA), VCR, and a PIFA-type antenna on the opposite side of the PCB board. The antenna is small and narrow-banded, about 50*30*3 mm^3, and bandwidth of 10 MHz. The antenna can be made small, if tuning is provided. The RF front end was accompanied with a low frequency analog tuner, that took care of the tuning of the VCR and varactor. The prototype is presented in Fig. 7

The main difference between the realised prototype and the simulations as well as the theoretical analysis, is that parasitic series inductances from hybrid to antenna and VCR are not modelled. Also RX loop reactances are not considered in the previous analysis. Both of these lead to increased reactances of the system, and hence to narrower band of the system. Also the realised antenna is narrower than simulated ($Q \approx 50$), making the antenna the limiting component for the bandwidth.

The actual RF front end was first demonstrated with vector network analyser (VNA). The measurement setup is presented in Fig. 8. The coupling to the antenna port is achieved with a reference antenna that is situated to a known distance of the antenna coupled to the RF front end. By knowing both antenna gains, the measurements of the antenna port are reduced to the power delivered to the antenna of the module. When similar calculation is made to take into account the power amplifier gain,the measurement results can be directly compared to the simulated and theoretical results. However, the PA gain is quite problematic to measure, as its gain depends on the output load. Hence error of 1 - 2 dB is to be considered for the measured results. The isolation and RX and TX gains of the RF front end are presented in Fig. 9.

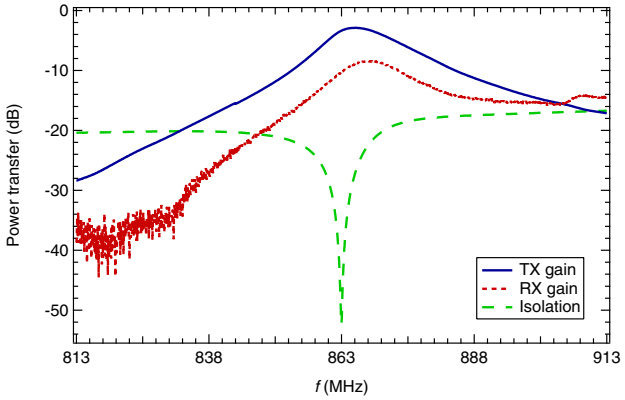

Fig. 9. Measurement of the prototype isolation and TX and RX gain.

In resonance, i.e. at 863 MHz, the isolation of even -50 dB is seen. The isolation is narrower than simulated, because the antenna of the prototype was narrower. Also VCR parasitics were not well enough included in the simulations. The TX gain is about -2.7 dB, and RX gain -7.0 dB, which are both a decibel less than simulated with $n = 3$. This probably due to the series losses, which were insufficiently modelled. In general, the shape and level of measured values comply well with both simulations and theoretical analysis.

The tuning of isolation over the European RFID band is shown in Fig. 10. The tuning range of the varactor capacitance is about one octave.

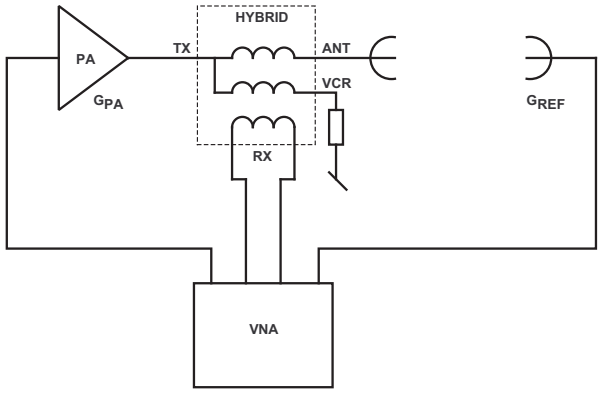

Fig. 8. Measurement setup of the prototype.

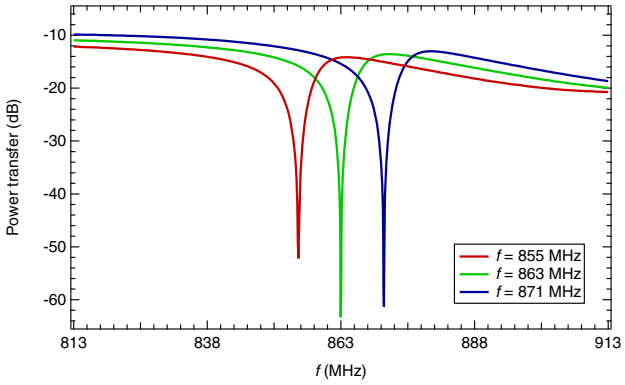

Fig. 10. Measurement of the isolation with different capacitance values of the antenna tuning varactor.

The RF front end was also tested with a RFID transceiver chip. The tuner used the output of quadrature mixers to tune the hybrid for maximum isolation. Here a reading distance of about 30-40 cm was achieved with transmit power of about 100 mW eirp regardless of the user hand or metal near the reader antenna.

VI. Conclusion

We have presented a hybrid transformer based RF front end for mobile UHF RFID readers. The solution has three main advantages: 1) power efficiency due to direct matching of antenna to PA output and narrow-band antenna; 2) small size, as circulator is not needed, and tunability allows a small, narrow-band antenna; 3) tunability delivers compensation for environmental reflections due to user hand near reader antenna, which increases read reliability.

The analysis and measurements show, that the solution is technically feasible. The hybrid delivers even -50 dB isolation between TX output and RX input. TX and RX gains depend from the ratio of VCR and antenna loads, i.e. the ratio $n = R_2/R_1$: The TX gain $G_{TX} \propto (1 + 1/n)^{-1}$ and RX gain $G_{RX} \propto 1/n^2$. Hence the more power is saved in the transmission, the more power is lost in the reception. These results were justified by theoretical analysis, simulations and measurements. Theoretically it was also shown, that the noise figure of the receiver increases as n^3.

The bandwidth of the system has several limits. The fundamental, maximum bandwidth of the system, is limited by the reactance of the hybrid branches. Theoretically a maximum relative bandwidth of about 0.3 is achievable. In this demonstration the toroidal coil having 6 nH/turn was used. Owing to this reasonable high inductance the maximum bandwidth was limited to about 100 MHz, which is just enough for covering the whole RFID UHF band tuning the antenna only. The bandwidth of antenna, which is about 20 MHz, is more than enough for 1 MHz data bandwidth used in UHF RFID.

The system includes also an RFID transceiver chip, and a analog tuner, that uses the output of the quadrature mixers to tune the hybrid for highest isolation. When using the prototype with the about 100 mW eirp transmit power, a reading distance of 30 - 40 cm was achieved regardless of the user hand or metal near the reader antenna.

The analysis, simulations and measurements show that a very power effective RFID reader can be realised by using a reactive power divider with a low output impedance PA directly connected into an antenna. The tunable antenna enables optimizing the antenna radiation efficiency and, in addition, it can be used to compensate for the reflections. Our first demonstrator clearly indicates its potential but further optimization of the whole system is still needed.

VII. Acknowledgments

This work has been financially supported of Perlos Corporation. The authors would like to thank Janne Toikka, Jukka Ranta, Dag Mårtensson, and Carl-Gustaf Blom from Perlos for fruitful discussions and valuable ideas.

References

[1] J.-P. Curty, M. Declercq, C. Dehollain, N. Joehl, *Design and Optimization of Passive UHF RFID Systems*, Springer, 2007.

[2] K. Choi, Y. Eo, S. Jung, I. Kwon, H-B. Lee, Y-J. Kim, "A Fully Integrated CMOS RF Transmitter for UHF Mobile RFID Reader Applications", *Proceedings of the 37th European Microwave Conference*, Munich, Germany, Oct. 2007, pp. 1648 – 1651.

[3] Y. Kim, I-J. Yoon, Y. Kim, "Internal Antenna Design of 900 MHz-Band Mobile Radio Frequency Identification System", *Microwave and optical technology letters*, Vol. 49, No. 9, Sep. 2007, pp. 2079 – 2082.

[4] P. D. L. Beasley, A. G. Stove, B. J. Reits, B-O. As, "Solving the Problems of a Single Antenna Frequency Modulated CW Radar", *Proc. IEEE Radar Conf.*, 1990, pp. 391 -? 395.

[5] J-G. Kim, S. Ko, S. Jeon, J-W. Park, S. Hong, "Balanced Topology to Cancel Tx Leakage in CW Radar", *IEEE Microwave and wireless components letters*, Vol. 14, No. 9, Sep. 2004, pp. 443 – 445.

Series title, number and report code of publication

VTT Publications 701
VTT-PUBS-701

Author(s)
Pursula, Pekka

Title

Analysis and Design of UHF and Millimetre Wave Radio Frequency Identification

Abstract

Radio frequency identification (RFID) is an asymmetric radio protocol, where uplink communication (from transponder to reader) is implemented with backscattering modulation. The idea was first demonstrated in the 1940's. One of the first consumer applications of RFID was access control, and key cards based on an inductive near field coupling are widely used even today. The introduction of Schottky diodes to CMOS processes enabled passive RFID, i.e. transponders without a battery, at ultra high frequencies (UHF) with reasonable cost and read range in the end of 1990's. This has opened up new applications and inspired new research on RFID.

This thesis studies the radio frequency (RF) components and general RF phenomena in RFID at UHF and millimetre waves. The theoretical analysis of the radio path reveals that the read range of a passive UHF system is ideally limited by the downlink, i.e. the power transfer from reader to the transponder. However, the architecture of the reader RF front end is critical, because the transmitted signal may couple a significant amount of noise to the receiver, overpowering the faint reflection from the transponder. In the thesis, two adaptive RF front ends are introduced to eliminate the noise coupling from the transmitter.

One of the most critical problems with UHF RFID has been the detuning of transponder antennas on different mounting platforms. The detuning may significantly diminish the read range of the transponder, especially on metal surfaces. In this thesis, two backscattering-based measurement techniques for the transponder antennas are presented. The detuning effect has been studied using these measurement techniques, and a platform tolerantantenna is introduced.

RFID at millimetre waves enables miniaturisation of the reader antenna, and widening the data bandwidth over short distances. This could be used to access wirelessly mass memories with wide data bandwidth. A semipassive or active transponder could communicate, e.g., with automotive radars. The millimetre wave identification (MMID) has been theoretically studied and experimentally verified at 60 GHz.

ISBN
978-951-38-7133-8 (soft back ed.)
978-951-38-7134-5 (URL: http://www.vtt.fi/publications/index.jsp)

Series title and ISSN
VTT Publications
1235-0621 (soft back ed.)
1455-0849 (URL: http://www.vtt.fi/publications/index.jsp)

Project number
25336

Date
December 2008

Language
English, Finnish abstr.

Pages
82 p. + app. 51 p.

Name of project

Commissioned by
The Finnish Foundation for Technology Promotion (TES), The Foundation of The Finnish Society of Electronics Engineers (EIS), The Espoo Culture Foundation

Keywords
radio frequency identification, RFID, ultra high frequency, UHF, millimetre, waves, millimetre wave identification, MMID, antenna, scattering, backscattering modulation, scattering measurement, reader device, adaptive rf front end

Publisher
VTT Technical Research Centre of Finland
P.O. Box 1000, FI-02044 VTT, Finland
Phone internat. +358 20 722 4520
Fax +358 20 722 4374

Julkaisun sarja, numero ja raporttikoodi

VTT Publications 701
VTT-PUBS-701

Tekijä(t)
Pursula, Pekka

Nimeke

UHF- ja millimetriaaltoalueen radiotunnistusjärjestelmien tutkimus ja suunnittelu

Tiivistelmä

Radiotunnistus (RFID) on lyhyen kantaman radioprotokolla, jossa yksinkertaisen tunnisteen muisti voidaan lukea langattomasti lukijalaitteen avulla. Tiedonsiirto tunnisteesta lukijalaitteeseen perustuu tunnisteen takaisinsironnan moduloimiseen. Tekniikka on osoitettu kokeellisesti toimivaksi jo 1940-luvulla. Radiotunnistuksen ensimmäisiä kuluttajasovelluksia on induktiivisiin kulkukortteihin ja lukulaitteisiin perustuva kulunvalvonta, jota käytetään tänäkin päivänä yleisesti. Passiivisten, eli paristottomien, tunnisteiden valmistaminen UHF-taajuusalueelle halpeni merkittävästi 1990-luvulla, kun Schottky-diodi integroitiin onnistuneesti CMOS-prosessiin.

Tässä väitöskirjassa on tutkittu radiotunnistusjärjestelmien radiotaajuisia komponentteja ja ilmiöitä UHF- ja millimetriaaltoalueella. Teoreettisen analyysin perusteella tehonsyöttö lukijalta tunnisteelle rajoittaa passiivisen UHF RFID -järjestelmän toimintaetäisyyden noin kymmeneen metriin. Lukijan vastaanottama signaali on tällä etäisyydellä heikko lähettimen kohinaan verrattuna. Tässä väitöskirjassa on esitetty kaksi mukautuvaa radioetuastetta lähettimen kohinan eristämiseksi vastaanottimesta.

Tunnisteantennin sivuunvirittyminen on yleinen ongelma radiotunnistuksessa. Antennin kiinnitysalustan johtavuus tai dielektrisyys muuttaa antennin resonanssitaajuutta, mikä voi estää tunnisteen havaitsemisen. Väitöskirjassa on kehitetty kaksi takaisinsirontaan perustuvaa antennimittausmenetelmää ilmiön tutkimiseksi. Lisäksi työssä esitellään antennirakenne, joka voidaan kiinnittää useille erityyppisille pinnoille antennin toiminnallisuuden heikentymättä.

Millimetriaaltoalueella radiotunnistuksessa voidaan käyttää erittäin laajaa tiedonsiirtokaistaa lyhyillä etäisyyksillä langattoman massamuistin nopeaan lukemiseen. Toisaalta pitkän kantaman sovelluksessa esimerkiksi autotutkia voitaisiin käyttää lukijalaitteina. Väitöskirjassa on tutkittu millimetriaaltojen käyttöä radiotunnistuksessa teoreettisesti sekä osoitettu tekniikan toimivuus kokeellisesti 60 GHz:n taajuudella.

ISBN
978-951-38-7133-8 (nid.)
978-951-38-7134-5 (URL: http://www.vtt.fi/publications/index.jsp)

Avainnimeke ja ISSN	Projektinumero
VTT Publications 1235-0621 (nid.) 1455-0849 (URL: http://www.vtt.fi/publications/index.jsp)	25336

Julkaisuaika	Kieli	Sivuja
Joulukuu 2008	Englanti, suom. tiiv.	82 s. + liitt. 51 s.

Projektin nimi	Toimeksiantaja(t)
	Tekniikan edistämissäätiö (TES), EIS – Elektroniikkainsinöörien seura ry., Espoon seudun kulttuurisäätiö

Avainsanat	Julkaisija
radio frequency identification, RFID, ultra high frequency, UHF, millimetre, waves, millimetre wave identification, MMID, antenna, scattering, backscattering modulation, scattering measurement, reader device, adaptive rf front end	VTT PL 1000, 02044 VTT Puh. 020 722 4520 Faksi 020 722 4374

This thesis studies the radio frequency (RF) components and phenomena in radio frequency identification (RFID) at UHF and millimetre waves. The radio path has been theoretically analysed to motivate the experimental work on all the RF components of an UHF RFID system. Two adaptive RF front ends for the reader have been designed and analysed, and an integrated circuit for a passive sensor application is introduced. Two scattering-based measurement techniques for small antennas have been developed, and the techniques have been used in the design and analysis of a platform-tolerant transponder antenna. In addition to UHF, the radio frequency identification at millimetre waves, or millimetre identification (MMID) is discussed. Communication by backscattering modulation is experimentally verified at 60 GHz.

Julkaisu on saatavana

VTT
PL 1000
02044 VTT
Puh. 020 722 4520
http://www.vtt.fi

Publikationen distribueras av

VTT
PB 1000
02044 VTT
Tel. 020 722 4520
http://www.vtt.fi

This publication is available from

VTT
P.O. Box 1000
FI-02044 VTT, Finland
Phone internat. + 358 20 722 4520
http://www.vtt.fi

ISBN 978-951-38-7133-8 (soft back ed.)
ISSN 1235-0621 (soft back ed.)

ISBN 978-951-38-7134-5 (URL: http://www.vtt.fi/publications/index.jsp)
ISSN 1455-0849 (URL: http://www.vtt.fi/publications/index.jsp)

VTT PUBLICATIONS 701

Analysis and Design of UHF and Millimetre Wave Radio Frequency Identification

Pekka Pursula